SMALL AMPLITUDE OSCILLATORY FLOWS OF NEMATIC LIQUID CRYSTAL POLYMERS

by
Eric P. Choate

A dissertation submitted to the faculty of the University of North Carolina at Chapel Hill in partial fulfillment of the requirements for the degree of Doctor of Philosophy in the Department of Mathematics.

Chapel Hill
2007

Approved by:

M. Gregory Forest

David Adalsteinsson

Richard M. McLaughlin

Peter J. Mucha

Ruhai Zhou

ABSTRACT

ERIC P. CHOATE: SMALL AMPLITUDE OSCILLATORY FLOWS OF NEMATIC LIQUID
CRYSTAL POLYMERS.
(Under the direction of M. Gregory Forest)

This dissertation presents two theoretical predictions of the behavior of solutions of nematic liquid crystal polymers when subjected to small amplitude flows that are oscillatory in time. First, we review theoretical models for predicting the behavior of nematic liquid crystals, including Leslie-Ericksen theory, which only attempts to capture the mean direction of molecular orientation, and Doi-Hess kinetic theory, which defines a probability density function on the unit sphere for the molecular orientation and also the mesocscopic orientation tensor models derived from it, which are the models that we will examine. In Chapter 2, we examine shear flow in the monodomain limit, in which there are no spatial gradients in molecular orientation, and we use multiple timescale perturbation analysis to capture very slowly developing effects in the dynamic moduli, similar to experimental observations. Then, in Chapter 3, we relax the monodomain restriction and examine the effect of heterogeneity in the molecular orientation and the choice of two special anchoring conditions for the orientation at the plates. We recover a Leslie-Ericksen-type prediction, formally connect imposed stress and imposed velocity boundary conditions in shear flow, and establish an equivalence at the level of the storage and loss moduli between shear flow and Poiseuille flow.

# ACKNOWLEDGMENTS

I am greatly indebted to my parents, Phil and Janice Choate. While there was very little higher mathematics that my father could teach me, he definitely instilled in me a curiosity and also a love of science. I am also thankful for my eighth grade algebra teach/football coach/track coach David Morris for teaching me that the study of math could be both interesting and enjoyable and something that I could do well. Also, Gary Hall's friendship and guidance during my undergraduate days are also very important to me, especially the time when on one of the tests he took off points because I failed to address the nonphysical solution to the differential equation used to model the system. "But you asked us to model this real-world situation, not solve a system of equations," I protested. He responded, "Why are you complaining, it was the only thing you missed on the test? In the long run, it won't matter, and you'll forget about this by next week." Well, Gary, it's been nearly ten years, and I still have not forgotten, and I still feel this is an important issue.

# TABLE OF CONTENTS

# LIST OF FIGURES

# Chapter 1

# Theory of Nematic Liquid Crystal Polymers

In this chapter, we define different types of models that are used to predict the behavior of a solution of nematic liquid crystal polymers in response to a fluid flow. The specific flows of interest are small amplitude oscillator shear flow and Poiseuille flow. Also, we will discuss some important orientation-dependent rheological properties that can be measured experimentally and also predicted once we have solved for the molecular orientation.

## 1.1  What are nematic liquid crystals?

In elementary school science classes, we learn that there are three distinct states of matter: solid, liquid, and gas. As is often the case with elementary school descriptions, later in life, we learn that the division of matter is somewhat more complicated. The example that we will examine in this dissertation is that of liquid crystals. These substances do not have the simple melting transition from solid to liquid of a substance like water, but instead they have distinct intermediate states in between the "solid" and "liquid" states. Specifically, liquid crystals are observed to "melt" from solid to the liquid crystal phase, and then "melt" again at a higher temperature to an isotropic liquid phase. In this intermediate liquid crystal state, called the nematic phase, the molecules lose their positional order making them liquid-like and allowing them to flow, but the molecules, which are roughly shaped like either long, thin rods or flat disks, still retain some degree of the orientational order found in a crystal.[1] Then at higher temperatures, in the isotropic state, this orientational order is also lost. Figure 1.1 shows a cartoon of the isotropic and nematic phases. Transitions from the isotropic phase back to the nematic phase

---

[1]There are other types of liquid crystal phases called smectic or cholesteric phases that retain a partial positional ordering in one or two dimensions. Additionally, some substances melt from a solid through one or more smectic phases before arriving at a nematic phase.
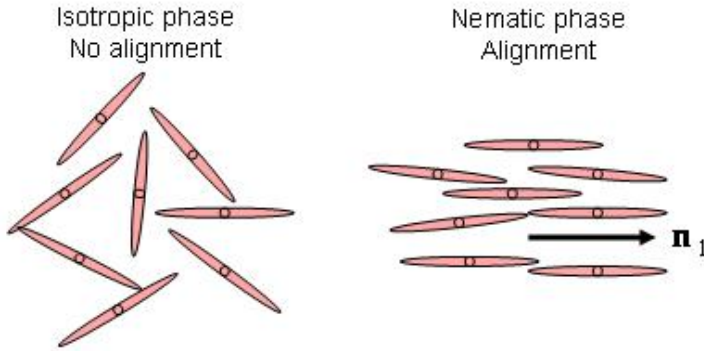
Figure 1.1: A cartoon illustrating the difference between solutions in the isotropic and nematic phases. In the nematic phase, the major director $\mathbf{n}_1$ represents the preferred direction of molecular alignment.

can be driven by decreasing the temperature, a *thermotropic* transition, or by increasing the concentration of a (usually dilute) solution of liquid crystals in a Newtonian solvent, a *lyotropic* transition. Some examples of nematic liquid crystals include $N$-($p$-methoxybenzylidene)-$p$-butylaniline (MBBA), poly-$\gamma$-benzyl-L-glutamate (PBLG) in $m$-cresol, and the tobacco mosaic virus in an aqueous solution.

In this chapter, we will review theoretical models used to predict when a substance is in the nematic phase and the nature of the molecular orientation of that phase. First, Leslie-Ericksen theory only attempts to describe the preferred direction of the molecules, and then the later kinetic theory of Doi and Hess attempts to refine this preferred orientation and provide a measure of the strength of this preference.

We will idealize these molecules as monodisperse rigid spheroids with an axis of symmetry with length $l$ and the transverse axis of length $d$. The aspect ratio is $R = \frac{l}{d}$, but it enters the theory mainly through the *molecular geometry parameter*

$$a = \frac{R^2 - 1}{R^2 + 1}. \tag{1.1}$$

Infinitely thin rods correspond to the limit $a \rightarrow 1$, spheres to $a = 0$, and infinitely thin disks to $a \rightarrow -1$. The majority of this dissertation will discuss finitely thin rods, usually with either
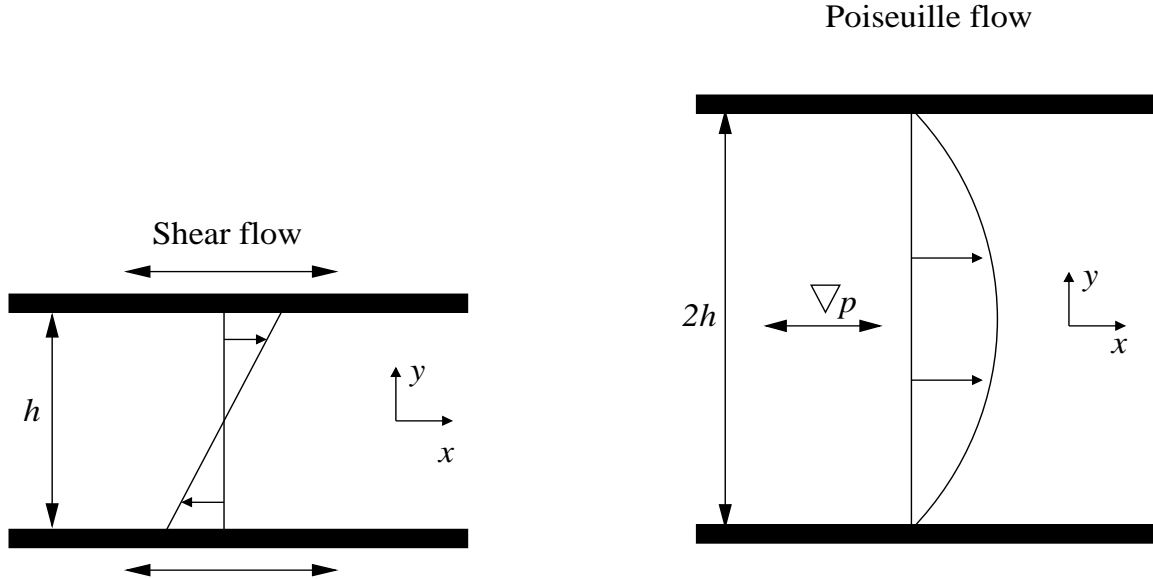
Figure 1.2: The geometries of our flows.

$a = 0.8$ or $a = 0.9$ . For disks, we use either $a = -0.8$ or $a = -0.9$. These spheroids are assumed to be uniformly dispersed in a dilute solution in a viscous solvent.

## 1.2   Small amplitude oscillatory shear and Poiseuille flows

In this dissertation, we will discuss two different types of flow between two parallel plates. In the shear flow studied in Chapters 2 and 3, the plates are moved parallel to each other in the $x$-direction, driven with either an imposed stress or an imposed velocity and inducing a flow by drag forces. In Chapter 3, we also examine Poiseuille flow in which the plates remain stationary and flow is induced by an oscillatory pressure gradient in the $x$-direction.

For both flow types, we center our coordinate axes at the midpoint between the plates, but for reasons discussed in Chapter 3, we will choose the gap separation to be $h$ for shear flow but $2h$ for Poiseuille flow, as depicted in Figure 1.2. We will choose $h = 10^{-4}$m as our characteristic length scale. By choosing uniform boundary conditions on both plates, we will assume throughout this dissertation that the fluid velocity takes the form

$$\mathbf{v} = (v_x(y), 0, 0)^T \tag{1.2}$$

3

and also that the nematic orientation is constant in the $x$- and $z$-directions. This allows us to focus on the one-dimensional structures that develop across the gap.

For the velocity $\mathbf{v}$, we define the velocity gradient as $(\nabla \mathbf{v})_{ij} = v_{i,j} = \frac{\partial v_i}{\partial x_j}$. The rate-of-strain tensor $\mathbf{D} = \frac{1}{2}\left(\nabla \mathbf{v} + \nabla \mathbf{v}^T\right)$ and the vorticity tensor $\mathbf{\Omega} = \frac{1}{2}\left(\nabla \mathbf{v} - \nabla \mathbf{v}^T\right)$ are respectively the symmetric and antisymmetric parts the velocity gradient. Under the geometrical restrictions above, we have

$$\mathbf{D} = \frac{1}{2}\frac{\partial v_x}{\partial y}\begin{pmatrix} 0 & 1 & 0 \\ 1 & 0 & 0 \\ 0 & 0 & 0 \end{pmatrix} \text{ and } \mathbf{\Omega} = \frac{1}{2}\frac{\partial v_x}{\partial y}\begin{pmatrix} 0 & 1 & 0 \\ -1 & 0 & 0 \\ 0 & 0 & 0 \end{pmatrix}. \tag{1.3}$$

## 1.3   Leslie-Ericksen Theory

An early theory for modeling a flowing nematic liquid crystal solution was developed by Leslie and Ericksen. Leslie-Ericksen (LE) theory attempts to provide only the *major director*, or the mean direction of the orientation of the molecules. For small-molecule nematics, when orientation is assumed to be instantaneous on the laboratory time scale, LE theory generally works well; however for slower molecular orientation times of larger polymeric nematics, LE theory begins to break down. (Larson, 1999)

First, Ericksen proposed a *transversely isotropic fluid* (TIF), which treats the major director $\mathbf{n}$ as the axis of symmetry of a rigid spheroid which is rotated by the surrounding flow, which results in the Jeffery orbit equation

$$\dot{\mathbf{n}} = \mathbf{\Omega} \cdot \mathbf{n} + \lambda_L(\mathbf{D} \cdot \mathbf{n} - \mathbf{D} : \mathbf{nnn}), \tag{1.4}$$

where $\lambda_L$ is known as the *Leslie tumbling parameter* for reasons outlined below. The $\mathbf{D} : \mathbf{nnn}$ term is included so that $\mathbf{n}$ remains a unit vector. This is coupled to the fluid velocity through a Navier-Stokes equation with the stress tensor

$$\boldsymbol{\tau} = 2\mu\mathbf{D} + 2\mu_1\mathbf{D} : \mathbf{nnnn} + \mu_2(\mathbf{nn} \cdot \mathbf{D} + \mathbf{D} \cdot \mathbf{nn}), \tag{1.5}$$

for three constant viscosities $\mu, \mu_1$, and $\mu_2$.

Leslie took Ericksen's TIF and added a molecular field $\mathbf{h}$ to account for the Frank distortional stresses generated by spatial variations in $\mathbf{n}$. In the absence of an electromagnetic field, $\mathbf{h}$ is written as the sum of three different types of distortional stresses—splay, twist, and bend:

$$
\begin{aligned}
\mathbf{h}_S &= K_1 \nabla (\nabla \cdot \mathbf{n}), \\
\mathbf{h}_T &= -K_2 (A \nabla \times \mathbf{n} + \nabla \times (A\mathbf{n})), \\
\mathbf{h}_B &= K_3 (\mathbf{B} \times (\nabla \times \mathbf{n}) + \nabla \times (\nabla \times \mathbf{B})),
\end{aligned}
\tag{1.6}
$$

where $A = \mathbf{n} \cdot (\nabla \times \mathbf{n})$ and $\mathbf{B} = \mathbf{n} \times (\nabla \times \mathbf{n})$. Often, the single-constant approximation

$$
K = K_1 = K_2 = K_3
\tag{1.7}
$$

is used so that $\mathbf{h}$ simplifies to

$$
\mathbf{h} = K \Delta \mathbf{n}.
\tag{1.8}
$$

Using this field, Leslie transformed (1.4) into

$$
\gamma_1 \mathbf{N} = -\gamma_2 (\mathbf{D} \cdot \mathbf{n} - \mathbf{D} : \mathbf{nnn}) + \mathbf{h} - \mathbf{h} \cdot \mathbf{nn},
\tag{1.9}
$$

for $\mathbf{N} = \dot{\mathbf{n}} - \boldsymbol{\Omega} \cdot \mathbf{n}$, and wrote the stress tensor in the form

$$
\boldsymbol{\tau} = \alpha_1 \mathbf{D} : \mathbf{nnnn} + \alpha_2 \mathbf{nN} + \alpha_3 \mathbf{Nn} + \alpha_4 \mathbf{D} + \alpha_5 \mathbf{nn} \cdot \mathbf{D} + \alpha_6 \mathbf{D} \cdot \mathbf{nn},
\tag{1.10}
$$

where the coefficients $\alpha_i$ are called the *Leslie viscosities*, and

$$
\gamma_1 = \alpha_3 - \alpha_2, \text{ and } \gamma_2 = \alpha_6 - \alpha_5.
\tag{1.11}
$$

Additionally, the Parodi relationship gives the constraint

$$
\alpha_6 = \alpha_2 + \alpha_3 + \alpha_5.
\tag{1.12}
$$

If $\mathbf{h} = \mathbf{0}$, then (1.9) reduces to (1.4) with the identification of the Leslie tumbling parameter as

$\lambda_L = -\frac{\gamma_2}{\gamma_1} = \frac{\alpha_2 + \alpha_3}{\alpha_2 - \alpha_3}.$

## 1.4 Kinetic theory

A more complicated theory was developed later by Doi and Hess (cf. (Doi and Edwards, 1986; Hess, 1976; Wang, 2002)) to account for variability in the degree of orientation of the molecules. In this kinetic theory, $f(\mathbf{m}, \mathbf{x}, t)$ denotes the probability density function corresponding to the probability that the axis of symmetry of a spheroidal molecule at location $\mathbf{x}$ is aligned with the direction $\mathbf{m}$ ($\|\mathbf{m}\| = 1$) at time $t$. The Smoluchowski equation for $f(\mathbf{m}, \mathbf{x}, t)$ is given by (Doi and Edwards, 1986):

$$\frac{df}{dt} = \mathcal{R} \cdot [\hat{D}_r(\mathbf{m})(\mathcal{R}f + \frac{1}{k_B T} f \mathcal{R}V)] - \mathcal{R} \cdot [\mathbf{m} \times \dot{\mathbf{m}} f], \tag{1.13}$$

where $\mathcal{R} = \mathbf{m} \times \frac{\partial}{\partial \mathbf{m}}$ is the rotational gradient operator, $k_B$ is the Boltzmann constant, $T$ is the absolute temperature, and $V$ is an excluded volume potential. For $a$ given by (1.1),

$$\dot{\mathbf{m}} = \boldsymbol{\Omega} \cdot \mathbf{m} + a[\mathbf{D} \cdot \mathbf{m} - \mathbf{D} : \mathbf{mmm}] \tag{1.14}$$

is the Jeffery orbit for a single molecule subjected to flow. The rotational diffusion coefficient $\hat{D}_r(\mathbf{m})$ is given by

$$\hat{D}_r(\mathbf{m}) = \begin{cases} D_r, & \text{for constant rotary diffusivity,} \\ \frac{D_r}{\left(\int_{\|\mathbf{m}'\|=1} \|\mathbf{m} \times \mathbf{m}'\| f(\mathbf{m}',t)d\mathbf{m}'\right)^2}, & \text{otherwise,} \end{cases} \tag{1.15}$$

$$= \begin{cases} D_r, & \text{for constant rotary diffusivity,} \\ \frac{D_r}{(1 - \mathbf{mm}:\mathbf{M})^2}, & \text{otherwise,} \end{cases} \tag{1.16}$$

with $D_r$ the averaged rotational diffusion rate. In this dissertation, we will use only the constant rotary model. The averaged rotational diffusion rate for a rod in a dilute solution is given by

$$D_r = \beta D_{r0}(\nu l^3)^{-2} \tag{1.17}$$

where $\beta = 10^4$, $\nu$ is the polymer number density, and the $D_{r0}$ is the dilute-solution rotational diffusion rate, which is given by the Kirkwood-Auer formula

$$D_{r0} = \frac{3k_BT(\ln(l/d) - \gamma)}{\pi \eta_s l^3}, \tag{1.18}$$

where $\gamma$ is a constant usually taken to be 0.8, and $\eta_s$ is the solvent viscosity (Larson, 1999).

For the excluded volume potential, we will use a modified version of the Marrucci-Greco potential (Wang, 2002)

$$V = -\tfrac{3}{2}Nk_BT\left[\left(1 + \tfrac{\mathcal{L}^2}{24}\Delta\right)\mathbf{M}:\mathbf{mm} + \tfrac{L^2}{48}\left(\nabla\nabla\mathbf{M}::\mathbf{mmmm} + (\nabla\nabla:\mathbf{M}_4):\mathbf{mm}\right)\right]. \tag{1.19}$$

The overall strength of the potential is characterized by the dimensionless polymer concentration parameter $N$. The two polymer interaction length scales introduced here, $\mathcal{L}$ and $L$, respectively represent strength of the isotropic and anisotropic distortional elastic stresses (Wang, 2002). In this context, *isotropic* means that there is no preferred mode of distortion in the splay, blend, or twist sense of (1.6). We define the nondimensional parameter $\theta = \frac{L^2}{\mathcal{L}^2}$ to characterize the relative strength of the anisotropic distortional elasticity so that $\theta = 0$ corresponds to the single Frank constant approximation of Leslie-Ericksen theory (1.7). Despite the notation, $\theta$ can take values in $[-1, \infty)$, being negative for disk-shaped molecules and positive for rods.

The potential (1.19) depends on $f$ through the second moment tensor

$$\mathbf{M} = \langle\mathbf{mm}\rangle = \int_{\|\mathbf{m}\|=1} \mathbf{mm}\, f(\mathbf{m}, t)\, d\mathbf{m}, \tag{1.20}$$

and the fourth moment $\mathbf{M}_4 = \langle\mathbf{mmmm}\rangle$. Note that $\mathbf{M}$ is symmetric and that since $\mathbf{m}$ is a unit vector, $\mathbf{M}$ has trace 1.

## 1.5 Mesoscopic Tensor Models

One way to attack the Smoluchowski equation (1.13) is by expanding $f$ in spherical harmonics (cf. (Forest *et al.*, 2005)); however in this dissertation we will approach (1.13) from a different direction and get information about $f$ through its second moment tensor $\mathbf{M}$, or the traceless

*mesoscopic orientational tensor*

$$\mathbf{Q} = \mathbf{M} - \frac{\mathbf{I}}{3}. \tag{1.21}$$

By multiplying (1.13) by $\mathbf{mm}$ and then integrating with respect to $\mathbf{m}$, we can get an equation for $\mathbf{M}$

$$
\begin{aligned}
\tfrac{d}{dt}\mathbf{M} = \quad & \boldsymbol{\Omega} \cdot \mathbf{M} - \mathbf{M} \cdot \boldsymbol{\Omega} + a(\mathbf{D} \cdot \mathbf{M} + \mathbf{M} \cdot \mathbf{D} - 2\mathbf{D} : \mathbf{M}_4) \\
& -6D_r \Big[ \mathbf{Q} - N(\mathbf{M} \cdot \mathbf{M} - \mathbf{M} : \mathbf{M}_4) - \tfrac{N\mathcal{L}^2}{48}(\Delta \mathbf{M} \cdot \mathbf{M} + \mathbf{M} \cdot \Delta \mathbf{M} - 2\Delta \mathbf{M} : \mathbf{M}_4) \\
& \quad - \tfrac{NL^2}{96}\big[ (\nabla\nabla\mathbf{M}) \vdots \mathbf{M}_4 + (\mathbf{M}_4 \vdots \nabla\nabla\mathbf{M})^T + \mathbf{M} \cdot (\nabla\nabla : \mathbf{M}_4 - 4\mathbf{M}_6 :: \nabla\nabla\mathbf{M}) \\
& \quad + ((\nabla\nabla\mathbf{M}) \vdots \mathbf{M}_4)^T + \mathbf{M}_4 \vdots \nabla\nabla\mathbf{M} + (\nabla\nabla : \mathbf{M}_4) \cdot \mathbf{M} - 2\mathbf{M}_4 : (\nabla\nabla : \mathbf{M}_4)\big] \Big],
\end{aligned}
\tag{1.22}
$$

where $\mathbf{M}_6 = \langle \mathbf{mmmmmm} \rangle$ is sixth moment of $f$. In order to close the system for $\mathbf{M}$ and $\mathbf{v}$, we apply the Doi approximations

$$\mathbf{M}_4 \quad \approx \quad \mathbf{MM}, \tag{1.23}$$

$$\mathbf{M}_6 \quad \approx \quad \mathbf{MMM}. \tag{1.24}$$

A discussion of other closure models is found in (Forest and Wang, 2003).

## 1.6  Stress Tensor

For our stress tensor, we use that of (Wang, 2002). We write the extra stress as the sum of four parts:

$$\boldsymbol{\tau} = \boldsymbol{\tau}^{Vis} + \boldsymbol{\tau}^{NE} + \boldsymbol{\tau}^{IE} + \boldsymbol{\tau}^{AE}. \tag{1.25}$$

Isotropic stresses will be lumped in with the pressure $p$. The viscous stress is represented by The elastic and viscous parts of the stress are respectively given by

$$\boldsymbol{\tau}^{Vis} = \quad 2\eta_s \mathbf{D} + 3\nu k_B T \left[ \zeta_1 \left( \mathbf{D} \cdot \mathbf{M} + \mathbf{M} \cdot \mathbf{D} \right) + \zeta_2 \mathbf{D} : \mathbf{M}_4 + \zeta_3 \mathbf{D} \right], \tag{1.26}$$

where

$$\zeta_1 = \zeta^{(0)}\left(\frac{1}{I_3} - \frac{1}{I_1}\right), \quad \zeta_2 = \zeta^{(0)}\left(\frac{J_1}{I_1 J_3} + \frac{1}{I_1} - \frac{2}{I_3}\right), \quad \zeta_3 = \frac{\zeta^{(0)}}{I_1},$$
$$I_1 = 2R\int_0^\infty \frac{dx}{(1+x)^3\sqrt{R^2+x}}, \quad I_3 = R(R^2+1)\int_0^\infty \frac{dx}{(1+x)^2(R^2+x)^{\frac{3}{2}}}, \tag{1.27}$$
$$J_1 = R\int_0^\infty \frac{x\,dx}{(1+x)^3\sqrt{(R^2+x)}}, \quad J_3 = R\int_0^\infty \frac{x\,dx}{(1+x)^2(R^2+x)^{\frac{3}{2}}},$$

where $\zeta^{(0)}$ is a free parameter with units of time to be experimentally characterized. In this dissertation we will use $\zeta^{(0)} = 0.01$ s.

The three remaining stresses are elastic in nature. The nematic elastic stress

$$\boldsymbol{\tau}^{NE} = 3a\nu k_B T[\mathbf{Q} - N(\mathbf{M}\cdot\mathbf{M} - \mathbf{M} : \mathbf{M}_4)] \tag{1.28}$$

arises from molecular orientation being locally out of nematic equilibrium. The isotropic distortional elastic stress is

$$\boldsymbol{\tau}^{IE} = \frac{\nu k_B T N \mathcal{L}^2}{32}\big[2(1-a)\mathbf{M}\cdot\Delta\mathbf{M} - 2(1+a)\Delta\mathbf{M}\cdot\mathbf{M}$$
$$+4a\Delta\mathbf{M} : \mathbf{M}_4 - M_{kl,i}M_{kl,j} + \mathbf{M} : \nabla\nabla\mathbf{M})\big], \tag{1.29}$$

and the anisotropic distortional elastic stress is

$$\boldsymbol{\tau}^{AE} = \frac{\nu k_B T N L^2}{32}\big[-(1+a)(\nabla\nabla\mathbf{M}\vdots\mathbf{M}_4 + (\mathbf{M}_4\vdots\nabla\nabla\mathbf{M})^T + (\nabla\nabla : \mathbf{M}_4)\cdot\mathbf{M})$$
$$+(1-a)((\nabla\nabla\mathbf{M}\vdots\mathbf{M}_4)^T + \mathbf{M}_4\vdots\nabla\nabla\mathbf{M} + \mathbf{M}\cdot(\nabla\nabla : \mathbf{M}_4)) \tag{1.30}$$
$$+a(4\mathbf{M}_6 :: \nabla\nabla\mathbf{M} + 2\mathbf{M}_4 : (\nabla\nabla : \mathbf{M}_4))\big].$$

The dimensionless linear momentum balance is

$$\frac{d\mathbf{v}}{dt} = \frac{1}{\rho}\nabla\cdot(-p\mathbf{I} + \boldsymbol{\tau}), \tag{1.31}$$

where $\rho$ is the fluid density.

## 1.7   In-plane Subspace and Spectral Representation

The orientation tensor $\mathbf{Q}$ is symmetric and has trace 0, and so it has five independent components. However, the system (1.22) and (1.31) has a reflection symmetry with respect to the $x$-$y$ plane, and so it possesses an "in-plane" subspace in which there are only three degrees of freedom in the orientation. In this dissertation, we will restrict to this subspace in which $\mathbf{Q}$ is forced to have the eigenvector $\mathbf{n}_3 = (0, 0, 1)$, which is equivalent to imposing $Q_{xz} = Q_{yz} = 0$. A result of this restriction is that if the major director $\mathbf{n}_1$ and the minor director $\mathbf{n}_2$ start in the flow-flow gradient plane, they remain in that plane.

We choose to represent these three degrees of freedom (two in the eigenvalues and one in the eigenvectors of $\mathbf{Q}$) in terms of the *in-plane director angle* $\psi$ and the scalar *order parameters* $s$ and $\beta$ as

$$\mathbf{Q} = s \left( \mathbf{n}_1 \mathbf{n}_1 - \tfrac{\mathbf{I}}{3} \right) + \beta \left( \mathbf{n}_2 \mathbf{n}_2 - \tfrac{\mathbf{I}}{3} \right), \tag{1.32}$$

$$\mathbf{n}_1 = (\cos\psi, \sin\psi, 0), \quad \mathbf{n}_2 = (-\sin\psi, \cos\psi, 0). \tag{1.33}$$

This is a standard "spectral representation" of the orientation tensor, where $\mathbf{n}_1$ and $\mathbf{n}_2$ are eigenvectors, and $s = d_1 - d_2$ and $\beta = d_2 - d_3$ are differences of the eigenvalues $d_i$ of $\mathbf{M}$ corresponding to the eigenvectors $\mathbf{n}_i$. The restrictions that $0 \leq d_i \leq 1$ and that $d_1 + d_2 + d_3 = 1$ place restrictions on the allowable values of $s$ and $\beta$, as illustrated in Figure 1.3.

In calling $\mathbf{n}_1$ the major director, we have assumed that $d_1$ is the unique largest eigenvalue of $\mathbf{M}$. (This corresponds to $s > \beta$ and $s > 0$.) However, there are situations in which this is not true. In a sense, if $d_2$ is the unique largest eigenvalue (This corresponds to $\beta > s, 0$.) then we have simply chosen the wrong alignment for which to assign $\psi = 0$, and there are no significant physical differences between these cases. However, if $d_3$ is the unique largest eigenvalue (or $s, \beta < 0$), then the major director is $\mathbf{n}_3 = (0, 0, 1)$, which corresponds to a *logrolling* state. This means that the molecules are on average aligned orthogonal to the $x$-$y$ plane rather than parallel to it.

Additionally, there are special states in which there are repeated eigenvalues. The state $d_1 = d_2 = d_3 = \frac{1}{3}$, that is $s = \beta = 0$, corresponds to the isotropic state of the fluid because the pdf $f(\mathbf{m}) \equiv \frac{1}{4\pi}$, and thus there are no distinguished directions. The situations in which
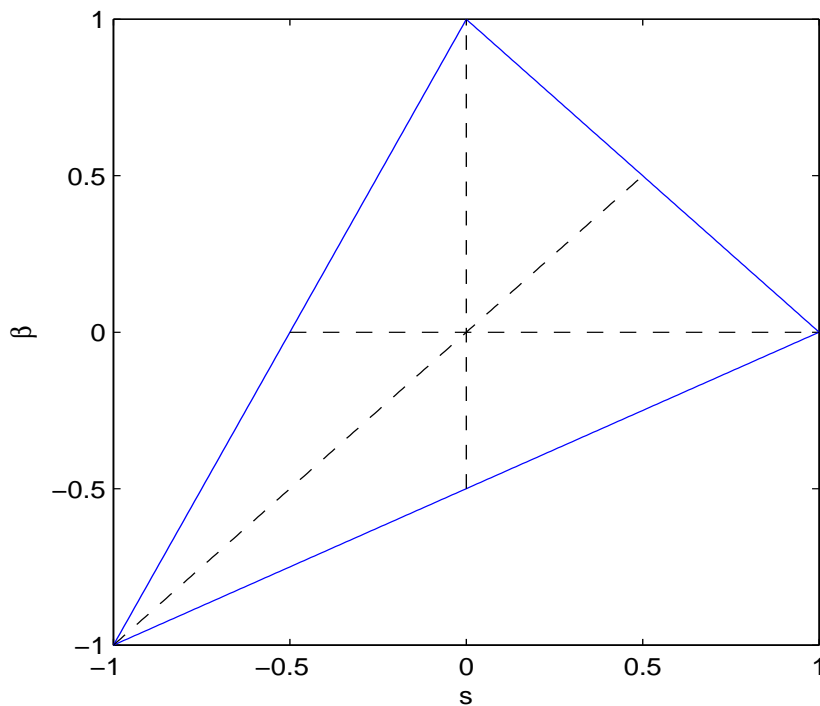
Figure 1.3: The allowable values of the order parameters lie inside a triangle in $s$-$\beta$ space. The dashed lines represent the uniaxial states.

there are only two distinct eigenvalues of $\mathbf{Q}$ are called *uniaxial states*, in contrast to the *biaxial* states in which there are three distinct eigenvalues. These are depicted by the dashed lines in Figure 1.3. The logrolling uniaxial state $d_3 > d_1 = d_2$ $(s = \beta < 0)$ is not significantly different than a biaxial logrolling state. However, when $d_1 = d_2 > d_3$ $(s = \beta > 0)$, the major director is not well-defined, a degenerate situation that we will call a *defect*. The main feature of a defect alignment is not that the molecules are on average *parallel* to a special vector, but instead the best that can be said is that on average, they are *orthogonal* to a special vector, in this case $\mathbf{n}_3$. In other words, there is not one "favored" direction, but instead the molecules only agree to reject one direction without reaching a consensus favorite. The two other uniaxial states with defects are $s = 0$ with $\beta < 0$ and $\beta = 0$ with $s < 0$, and they are aligned orthogonal to $\mathbf{n}_2$ and $\mathbf{n}_1$, respectively.

In terms of the probability density function $f$, in a biaxial state $f(\mathbf{m})$ is an ellipsoid, but at a uniaxial state, $f$ is a spheroid. The defect states correspond to $f$ being a oblate spheroid. The alignments of remaining non-defect uniaxial states $s = 0$ with $\beta > 0$ and $\beta = 0$ with $s > 0$,

in which $f$ is an prolate spheroid, are not significantly different from those biaxial states nearby in $s$-$\beta$ space.

The system for $s, \beta, \psi$, and $v_x$ that we will analyze in this dissertation is

$$\frac{\partial s}{\partial t} = \frac{a}{3}\frac{\partial v_x}{\partial y}g_0(s,\beta)\sin 2\psi - 6D_r\left(U(s) + \frac{2Ns\beta}{3}(1-s+\beta)\right)$$
$$- \frac{D_r N\mathcal{L}^2}{6}\left((s-\beta)g_0(s,\beta)\left(\frac{\partial\psi}{\partial y}\right)^2 + \frac{1}{2}g_1(s,\beta)\frac{\partial^2 s}{\partial y^2} + \frac{1}{2}g_2(s,\beta)\frac{\partial^2\beta}{\partial y^2}\right)$$
$$+ \frac{D_r NL^2}{48}\left[g_3(s,\beta,\psi)\frac{\partial^2\psi}{\partial y^2} + (g_4(s,\beta) + g_5(s,\beta)\cos 2\psi)\frac{\partial^2 s}{\partial y^2}\right.$$
$$+ (g_6(s,\beta) + g_7(s,\beta)\cos 2\psi)\frac{\partial^2\beta}{\partial y^2} + (g_8(s,\beta) + g_9(s,\beta)\cos 2\psi)\left(\frac{\partial\psi}{\partial y}\right)^2 \qquad (1.34)$$
$$+ \frac{2}{3}(-1 + 3\cos 2\psi)g_1(s,\beta)\left(\frac{\partial s}{\partial y}\right)^2 - \frac{2}{3}(1 + 3\cos 2\psi)g_2(s,\beta)\left(\frac{\partial\beta}{\partial y}\right)^2$$
$$+ \sin 2\psi\left(g_{10}(s,\beta)\frac{\partial s}{\partial y} + g_{11}(s,\beta)\frac{\partial\beta}{\partial y}\right)\frac{\partial\psi}{\partial y}$$
$$+ \frac{2}{3}\left(-(1 + 3\cos 2\psi)g_1(s,\beta) + (-1 + 3\cos 2\psi)g_2(s,\beta)\right)\frac{\partial s}{\partial y}\frac{\partial\beta}{\partial y}\right],$$

$$\frac{\partial\beta}{\partial t} = -\frac{a}{3}\frac{\partial v_x}{\partial y}g_0(\beta,s)\sin 2\psi - 6D_r\left(U(\beta) + \frac{2Ns\beta}{3}(1-\beta+s)\right)$$
$$- \frac{D_r N\mathcal{L}^2}{6}\left((s-\beta)g_0(\beta,s)\left(\frac{\partial\psi}{\partial y}\right)^2 + \frac{1}{2}g_1(\beta,s)\frac{\partial^2\beta}{\partial y^2} + \frac{1}{2}g_2(\beta,s)\frac{\partial^2 s}{\partial y^2}\right)$$
$$+ \frac{D_r NL^2}{48}\left[-g_3(\beta,s,\psi)\frac{\partial^2\psi}{\partial y^2} + (g_4(\beta,s) - g_5(\beta,s)\cos 2\psi)\frac{\partial^2\beta}{\partial y^2}\right.$$
$$+ (g_6(\beta,s) - g_7(\beta,s)\cos 2\psi)\frac{\partial^2 s}{\partial y^2} + (g_8(\beta,s) - g_9(\beta,s)\cos 2\psi)\left(\frac{\partial\psi}{\partial y}\right)^2 \qquad (1.35)$$
$$- \frac{2}{3}(1 + 3\cos 2\psi)g_1(\beta,s)\left(\frac{\partial\beta}{\partial y}\right)^2 - \frac{2}{3}(1 - 3\cos 2\psi)g_2(\beta,s)\left(\frac{\partial s}{\partial y}\right)^2$$
$$+ \sin 2\psi\left(-g_{10}(\beta,s)\frac{\partial\beta}{\partial y} - g_{11}(\beta,s)\frac{\partial s}{\partial y}\right)\frac{\partial\psi}{\partial y}$$
$$+ \frac{2}{3}\left((-1 + 3\cos 2\psi)g_1(\beta,s) - (1 + 3\cos 2\psi)g_2(\beta,s)\right)\frac{\partial s}{\partial y}\frac{\partial\beta}{\partial y}\right],$$

$$\frac{\partial\psi}{\partial t} = -\frac{1}{2}\frac{\partial v_x}{\partial y}\left(1 - \frac{a}{3}\frac{s+\beta+2}{s-\beta}\cos 2\psi\right) + \frac{D_r N\mathcal{L}^2}{24}\frac{s+\beta+2}{(s-\beta)^2}\frac{\partial}{\partial y}\left((s-\beta)^2\frac{\partial\psi}{\partial y}\right)$$
$$+ \frac{D_r NL^2}{16}(2+s+\beta)\left[\frac{1}{9(s-\beta)^2}\frac{\partial}{\partial y}\left((2+s+\beta)(s-\beta)^2\frac{\partial\psi}{\partial y}\right)\right.$$
$$+ \sin 2\psi\left(\frac{1+5s-4\beta}{54(s-\beta)}\frac{\partial^2 s}{\partial y^2} + \frac{1+5\beta-4s}{54(s-\beta)}\frac{\partial^2\beta}{\partial y^2} + \frac{s-\beta}{3}\left(\frac{\partial\psi}{\partial y}\right)^2\right) \qquad (1.36)$$
$$- \cos 2\psi\left(\left(\frac{\partial s}{\partial y} + \frac{\partial\beta}{\partial y}\right)\frac{\partial\psi}{\partial y} + \frac{s-\beta}{3}\frac{\partial^2\psi}{\partial y^2}\right)\right],$$

$$\frac{\partial v_x}{\partial t} = \frac{1}{\rho}\left(-\frac{\partial p}{\partial x} + \frac{\partial\tau_{xy}}{\partial y}\right), \qquad (1.37)$$

for the shear stress

$$\tau_{xy} = \left[\eta_s + 3\nu k_B T\left(\frac{\zeta_1}{6}(s+\beta+2) + \frac{\zeta_2}{4}(s-\beta)^2\sin^2 2\psi + \frac{\zeta_3}{2}\right)\right]\frac{\partial v_x}{\partial y}$$
$$+ \frac{3a\nu k_B T}{2}\sin 2\psi\left[U(s) - U(\beta) - \frac{4Ns\beta}{3}(s-\beta)\right]$$
$$+ \frac{\nu k_B TN\mathcal{L}^2}{16}\left[\left(1 - \frac{a}{3}\frac{s+\beta+2}{s-\beta}\cos 2\psi\right)\frac{\partial}{\partial y}\left((s-\beta)^2\frac{\partial\psi}{\partial y}\right)\right.$$
$$\left.+ \frac{a}{3}\sin 2\psi\left(h_0(\beta,s)\frac{\partial^2\beta}{\partial y^2} - h_0(s,\beta)\frac{\partial^2 s}{\partial y^2} + 2(s-\beta)(g_0(s,\beta)+g_0(\beta,s))\left(\frac{\partial\psi}{\partial y}\right)^2\right)\right]$$
$$+ \frac{\nu k_B TNL^2}{32}\left[h_1(s,\beta,\psi)\frac{\partial^2\psi}{\partial y^2} + h_2(s,\beta,\psi)\frac{\partial^2 s}{\partial y^2} - h_2(\beta,s,\psi)\frac{\partial^2\beta}{\partial y^2} + h_3(s,\beta,\psi)\left(\frac{\partial\psi}{\partial y}\right)^2\right.$$
$$+ \frac{a}{9}\sin 2\psi\left((-1+3\cos 2\psi)h_0(s,\beta)\left(\frac{\partial s}{\partial y}\right)^2 + (1+3\cos 2\psi)h_0(\beta,s)\left(\frac{\partial\beta}{\partial y}\right)^2\right)$$
$$+ (h_3(s,\beta) + h_4(s,\beta)\cos 2\psi)\frac{\partial s}{\partial y} + (h_3(\beta,s) - h_4(\beta,s)\cos 2\psi)\frac{\partial\beta}{\partial y})\frac{\partial\psi}{\partial y}$$
$$\left.+ h_5(s,\beta,\psi)\frac{\partial s}{\partial y}\frac{\partial\beta}{\partial y}\right]$$

(1.38)

where

$$U(s) = s\left(1 - \frac{N}{3}(1-s)(2s+1)\right), \quad g_0(s,\beta) = 1 + 2s - \beta + 3s\beta - 3s^2,$$
$$g_1(s,\beta) = (s-1)(1+2s-\beta), \quad g_2(s,\beta) = s(1-s+2\beta),$$
$$g_3(s,\beta,\psi) = 2\sin 2\psi(1+s)(s-\beta)(1+s+\beta-2(s^2-s\beta+\beta^2)),$$
$$g_4(s,\beta) = -\frac{1}{3}(1+s)(8s^2+s\beta-4s-4-\beta^2+5\beta)$$
$$g_5(s,\beta) = \frac{1}{9}(2(s-1)(1+2s)(5+18s)+17\beta+22s\beta-99s^2\beta+45s\beta^2-7\beta^2),$$
$$g_6(s,\beta) = \frac{1}{3}s(s^2+4s-17\beta-s\beta-8\beta^2-5)$$
$$g_7(s,\beta) = \frac{1}{9}(17s+20s^2-9s^3+99s^2\beta-5s\beta-16\beta^2-72s\beta^2+8\beta+8),$$
$$g_8(s,\beta) = -\frac{2}{3}(s-\beta)(4+13s-8s^2-9s^3-5\beta+11s\beta+\beta^2+9s\beta^2),$$
$$g_9(s,\beta) = -2(s-\beta)(-2+13s^3+\beta+\beta^2-4s^2-22s^2\beta-7s+3s\beta+13s\beta^2)),$$
$$g_{10}(s,\beta) = -4(-1+4s^3-5s^2\beta+\beta^2+s(-3+\beta(3\beta-1))),$$
$$g_{11}(s,\beta) = -4(1+2s-3s^3+\beta+2s\beta+5s^2\beta-2\beta^2-4s\beta^2),$$

(1.39)

13

$$h_0(s,\beta) = (1-\beta+2s)(1+\beta-s),$$

$$h_1(s,\beta,\psi) = \tfrac{1}{3}(s-\beta)^2(2+s+\beta-3(s-\beta)\cos 2\psi) - \tfrac{a}{18}(s-\beta)^2\Big(2\cos 2\psi\tfrac{(2+s+\beta)^2}{s-\beta}$$

$$-3\big(1+2(s^2-s\beta+\beta^2)+\cos 4\psi(3-2s^2+2\beta-2\beta^2+2s+2s\beta)\big)\Big),$$

$$h_2(s,\beta,\psi) = \tfrac{1}{18}\sin 2\psi\Big[a(8s^3+4s^2-7s^2\beta+3\beta^2+\beta^2-8s-11s\beta-2s\beta^2-4$$

$$-3\cos 2\psi(s-\beta)(8s^2+5\beta^2-\beta-3s-11s\beta-3))+(1+5s-4\beta)(s-\beta)\Big],$$

$$h_3(s,\beta,\psi) = \sin 2\psi(s-\beta)\Big((s-\beta)^2 - \tfrac{a}{9}\big(9s^3+7s^2-9s^2\beta-8s-9s\beta^2-13s\beta+$$

$$+9\beta^3-7\beta^2-8\beta-8+3(s-\beta)\cos 2\psi(10-13s^2+6s+22s\beta+6\beta-13\beta^2)\big)\Big),$$

$$h_4(s,\beta) = -3(s-\beta)^2 - \tfrac{a}{9}(2+s+\beta)(4+3s+\beta),$$

$$h_5(s,\beta,\psi) = \tfrac{a}{9}\sin 2\psi\Big((s-\beta)(s+\beta-1)$$

$$+3\cos 2\psi(3s^2+(\beta-1)(2+3\beta)-s(1+6\beta))\Big).$$

$$(1.40)$$

## 1.8 Rheological Properties

One motivation for solving the system (1.34)-(1.38) is that once the stress tensor is known, we are able to make predictions of certain rheological properties that can be measured in laboratory experiments (Larson, 1999).

### 1.8.1 Storage and Loss Moduli

In a perfectly neo-Hookean solid, the shear stress is proportional to the shear strain $\gamma$:

$$\tau_{xy}^{neo-Hookean} = G\gamma, \qquad (1.41)$$

for the shear modulus $G$. For a perfectly Newtonian fluid, however, the shear stress is proportional to the strain rate $\dot\gamma$:

$$\tau_{xy}^{Newtonian} = \eta\dot\gamma, \qquad (1.42)$$

for the shear viscosity $\eta$. It is assumed that the strain and strain rate are macroscopic quantities defined for the system as a whole, and not defined locally inside the substance so that the stress response is also homogeneous, and the shear modulus and viscosity are material properties.

A complex fluid such as a solution of nematic liquid crystal polymers possesses properties

similar to both a neo-Hookean solid and a Newtonian fluid. One method to probe the combination of these two dissimilar elements is through *linear viscoelasticity*. In this case, it is expected that the velocity gradient is approximately linear in $y$ and oscillatory in time so that the macroscopic shear strain can be written as

$$\gamma = \gamma_0 \sin \omega t. \tag{1.43}$$

The macroscopic strain rate is then just

$$\dot{\gamma} = \dot{\gamma}_0 \cos \omega t, \tag{1.44}$$

where $\dot{\gamma}_0 = \gamma_0 \omega$. Thus, a measure of a substance's solid-like and liquid-like properties can be made if the shear stress $\tau_{xy}$ can be decomposed into the sum of a part in-phase with the strain and another out-of-phase (or in-phase with the strain rate):

$$\tau_{xy} = \gamma_0 \left( G'(\omega) \sin \omega t + G''(\omega) \cos \omega t \right). \tag{1.45}$$

The in-phase term $G'(\omega)$ is called the *storage modulus* and the out-of-phase term $G''(\omega)$ is called the *loss modulus*. To mimic the notation in (1.43), the *complex modulus* is

$$G^* = G' + iG''. \tag{1.46}$$

Alternatively, from the perspective of (1.44), the *complex viscosity* is defined as

$$\eta^* = \eta' - i\eta'' = \frac{G^*}{i\omega}. \tag{1.47}$$

The ratio

$$\frac{G''}{G'} = \tan \delta \tag{1.48}$$

is known as the *loss tangent*, and it is large for a substance that is more liquid-like and small for a substance is more solid-like.

The ultimate goals of the chapters that follow are to make predictions of the storage and lose moduli.

## 1.8.2 Normal Stress Differences

Two other important rheological properties are the first and second normal stress differences, defined by

$$
\begin{aligned}
N_1 &= \tau_{xx} - \tau_{yy}, \\
N_2 &= \tau_{yy} - \tau_{zz},
\end{aligned}
\tag{1.49}
$$

respectively. Non-zero normal stress differences indicate a force exerted by the fluid pushing the plates apart or pulling them together.

# Chapter 2

# Shear flow in the monodomain Limit

In the so-called "monodomain limit," it is assumed that there are no spatial gradients in the orientation variables, which in turn allows us to remove hydrodynamic feedback from the problem. Therefore, it allows us to impose a linear velocity profile and then compute the orientation's reaction. A modified version of this chapter appears in Choate and Forest (2006).

## 2.1 Monodomain limit and nondimensionalization

In the monodomain limit, the interaction lengths $\mathcal{L}$ and $L$ are assumed to be small compared to the length scale over which distortions occur, allowing us to effectively ignore the spatial gradients in the system (1.34)-(1.38). Thus, we can assume that for small amplitude oscillatory shear flow the velocity is simply linear in $y$, and we will write it as

$$v_x = \dot{\gamma}_0 y \cos \omega t, \tag{2.1}$$

where $\dot{\gamma}_0 = \frac{A_0 \omega}{h}$ is a shear rate composed of the gap width $h$, the maximum relative amplitude of the oscillatory displacement of the parallel plates $A_0$, and the frequency of the oscillation $\omega$. This crude simplification is indeed shown to be physically relevant for the fluid near the center of the channel when the plate separation is wide.

Under these restriction that $s$, $\beta$, and $\psi$ are functions of time only, the system (1.34)-(1.36) reduces to

$$
\begin{aligned}
\dot{s} =& \ -6D_r\left(U(s) + \tfrac{2Ns\beta}{3}(1 - s + \beta)\right) + \tfrac{a}{3}\dot{\gamma}_0 \cos \omega t(1 + 2s - \beta + 3s\beta - 3s^2)\sin 2\psi, \\
\dot{\beta} =& \ -6D_r\left(U(\beta) + \tfrac{2Ns\beta}{3}(1 - \beta + s)\right) - \tfrac{a}{3}\dot{\gamma}_0 \cos \omega t(1 + 2\beta - s + 3s\beta - 3\beta^2)\sin 2\psi, \\
\dot{\psi} =& \ -\tfrac{1}{2}\dot{\gamma}_0 \cos \omega t\left(1 - \tfrac{a}{3}\tfrac{s+\beta+2}{s-\beta}\cos 2\psi\right),
\end{aligned}
\tag{2.2}
$$

and it is this system of ordinary differential equations that we we analyze in this chapter.

As a characteristic timescale we choose $t_r = (6D_r)^{-1}$, the timescale of molecular rotational diffusion. For small molecule liquid crystals, this timescale is quite fast; however, from (1.18), for the larger polymeric molecules of the present discussion, the rotational diffusion is slow enough to have an observable effect. In this dissertation, we will use $D_r = 35$ s$^{-1}$. Thus, the nondimensional velocity is

$$v_x = De\, y \cos \omega t \tag{2.3}$$

where we have defined the nondimensional *Deborah number*

$$De = \frac{\dot{\gamma}_0}{6D_r} \tag{2.4}$$

as the ratio of the shear rate to the rate of rotational diffusion so that the small amplitude limit is $De << 1$. The system (2.2) reduces to

$$\dot{s} = -U(s) - \frac{2Ns\beta}{3}(1 - s + \beta) + \frac{a}{3}De \cos \omega t(1 + 2s - \beta + 3s\beta - 3s^2)\sin 2\psi, \tag{2.5}$$

$$\dot{\beta} = -U(\beta) - \frac{2Ns\beta}{3}(1 - \beta + s) - \frac{a}{3}De \cos \omega t(1 + 2\beta - s + 3s\beta - 3\beta^2)\sin 2\psi, \tag{2.6}$$

$$\dot{\psi} = -\frac{1}{2}De \cos \omega t \left(1 - \frac{a}{3}\frac{s+\beta+2}{s-\beta}\cos 2\psi\right). \tag{2.7}$$

## 2.2   Degenerate quiescent equilibrium

The system (2.5)-(2.7) possesses very special equilibrium solutions when there is no flow, that is, when $De = 0$. In this case we find that (2.5)-(2.7) reduces to

$$\dot{s} = -U(s) - \frac{2Ns\beta}{3}(1 - s + \beta) \tag{2.8}$$

$$\dot{\beta} = -U(\beta) - \frac{2Ns\beta}{3}(1 - \beta + s) \tag{2.9}$$

$$\dot{\psi} = 0, \tag{2.10}$$

or in its equivalent tensor form

$$\dot{\mathbf{Q}} = \mathbf{Q} - N(\mathbf{M} \cdot \mathbf{M} - \mathbf{M} : \mathbf{MM}). \tag{2.11}$$

From (1.39), $U(s) = s(1 - \frac{N}{3}(1-s)(2s+1))$, and so the only material parameter in this system is the nondimensional concentration parameter $N$.

In general, the equilibrium order parameter system (2.8)-(2.9) has seven steady solutions, but for the purposes of this dissertation, we will ignore the five solutions that are unstable to perturbations in the form of a shear flow for all $N > 0$ (Forest and Wang, 2003)). One of the remaining two solutions is the isotropic solution

$$(s, \beta) = (0, 0), \tag{2.12}$$

which exists for all $N > 0$ but is only stable for $0 < N < 3$. This solution corresponds to the state in which the molecules have no preferred orientation either because the concentration is too low for the molecules to effective communicate with each other or because the temperature is too high.

Additionally, if the concentration is sufficiently high, $N > \frac{8}{3}$, then there is also the uniaxial nematic equilibrium solution

$$(s, \beta) = (s_{eq}, 0) \tag{2.13}$$

for

$$s_{eq} = \frac{1}{4}\left(1 + 3\sqrt{1 - \frac{8}{3N}}\right). \tag{2.14}$$

This solution is stable if it is defined. Thus, in the region $\frac{8}{3} < N < 3$, the isotropic and nematic solutions are bistable, but when $N > 3$, $(s_{eq}, 0)$ is the only solution stable to shear perturbations. For the remainder of this dissertation, we will assume that $N$ is well into the nematic range, using $N = 6$ so that $s_{eq} = 0.809$.

While the concentration selects the degree to which the molecules are ordered, in the absence

of flow, the preferred direction of this ordering is not selected. Indeed, from (2.10), any constant value

$$\psi \equiv \Psi_0 \tag{2.15}$$

is a solution. (We choose $-\frac{\pi}{2} < \Psi_0 \leq \frac{\pi}{2}$.) Several authors (cf. (Forest *et al.*, 2003; Hess and Kröger, 2004; Lee *et al.*, 2006; Marrucci and Greco, 1993; Rienäcker and Hess, 1999; Rienäcker *et al.*, 2002a,b)) have explored the role of this orientational degeneracy in steady shear.

In the following, we will use this orientationally degenerate equilibrium solution as our initial conditions for (2.5)-(2.7):

$$s(t=0) = s_{eq}, \quad \beta(t=0) = 0, \quad \psi(t=0) = \Psi_0. \tag{2.16}$$

We shall see that some phenomena are sensitive to the initial value of the director angle.

## 2.3 Weak steady shear flow

Before we examine weak oscillatory shear, we will first look at weak steady shear, or $De << 1$ with $\omega = 0$ in (2.5)-(2.7).[1] We will employ "two-timing" asymptotic analysis similar to that used in (Vicente Alonso *et al.*, 2003) for a Landau-de Gennes model. The utility of this asymptotic analysis is that one can effectively diagonalize the fast and slow response of the director and order parameters, and thereby solve the system (2.5)-(2.7) in a hierarchy of simpler, lower dimensional equations. The molecular relaxation timescale

$$T_0 = t \tag{2.17}$$

dominates the order parameter equations (2.5)-(2.6) while the director angle equation (2.7) is on the slower shear flow timescale

$$T_1 = De\ t. \tag{2.18}$$

---

[1]As defined by (2.4), when $\omega = 0$, then $De = 0$, and indeed, $v_x$ in (2.1) is 0. Therefore in steady shear, we will define the Deborah number as $De = \frac{\dot{\gamma}_0}{D_r}$ where $\dot{\gamma}_0$ is the imposed shear rate and use $v_x = De\ y$.

We treat the initial slow time as zero, but we allow for the initial value of the fast time $T_{00} = t_0$ to be a free parameter, the role of which will be discussed below. We will use the expansions

$$s = s_{eq} + De\, s_1^{ss}(T_0, T_1) + O(De^2), \tag{2.19}$$

$$\beta = 0 + De\, \beta_1^{ss}(T_0, T_1) + O(De^2), \tag{2.20}$$

$$\psi = \psi_0^{ss}(T_0, T_1) + De\, \psi_1^{ss}(T_0, T_1) + O(De^2), \tag{2.21}$$

where the superscript $ss$ denotes steady shear. Alternatively, the orientation tensor can be expanded as

$$\begin{aligned}
\mathbf{Q} = \;& s_{eq}\left(\mathbf{n}_{1,0}^{ss}\mathbf{n}_{1,0}^{ss} - \tfrac{\mathbf{I}}{3}\right) \\
& +De\left[s_1^{ss}\left(\mathbf{n}_{1,0}^{ss}\mathbf{n}_{1,0}^{ss} - \tfrac{\mathbf{I}}{3}\right) + \beta_1^{ss}\left(\mathbf{n}_{2,0}^{ss}\mathbf{n}_{2,0}^{ss} - \tfrac{\mathbf{I}}{3}\right) + s_{eq}\psi_1^{ss}\left(\mathbf{n}_{1,0}^{ss}\mathbf{n}_{2,0}^{ss} + \mathbf{n}_{2,0}^{ss}\mathbf{n}_{1,0}^{ss}\right)\right] \\
& +O(De^2),
\end{aligned} \tag{2.22}$$

where $\mathbf{n}_{1,0}^{ss} = (\cos\psi_0^{ss}, \sin\psi_0^{ss}, 0)$ and $\mathbf{n}_{2,0}^{ss} = (-\sin\psi_0^{ss}, \cos\psi_0^{ss}, 0)$.

At zeroth order in $De$, we quickly see that $\frac{\partial \psi_0^{ss}}{\partial T_0} = 0$, and so at first order (2.7) yields

$$\frac{\partial \psi_1^{ss}}{\partial T_0} = -\frac{d\psi_0^{ss}}{dT_1} - \tfrac{1}{2}\left(1 - \lambda_0 \cos 2\psi_0^{ss}(T_1)\right), \tag{2.23}$$

where we have define the Leslie tumbling parameter $\lambda_0 = \lambda(s_{eq}, 0)$ with

$$\lambda(s, \beta) = \frac{a}{3}\frac{2 + s + \beta}{s - \beta}. \tag{2.24}$$

Integrating (2.23) with respect to $T_0$, we see that

$$\psi_1^{ss}(T_0, T_1) = -T_0\left(\frac{d\psi_0^{ss}}{dT_1} + \tfrac{1}{2}\left(1 - \lambda_0 \cos 2\psi_0^{ss}(T_1)\right)\right) + \bar{\psi}_1^{ss}(T_1), \tag{2.25}$$

The solvability condition that $\psi_1^{ss}$ remains bounded as a function of $T_0$ yields

$$\frac{d\psi_0^{ss}}{dT_1} = -\tfrac{1}{2}\left(1 - \lambda_0 \cos 2\psi_0^{ss}\right). \tag{2.26}$$

Thus one recovers the well-known director angle equation from Leslie-Ericksen theory, which

comes from (1.4) in the in-plane monodomain limit. It is separable and can be integrated in closed form, which we represent by $\psi_0^{ss}(T_1) = \Psi(T_1 + \phi_0)$, where

$$
\Psi(x) = \begin{cases}
\tan^{-1}\left( \frac{\sqrt{1-\lambda_0^2}}{1+\lambda_0} \tan\left( -\frac{\sqrt{1-\lambda_0^2}}{2} x \right) \right), & \text{if } |\lambda_0| < 1, \\
\tan^{-1}\left( \tan\psi_L \tanh\left( \frac{\sqrt{\lambda_0^2-1}}{2} x \right) \right), & \text{if } |\lambda_0| > 1 \text{ and } |\Psi_0| < |\psi_L|, \\
\tan^{-1}\left( \tan\psi_L \coth\left( \frac{\sqrt{\lambda_0^2-1}}{2} x \right) \right), & \text{if } |\lambda_0| > 1 \text{ and } |\psi_L| < |\Psi_0| < \frac{\pi}{2},
\end{cases}
\tag{2.27}
$$

where

$$
\psi_L = \tan^{-1}\left( \frac{\sqrt{\lambda_0^2 - 1}}{\lambda_0 + 1} \right)
\tag{2.28}
$$

is the classical Leslie angle, and

$$
\phi_0 = \begin{cases}
-\frac{2}{\sqrt{1-\lambda_0^2}} \tan^{-1}\left( \frac{1+\lambda_0}{\sqrt{1-\lambda_0^2}} \tan\Psi_0 \right), & \text{if } |\lambda_0| < 1, \\
\frac{2}{\sqrt{\lambda_0^2-1}} \tanh^{-1}\left( \frac{\tan\Psi_0}{\tan\psi_L} \right), & \text{if } |\lambda_0| > 1 \text{ and } |\Psi_0| < |\psi_L|, \\
\frac{2}{\sqrt{\lambda_0^2-1}} \coth^{-1}\left( \frac{\tan\Psi_0}{\tan\psi_L} \right), & \text{if } |\lambda_0| > 1 \text{ and } |\psi_L| < |\Psi_0| < \frac{\pi}{2}.
\end{cases}
\tag{2.29}
$$

Thus if $|\lambda_0| < 1$, then $\psi_0^{ss}(De\,t)$ is periodic with period $T^{ss} = \frac{2\pi}{De\sqrt{1-\lambda_0^2}}$, meaning that the director tumbles. However, if $|\lambda_0| > 1$, then the director aligns relative to the flow with $\psi_0^{ss}(De\,t)$ decaying to the Leslie alignment angle $\psi_L$. These two different behaviors are depicted for rods in Figure 2.1 and for disks in Figure 2.2.

To our knowledge the exact role of the initial director angle $\Psi_0$ has not been previously amplified. It is often hidden in a generic constant of integration and sometimes taken to be zero. This is understandable since the qualitative effect of $\Psi_0$ on $\psi_0^{ss}$ is not significant, introducing only a phase shift in the tumbling regime, and in the flow-aligning case only affecting the direction from which the director approaches the Leslie angle ($\psi_0^{ss}$ will not pass through $-\psi_L$ on its way to $\psi_L$), as illustrated in Figure 2.1. We shall show below, however, that the effect of $\Psi_0$ is qualitatively significant for oscillatory shear.
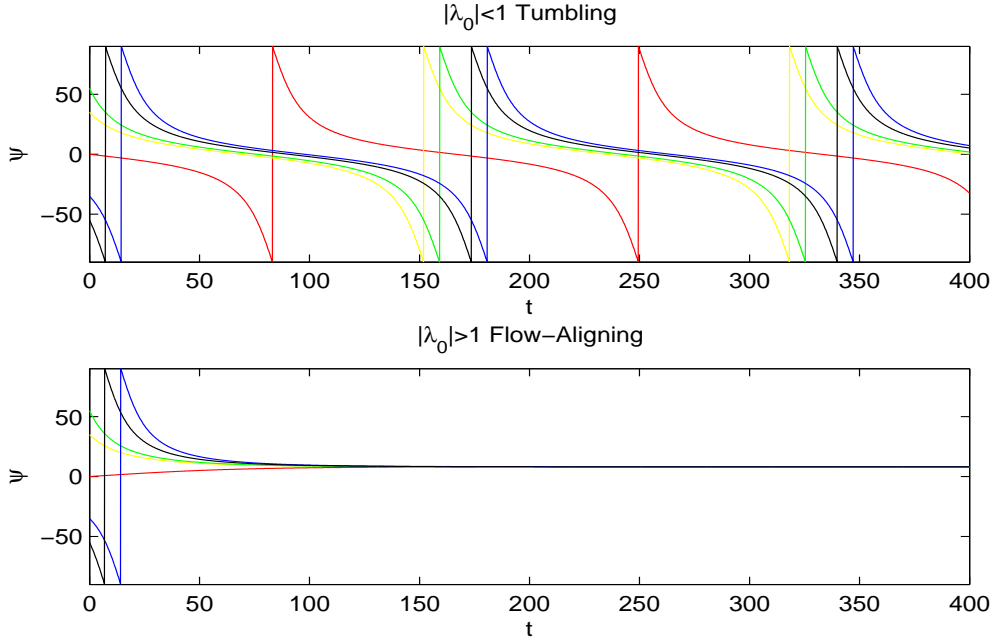
Figure 2.1: The two different responses, tumbling and flow-aligning, to steady shear for rods with $a = 0.8$ ($\lambda_0 = 0.926$) and $0.9$ ($\lambda_0 = 1.042$) for $\Psi_0 = -55°, -35°, 0°, 35°$, and $55°$. For $a = 0.9$, $\psi_L = 8.128°$. [$N = 6$, $De = 0.1$.]
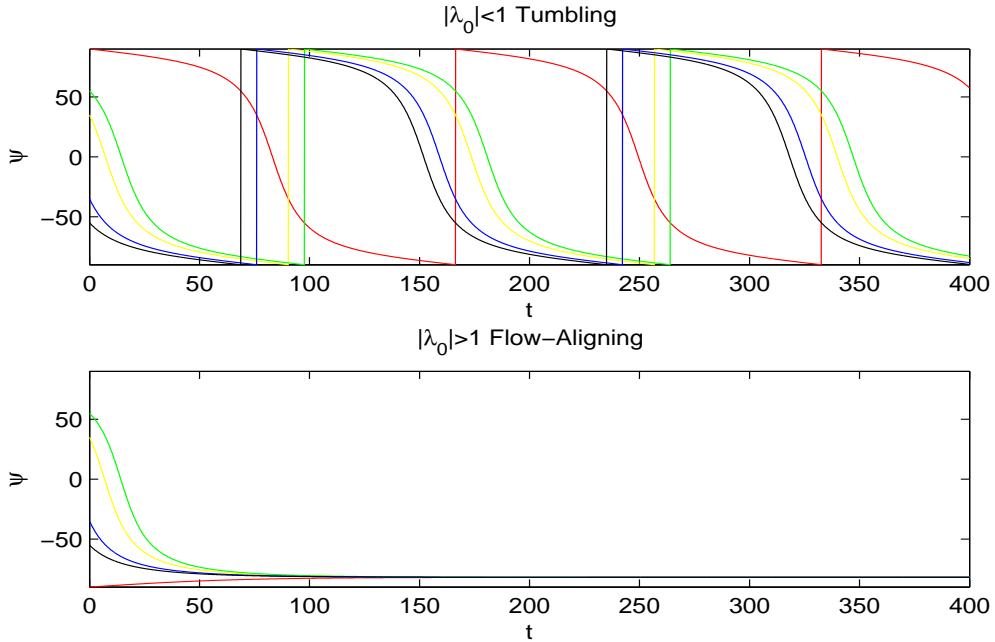


Figure 2.2: The two steady shear responses for disks with $a = -0.8$ ($\lambda_0 = -0.926$) and $-0.9$ ($\lambda_0 = -1.042$) for $\Psi_0 = -55°, -35°, 35°, 55°$, and $\pm 90°$. For $a = -0.9$, $\psi_L = -81.87°$. [$N = 6$, $De = 0.1$.]

Using $\psi_0^{ss}(T_1)$, the $O(De)$ order parameter equations are triangular system

$$\begin{aligned}
\frac{\partial \beta_1^{ss}}{\partial T_0} &= -a_1 \beta_1^{ss} + a a_4 \sin 2\psi_0^{ss}(T_1), \\
\frac{\partial s_1^{ss}}{\partial T_0} &= -a_2 s_1^{ss} + a_3 \beta_1^{ss} + a a_5 \sin 2\psi_0^{ss}(T_1),
\end{aligned} \tag{2.30}$$

where

$$\begin{aligned}
a_1 &= \frac{N}{3}\left(2s_{eq}^2 + 2s_{eq} - 1 + \frac{3}{N}\right) = N s_{eq} \\
a_2 &= \frac{N}{3}\left(6s_{eq}^2 - 2s_{eq} - 1 + \frac{3}{N}\right) = \frac{N}{3}\left(s_{eq} + 2 - \frac{6}{N}\right), \\
a_3 &= \frac{2N}{3}\left(s_{eq}^2 - s_{eq}\right) = \frac{1}{2}(a_2 - a_1), \\
a_4 &= \frac{1}{3}(s_{eq} - 1), \\
a_5 &= \frac{1}{3}\left(1 + 2s_{eq} - 3s_{eq}^2\right) = \frac{1}{6}(s_{eq} - 1 + \frac{9}{N}).
\end{aligned} \tag{2.31}$$

This can be solved exactly by quadrature:

$$\begin{aligned}
\beta_1^{ss}(T_0, T_1) &= a \sin 2\psi_0^{ss}(T_1)\frac{a_4}{a_1}\left(1 - e^{a_1(T_{00} - T_0)}\right), \\
s_1^{ss}(T_0, T_1) &= a \sin 2\psi_0^{ss}(T_1)\left(\frac{a_3 a_4 + a_5 a_1}{a_1 a_2} - \frac{a_4}{2a_1}e^{a_1(T_{00} - T_0)} + \frac{a_4 - 2a_5}{2a_2}e^{a_2(T_{00} - T_0)}\right),
\end{aligned} \tag{2.32}$$

The two order parameter relaxation rates $a_1$ and $a_2$ are the same rates identified in (Larson and Mead, 1989a). In the nematic region $N > 3$, $a_1 > a_2 > \frac{1}{2}$. However, in the bistable region $\frac{8}{3} < N < 3$, $a_2 \to 0$ as $N \to \frac{8}{3}$.

Thus for steady shear, at leading order the tensor model predicts the same director behavior as Leslie-Ericksen theory coupled with order parameters that decay exponentially to the quiescent uniaxial values modified by $O(De)$ corrections that are proportional to $\sin 2\psi_0^{ss}$. The main parameter in determining qualitative behavior is the Leslie "material parameter" $\lambda_0$ which is identified for nematic polymers as dependent on aspect ratio through $a$ and concentration through $s_{eq}$ (Forest and Wang, 2003).

Using (2.32), the analysis can be continued to get $\bar{\psi}_1^{ss}$. At $O(De^2)$, (2.7) is

$$\begin{aligned}
\frac{\partial \psi_2^{ss}}{\partial T_0} &= -\frac{d\bar{\psi}_1^{ss}}{dT_1} - \frac{a^2}{3s_{eq}^2}\Big((s_{eq}(s_{eq} + 2)\bar{\psi}_1^{ss}\sin 2\psi_0^{ss} + \\
&\quad \frac{a}{2}\sin 4\psi_0^{ss}\left(\frac{a_3 a_4 + a_1 a_5 - a_2 a_4(1 + s_{eq})}{a_1 a_2} + \frac{a_4(2s_{eq} - 1)}{2a_1}e^{a_1(T_{00} - T_0)} + \frac{a_4 - 2a_5}{2a_2}e^{a_2(T_{00} - T_0)}\right)\Big).
\end{aligned} \tag{2.33}$$

We observe that for $\psi_2^{ss}$ to be bounded as a function of $T_0$, we must require that $\frac{d\bar{\psi}_1^{ss}}{dT_1} = 0$. In

24

the flow-aligning regime, it is easy to solve (2.33) for this constant $\bar{\psi}_1^{ss}$ in the limit $T_0 \to \infty$. This can improve the approximation to the flow-alignment angle to

$$\psi_L + De\frac{3((s_{eq} + 1)a_4a_2 - a_3a_4 - a_1a_5)}{a_1a_2(s_{eq} + 2)^2}. \tag{2.34}$$

Also, the first order asymptotic expressions for the order parameters are

$$
\begin{aligned}
s &= s_{eq} + De\frac{a(a_3a_4 + a_5a_1)}{a_1a_2}\sin 2\psi_L, \\
\beta &= De\frac{aa_4}{a_1}\sin 2\psi_L.
\end{aligned} \tag{2.35}
$$

## 2.4 Weak Oscillatory Shear Flow

### 2.4.1 Leslie-Ericksen for weak oscillatory shear flow

Anticipating a similar relationship between the tensor and Leslie-Ericksen models for the more complicated dynamics of oscillatory shear, we begin our investigation of oscillatory shear with the non-autonomous generalization of the LE director angle equation,

$$\frac{d\psi_{LE}}{dt} = -\frac{1}{2}De\cos\omega t\left(1 - \lambda_0\cos 2\psi_{LE}\right). \tag{2.36}$$

This equation can also be solved exactly:

$$\psi_{LE}(t) = \Psi\left(De\frac{\sin\omega t - \sin\omega t_0}{\omega} + \phi_0\right), \tag{2.37}$$

where the function $\Psi$ is defined by (2.27). This solution predicts an oscillatory response for both "tumbling" and "flow-aligning" nematic liquids as classified based on their steady shear response. This oscillatory behavior is a consequence of the "internal clock," $\frac{De}{\omega}\sin\omega t$, which oscillates between $\pm\frac{De}{\omega}$, on which the with function $\Psi$ is evaluated. Thus the director angle oscillates about the initial angle $\Psi_0$.

Figure 2.3 compares $\psi_{LE}$ to a numerical solution of the tensor model (2.5)-(2.7) where $\psi$, $s$, and $\beta$ are coupled. We observe: $\psi_{LE}$ accurately captures the oscillatory nature of the director angle *for small times*, a few dozen periods of the plates. However, for larger times, a slow drift of the mean director angle of the tensor model emerges, and furthermore the drift dynamics

25
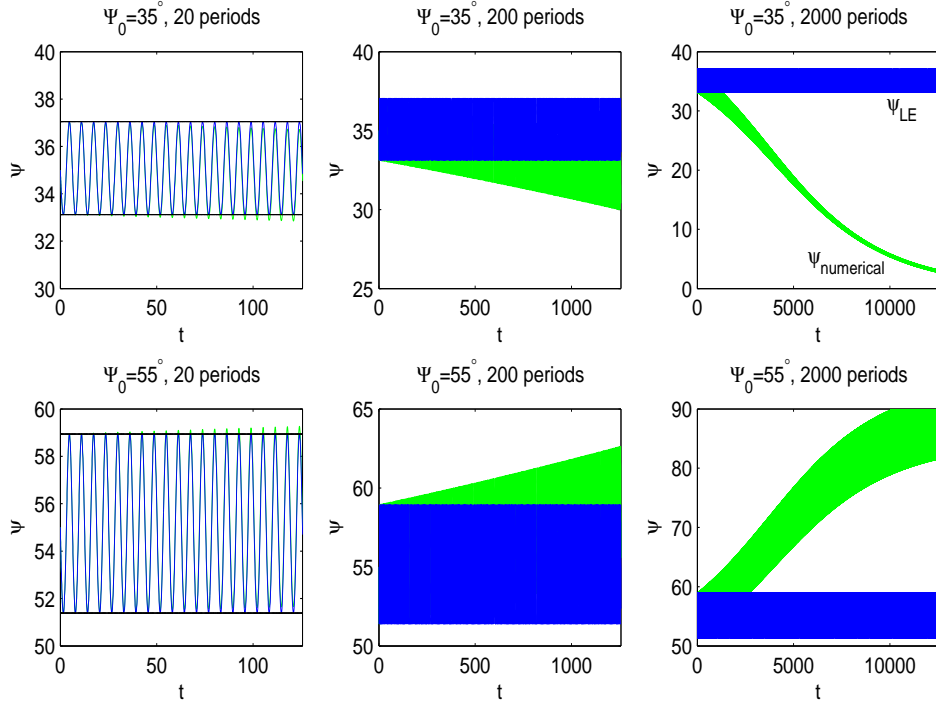
Figure 2.3: The Leslie-Ericksen theory prediction (dark band) of oscillation around the initial value $\Psi_0$ coincides with the numerical solution (light band) for the first few plate oscillations, but the mean of the numerical solution slowly drifts toward either $0°$ (if $|\Psi_0| < 45°$) or $\pm 90°$ (if $45° < |\Psi_0| < 90°$). $[N = 6, a = 0.8 \, (\lambda_0 = 0.926), De = 0.1$, and $\omega = 1$ for $\Psi_0 = 35°$ and $\Psi_0 = 55°$.]

are sensitive to initial data.

More complete numerical studies show the asymptotic value of the mean angle is parallel to the plates when $|\Psi_0| < \frac{\pi}{4}$ or perpendicular to the plates when $\frac{\pi}{4} < |\Psi_0| < \frac{\pi}{2}$. For the LE model, the asymptotic value of the mean is simply $\Psi_0$, independent of the initial data, *and* independent of the Leslie parameter $\lambda_0$.

### 2.4.2 Failure of the two-timing argument used for steady shear

Before using multiple timescale perturbation analysis in oscillatory shear, we must briefly discuss the additional timescale introduced when $\omega \neq 0$. We limit the present discussion to relatively fast plate oscillation, or $\omega >> De$, and use $\cos \omega t = \cos \omega T_0$ when time appears explicitly in (2.5)-(2.7). Additionally we note that we have used the term "mean" loosely, for indeed $\frac{\omega}{2\pi} \int_{t-\frac{\pi}{\omega}}^{t+\frac{\pi}{\omega}} \psi_{LE}(t') \, dt' \neq \Psi_0$ (unless $\Psi_0 = 0$), but instead $\int_{t-\frac{\pi}{\omega}}^{t+\frac{\pi}{\omega}} sgn(\psi_{LE}(t') - \Psi_0) \, dt' = 0$. For the

remainder of the paper we use "mean" to refer to integrating with respect to $T_0$ only over one period allowing the mean to remain a function of the slow time $T_1$.

If the two-timing argument from Section 2.3 is followed again for oscillatory shear, we still have $\frac{\partial \psi_0}{\partial T_0} = 0$ so that $\psi_0(T_0, T_1) \equiv \tilde{\psi}_0(T_1)$, but (2.25) becomes

$$\frac{\partial \psi_1}{\partial T_0} = -\frac{d\tilde{\psi}_0}{dT_1} - \frac{1}{2} \cos \omega T_0 \left(1 - \lambda_0 \cos 2\tilde{\psi}_0(T_1)\right). \tag{2.38}$$

After integration with respect to $T_0$, one finds that

$$\psi_1(T_0, T_1) \quad = -(T_0 - T_{00})\frac{d\tilde{\psi}_0}{dT_1} - \frac{\sin \omega T_0 - \sin \omega T_{00}}{2\omega} \left(1 - \lambda_0 \cos 2\tilde{\psi}_0\right) + \tilde{\psi}_1(T_1). \tag{2.39}$$

Thus, the solvability condition for $\psi_1$ to remain bounded as a function of $T_0$ is now $\frac{d\tilde{\psi}_0}{dT_1} = 0$, implying that $\psi_0(T_0, T_1) \equiv \Psi_0$, which clearly does *not* capture the long time dynamics of the numerical solutions shown in Figure 2.3. We shall see that in fact this longtime drift of the mean of the oscillation arises from the emergence of higher harmonics in the $O(De^2)$ balance, arising precisely through the small amplitude oscillations of the tumbling parameter $\lambda(s, \beta)$. Thus, LE theory with its constant order parameter cannot yield this effect.

### 2.4.3 A third slower timescale

Since the two times $T_0 = t$ and $T_1 = De\,t$ do not prove to be enough to capture the drift in Figure 2.3, we will introduce a new, slower time $T_2 = De^2 t$. Instead of $\psi_0(T_0, T_1) \equiv \Psi_0$ of the previous section, we now allow $\psi_0(T_0, T_1, T_2) \equiv \bar{\psi}_0(T_2)$, and replace $\tilde{\psi}_1(T_1)$ in (2.39) with $\tilde{\psi}_1(T_1, T_2)$.

Even though $\bar{\psi}_0(T_2)$ is not yet known, it does not prevent us from solving the system for the order parameters at $O(De)$:

$$\begin{aligned}
\frac{\partial \beta_1}{\partial T_0} &= -a_1\beta_1 + aa_4 \cos \omega T_0 \sin 2\bar{\psi}_0(T_2), \\
\frac{\partial s_1}{\partial T_0} &= -a_2 s_1 + a_3\beta_1 + aa_5 \cos \omega T_0 \sin 2\bar{\psi}_0(T_2),
\end{aligned} \tag{2.40}$$

where the $a_i$ are given by (2.31). This system can be solved by quadrature, and we see that the order parameters quickly decay to sinusoidal states with an amplitude that may vary slowly

with time:

$$
\begin{aligned}
\beta_1 &= a\sin 2\bar{\psi}_0(T_2)\left(a_{\beta_1}\cos\omega T_0 + b_{\beta_1}\sin\omega T_0 + c_{\beta_1}e^{a_1(T_{00}-T_0)}\right)\\
s_1 &= a\sin 2\bar{\psi}_0(T_2)\left(a_{s_1}\cos\omega T_0 + b_{s_1}\sin\omega T_0 + \tfrac{c_{\beta_1}}{2}e^{a_1(T_{00}-T_0)} + c_{s_1}e^{a_2(T_{00}-T_0)}\right),
\end{aligned}
\tag{2.41}
$$

where

$$
\begin{aligned}
a_{\beta_1} &= \tfrac{a_1 a_4}{a_1^2+\omega^2}, \quad b_{\beta_1} = \tfrac{\omega a_4}{a_1^2+\omega^2}, \quad c_{\beta_1} = -a_{\beta_1}\cos\omega T_{00} - b_{\beta_1}\sin\omega T_{00},\\
a_{s_1} &= \tfrac{a_3(a_2 a_{\beta_1}-\omega b_{\beta_1})+a_5 a_2}{a_2^2+\omega^2}, \quad b_{s_1} = \tfrac{a_3(\omega a_{\beta_1}+a_2 b_{\beta_1})+a_5\omega}{a_2^2+\omega^2},\\
c_{s_1} &= -a_{s_1}\cos\omega T_{00} - b_{s_1}\sin\omega T_{00} - \tfrac{c_{\beta_1}}{2}.
\end{aligned}
\tag{2.42}
$$

We briefly pause to note that we have the freedom to add functions of $T_1$ and $T_2$ to $c_{\beta_1}$ and $c_{s_1}$, but we will suppress these terms since they would be quickly killed by the exponentially decaying factors. We also observe that judiciously fine tuning $T_{00}$ can make either $c_{\beta_1} = 0$ or $c_{s_1} = 0$, thereby eliminating our choice of terms that decay exponentially with rates $a_1$ or $a_2$, leaving us with only one decay rate in the first order terms.

Now that we have $s_1$ and $\beta_1$ given by (2.41), we can better approximate the tumbling parameter $\lambda(s,\beta)$ with

$$
\lambda(s_{eq}+De s_1, De\beta_1) = \lambda_0 + De\lambda_1 + O(De^2),
\tag{2.43}
$$

where

$$
\begin{aligned}
\lambda_1 &= \tfrac{2a}{3s_{eq}^2}\left((1+s_{eq})\beta_1 - s_1\right)\\
&= \sin 2\bar{\psi}_0(T_2)\left(2B_1\cos\omega T_0 + 2B_2\sin\omega T_0 + B_3 e^{a_1(T_{00}-T_0)} + B_4 e^{a_2(T_{00}-T_0)}\right)
\end{aligned}
\tag{2.44}
$$

where

$$
\begin{aligned}
B_1 &= \tfrac{a^2}{3s_{eq}^2}\left((1+s_{eq})a_{\beta_1} - a_{s_1}\right),\\
B_2 &= \tfrac{a^2}{3s_{eq}^2}\left((1+s_{eq})b_{\beta_1} - b_{s_1}\right),\\
B_3 &= \tfrac{a^2}{3s_{eq}^2}c_{\beta_1}(2s_{eq}+1), \quad B_4 = -\tfrac{2a^2}{3s_{eq}^2}c_{s_1}.
\end{aligned}
\tag{2.45}
$$

Thus, at second order, (2.7) simplifies to

$$
\begin{aligned}
\frac{\partial \psi_2}{\partial T_0} = & \; -\frac{\partial \tilde{\psi}_1}{\partial T_1} - \frac{d\bar{\psi}_0}{dT_2} + \tfrac{1}{2} \cos \omega T_0 \left( -2\lambda_0 \psi_1 \sin 2\bar{\psi}_0 + \lambda_1 \cos 2\bar{\psi}_0 \right) \\
= & \; -\frac{\partial \tilde{\psi}_1}{\partial T_1} - \frac{d\bar{\psi}_0}{dT_2} \\
& -\lambda_0 \cos \omega T_0 \sin 2\bar{\psi}_0 (\tilde{\psi}_1 + \tfrac{1}{2\omega}(1 - \lambda_0 \cos 2\bar{\psi}_0)(\sin \omega T_0 - \sin \omega T_{00})) \\
& +\tfrac{\sin 4\bar{\psi}_0}{4} \left( 2B_1 \cos^2 \omega T_0 + 2B_2 \sin \omega T_0 \cos \omega T_0 \right. \\
& \qquad \left. + \cos \omega T_0 (B_3 e^{a_1(T_{00}-T_0)} + B_4 e^{a_2(T_{00}-T_0)}) \right).
\end{aligned}
\tag{2.46}
$$

Integrating with respect to $T_0$, we find

$$
\begin{aligned}
\psi_2 = & \; (T_0 - T_{00}) \left( -\frac{d\bar{\psi}_0}{dT_2} - \frac{\partial \tilde{\psi}_1}{\partial T_1} + \frac{B_1}{4} \sin 4\bar{\psi}_0 \right) + \frac{B_1}{8\omega} \sin 4\bar{\psi}_0 (\sin 2\omega T_0 - \sin 2\omega T_{00}) \\
& - \left( \frac{B_2}{8\omega} \sin 4\bar{\psi}_0 + \frac{\lambda_0}{8\omega^2} \sin 2\bar{\psi}_0 (1 - \lambda_0 \cos 2\bar{\psi}_0) \right) (\cos 2\omega T_0 - \cos 2\omega T_{00}) \\
& - \lambda_0 \sin 2\bar{\psi}_0 \left( \tilde{\psi}_1 + (1 - \lambda_0 \cos 2\bar{\psi}_0) \frac{\sin \omega T_{00}}{2\omega} \right) \frac{\sin \omega T_0 - \sin \omega T_{00}}{\omega} + \tilde{\psi}_2(T_1, T_2) \\
& - \frac{B_3 \sin 4\bar{\psi}_0}{4(a_1^2+\omega^2)} \left( (a_1 \cos \omega T_0 - \omega \sin \omega T_0) e^{a_1(T_{00}-T_0)} - (a_1 \cos \omega T_{00} - \omega \sin \omega T_{00}) \right) \\
& - \frac{B_4 \sin 4\bar{\psi}_0}{4(a_2^2+\omega^2)} \left( (a_2 \cos \omega T_0 - \omega \sin \omega T_0) e^{a_2(T_{00}-T_0)} - (a_2 \cos \omega T_{00} - \omega \sin \omega T_{00}) \right).
\end{aligned}
\tag{2.47}
$$

In order for $\psi_2$ to be a bounded function of $T_0$, we impose the solvability condition

$$
\frac{d\bar{\psi}_0}{dT_2} + \frac{\partial \tilde{\psi}_1}{\partial T_1} - \frac{B_1}{4} \sin 4\bar{\psi}_0 = 0.
\tag{2.48}
$$

Integrating with respect to $T_1$, we have

$$
\tilde{\psi}_1(T_1, T_2) = -T_1 \left( \frac{d\bar{\psi}_0}{dT_2} - \frac{B_1}{4} \sin 4\bar{\psi}_0 \right) + \bar{\psi}_1(T_2).
\tag{2.49}
$$

In order for $\tilde{\psi}_1$ to be bounded as a function of $T_1$, we impose the solvability condition

$$
\frac{d\bar{\psi}_0}{dT_2} = \frac{B_1}{4} \sin 4\bar{\psi}_0
\tag{2.50}
$$

This equation is separable and can be integrated in closed form to get

$$
\bar{\psi}_0(T_2) = \tfrac{1}{2} \tan^{-1}(e^{B_1 T_2} \tan 2\Psi_0) + \frac{\pi(sgn(\Psi_0) - sgn(\tan 2\Psi_0))}{4},
\tag{2.51}
$$

where the $sgn(\Psi_0) - sgn(\tan 2\Psi_0)$ term is included to allow $\tfrac{1}{2} \tan^{-1}$ to return values onto the

29

intervals $(-\frac{\pi}{2}, -\frac{\pi}{4})$ and $(\frac{\pi}{4}, \frac{\pi}{2})$ when appropriate.

The slow-time effect of $\bar{\psi}_0(T_2)$ is term is the most important term, driving all the slow effects. However, before we analyze those effects in the next section, we first continue the asymptotic analysis, and since $\psi_0(T_0, T_1, T_2) = \bar{\psi}_0(T_2)$, we will drop the bar on $\bar{\psi}_0(T_2)$. Proceeding to the second order balance for the order parameters, we find to be

$$
\begin{aligned}
\frac{\partial \beta_2}{\partial T_0} &= -a_1\beta_2 + 2N(2s_{eq}+1)(\beta_1^2 - 2s_1\beta_1) \\
&\quad + a\cos\omega T_0 \left(2a_4\psi_1\cos 2\psi_0 + \tfrac{1}{3}(s_1 - (2+3s_+)\beta_1)\sin 2\psi_0\right) \\
&= -a_1\beta_2 + a^2 \sin 2\psi_0 \left(f_1\cos^2\omega T_0 + f_2\sin^2\omega T_0 + f_3\sin\omega T_0\cos\omega T_0 \right. \\
&\quad + e^{a_1(T_{00}-T_0)}(f_4\cos\omega T_0 + f_5\sin\omega T_0) + e^{a_2(T_{00}-T_0)}(f_6\cos\omega T_0 + f_7\sin\omega T_0) \\
&\quad \left. + f_8 e^{(a_1+a_2)(T_{00}-T_0)}\right) - \tfrac{aa_4}{\omega}\cos 2\psi_0(1 - \lambda_0\cos 2\psi_0)\cos\omega T_0\sin\omega T_0 \\
&\quad + aa_4\cos 2\psi_0\left((1 - \lambda_0\cos 2\psi_0)\tfrac{\sin\omega T_{00}}{\omega} + 2\bar{\psi}_1\right)\cos\omega T_0,
\end{aligned}
\tag{2.52}
$$

where

$$
\begin{aligned}
f_1 &= \tfrac{N}{3}(2s_{eq}+1)(a_{\beta_1}^2 - 2a_{s_1}a_{\beta_1}) + \tfrac{1}{3}(a_{s_1} - (2+3s_+)a_{\beta_1}), \\
f_2 &= \tfrac{N}{3}(2s_{eq}+1)(b_{\beta_1}^2 - 2b_{s_1}b_{\beta_1}) \\
f_3 &= \tfrac{N}{3}(2s_{eq}+1)(2a_{\beta_1}b_{\beta_1} - (a_{s_1}b_{\beta_1} + a_{\beta_1}b_{s_1})) + \tfrac{1}{3}(b_{s_1} - (2+3s_{eq})b_{\beta_1}), \\
f_4 &= \tfrac{N}{3}(2s_{eq}+1)c_{\beta_1}(a_{\beta_1} - 2a_{s_1}) - \tfrac{c_{\beta_1}}{6}(3 + 6s_{eq}), \\
f_5 &= \tfrac{N}{3}(2s_{eq}+1)c_{\beta_1}(b_{\beta_1} - 2b_{s_1}), \quad f_6 = -\tfrac{2N}{3}(2s_{eq}+1)a_{\beta_1}c_{s_1} - \tfrac{1}{3}c_{s_1}, \\
f_7 &= -\tfrac{2N}{3}(2s_{eq}+1)b_{\beta_1}c_{s_1}, \quad f_8 = -\tfrac{2N}{3}(2s_{eq}+1)c_{\beta_1}c_{s_1}.
\end{aligned}
\tag{2.53}
$$

We can solve (2.52) to get

$$
\begin{aligned}
\beta_2 = \quad & a^2\sin^2 2\psi_0 \left[a_{\beta_2} + b_{\beta_2}\cos 2\omega T_0 + c_{\beta_2}\sin 2\omega T_0 + i_{\beta_2}e^{(a_1+a_2)(T_{00}-T_0)}\right. \\
&\quad + e^{a_1(T_{00}-T0)}(d_{\beta_2} + e_{\beta_2}\cos\omega T_0 + f_{\beta_2}\sin\omega T_0) \\
&\quad \left. + e^{a_2(T_{00}-T0)}(g_{\beta_2}\cos\omega T_0 + h_{\beta_2}\sin\omega T_0)\right] \\
&+ a\cos 2\psi_0(1 - \lambda_0\cos 2\psi_0)\left[(j_{\beta_2}\cos 2\omega T_0 + k_{\beta_2}\sin 2\omega T_0 + l_{\beta_2}\cos\omega T_0\right. \\
&\quad \left. + m_{\beta_2}\sin\omega T_0 + p_{\beta_2}e^{a_1(T_{00}-T_0)}\right] \\
&+ a\bar{\psi}_1\cos 2\psi_0(n_{\beta_2}\cos\omega T_0 + o_{\beta_2}\sin\omega T_0 + q_{\beta_2}e^{a_1(T_{00}-T_0)})
\end{aligned}
\tag{2.54}
$$

where

$$
\begin{aligned}
a_{\beta_2} &= \frac{f_1+f_2}{2a_1}, b_{\beta_2} = \frac{a_1(f_1-f_2)-2\omega f_3}{2(a_1^2+4\omega^2)}, \quad c_{\beta_2} = \frac{2\omega(f_1-f_2)+a_1 f_3}{2(a_1^2+4\omega^2)}, \\
d_{\beta_2} &= -a_{\beta_2} - b_{\beta_2}\cos 2\omega T_{00} - c_{\beta_2}\sin 2\omega T_{00} - (e_{\beta_2}+g_{\beta_2})\cos\omega T_{00} \\
&\quad -(f_{\beta_2}+h_{\beta_2})\sin\omega T_{00} - i_{\beta_2}, \quad e_{\beta_2} = -\frac{f_5}{\omega}, \quad f_{\beta_2} = \frac{f_4}{\omega}, \\
g_{\beta_2} &= \frac{(a_1-a_2)f_6-\omega f_7}{(a_1-a_2)^2+\omega^2}, \qquad h_{\beta_2} = \frac{(a_1-a_2)f_7+\omega f_6}{(a_1-a_2)^2+\omega^2}, \qquad i_{\beta_2} = -\frac{f_8}{a_2}, \\
j_{\beta_2} &= -\frac{a_4}{a_1^2+4\omega^2}, \quad k_{\beta_2} = \frac{a_1 a_4}{2\omega(a_1^2+4\omega^2)}, \quad l_{\beta_2} = -\frac{a_1 a_4}{a_1^2+\omega^2}\frac{\sin\omega T_{00}}{\omega}, \\
m_{\beta_2} &= -\frac{a_4\sin\omega T_{00}}{a_1^2+\omega^2}, \quad n_{\beta_2} = \frac{2a_1 a_4\sin\omega T_{00}}{a_1^2+\omega^2}, \quad o_{\beta_2} = \frac{2a_4\omega\sin\omega T_{00}}{a_1^2+\omega^2}, \\
p_{\beta_2} &= -j_{\beta_2}\cos 2\omega T_{00} - k_{\beta_2}\sin 2\omega T_{00} - l_{\beta_2}\cos\omega T_{00} - m_{\beta_2}\sin\omega T_{00}, \\
q_{\beta_2} &= -n_{\beta_2}\cos\omega T_{00} - o_{\beta_2}\sin\omega T_{00}.
\end{aligned}
\tag{2.55}
$$

Similarly, we see that

$$
\begin{aligned}
\frac{\partial s_2}{\partial T_0} &= -a_2 s_2 + a_3 \beta_2 + \frac{N}{3}\left((1-6s_{eq})s_1^2 + (4s_{eq}-2)s_1\beta_1 - 2s_{eq}\beta_1^2\right) \\
&\quad + a\cos\omega T_0\left(2a_5\psi_1\cos 2\psi_0 + \frac{1-3s_{eq}}{3}(2s_1-\beta_1)\sin 2\psi_0\right) \\
&= -a_2 s_2 + a^2\sin 2\psi_0\left(g_0 + g_1\cos 2\omega T_0 + g_2\sin 2\omega T_0 + g_7 e^{(a_1+a_2)(T_{00}-T_0)} + \right. \\
&\quad\quad e^{a_1(T_{00}-T_0)}g_3(\cos\omega T_0 + g_4\sin\omega T_0) + e^{a_2(T_{00}-T_0)}(g_5\cos\omega T_0 + g_6\sin\omega T_0) \\
&\quad\quad \left. + g_8 e^{2a_1(T_{00}-T_0)} + g_9 e^{2a_2(T_{00}-T_0)} + g_{10}e^{a_1(T_{00}-T_0)}\right) \\
&\quad + a\cos 2\psi_0(1-\lambda_0\cos 2\psi_0)\left(g_{11}\cos 2\omega T_0 + g_{12}\sin 2\omega T_0 + g_{13}\cos\omega T_0 \right.\\
&\quad\quad \left. + g_{14}\sin\omega T_0 + g_{15}e^{a_1(T_{00}-T_0)}\right) \\
&\quad + a\bar\psi_1\cos 2\psi_0\left(g_{16}\cos\omega T_0 + g_{17}\sin\omega T_0 + g_{18}e^{a_1(T_{00}-T_0)}\right),
\end{aligned}
\tag{2.56}
$$

where

$$g_0 = \frac{N}{6}\left((1 - 6s_{eq})(a_{s_1}^2 + b_{s_1}^2) + (4s_{eq} - 2)(a_{s_1}a_{\beta_1} + b_{s_1}b_{\beta_1}) - 2s_{eq}(a_{\beta_1}^2 + b_{\beta_1}^2)\right)$$

$$+ a_3 a_{\beta_2} + \frac{1 - 3s_{eq}}{6}(2(a_{s_1} + b_{s_1}) - a_{\beta_1} - b_{\beta_1}), \quad g_{12} = a_3 k_{\beta_2} - \frac{a_5}{2\omega},$$

$$g_1 = \frac{N}{6}\left((1 - 6s_{eq})(a_{s_1}^2 - b_{s_1}^2) + (4s_{eq} - 2)(a_{s_1}a_{\beta_1} - b_{s_1}b_{\beta_1}) - 2s_+(a_{\beta_1}^2 - b_{\beta_1}^2)\right)$$

$$+ a_3 b_{\beta_2} + \frac{1 - 3s_{eq}}{6}(2(a_{s_1} - b_{s_1}) - a_{\beta_1} + b_{\beta_1}), \quad g_{10} = a_3 d_{\beta_2}, \quad g_{11} = a_3 j_{\beta_2},$$

$$g_2 = a_3 c_{\beta_2} + \frac{N}{3}\left((1 - 6s_{eq})a_{s_1}b_{\beta_1} + (2s_{eq} - 1)(a_{s_1}b_{\beta_1} + a_{\beta_1}b_{s_1}) - 2s_{eq}a_{\beta_1}b_{\beta_1}\right)$$

$$+ \frac{1 - 3s_{eq}}{6}(2b_{s_1} - b_{\beta_1}), \quad g_{13} = a_3 l_{\beta_2} + \frac{a_5 \sin\omega T_{00}}{\omega}, \quad g_{14} = a_3 m_{\beta_2},$$

$$g_3 = a_3 e_{\beta_2} + \frac{N}{3}\left((1 - 6s_{eq})a_{s_1}c_{\beta_1} + (2s_{eq} - 1)(2a_{s_1} + a_{\beta_1})c_{\beta_1} - 4s_{eq}a_{\beta_1}c_{\beta_1}\right),$$

$$g_4 = a_3 f_{\beta_2} + \frac{N}{3}\left((1 - 6s_{eq})b_{s_1}c_{\beta_1} + (2s_{eq} - 1)(2b_{s_1} + b_{\beta_1})c_{\beta_1} - 4s_{eq}b_{\beta_1}c_{\beta_1}\right),$$

$$g_5 = a_3 g_{\beta_2} + \frac{N}{3}\left((2 - 12s_{eq})c_{s_1}a_{\beta_1} + (4s_{eq} - 2)a_{s_1}c_{s_1}\right) + \frac{1 - 3s_{eq}}{3}2c_{s_1}, \qquad (2.57)$$

$$g_6 = a_3 h_{\beta_2} + \frac{N}{3}\left((2 - 12s_{eq})c_{s_1}b_{\beta_1} + (4s_{eq} - 2)b_{s_1}c_{s_1}\right), \quad g_{16} = a_3 n_{\beta_2} + 2a_5,$$

$$g_7 = a_3 i_{\beta_2} - \frac{N}{3}(2s_{eq} + 1)c_{s_1}c_{\beta_1}, \quad g_8 = \frac{N}{12}(2s_{eq} - 7)c_{\beta_1}^2,$$

$$g_9 = \frac{N}{3}(1 - 6s_{eq})c_{s_1}^2, \quad g_{15} = a_3 p_{\beta_2}, \quad g_{17} = a_3 o_{\beta_2}, \quad g_{18} = a_3 q_{\beta_2},$$

As before, we can solve (2.56) to get

$$s_2 = a^2 \sin^2 2\psi_0 \left(a_{s_2} + b_{s_2}\cos 2\omega T_0 + c_{s_2}\sin 2\omega T_0\right.$$

$$+ e^{a_1(T_{00} - T0)}(d_{s_2} + e_{s_2}\cos\omega T_0 + f_{s_2}\sin\omega T_0) + i_{s_2}e^{(a_1 + a_2)(T_{00} - T_0)}$$

$$+ e^{a_2(T_{00} - T0)}(s_{s_2} + g_{s_2}\cos\omega T_0 + h_{s_2}\sin\omega T_0) + r_{s_2}e^{2a_2(T_{00} - T_0)})$$

$$+ a\cos 2\psi_0(1 - \lambda_0\cos 2\psi_0)\left(j_{s_2}\cos 2\omega T_0 + k_{s_2}\sin 2\omega T_0 + l_{s_2}\cos\omega T_0\right. \qquad (2.58)$$

$$+ m_{s_2}\sin\omega T_0 + p_{s_2}e^{a_1(T_{00} - T_0)} + t_{s_2}e^{a_2(T_{00} - T_0)})$$

$$+ a\bar{\psi}_1\cos 2\psi_0(n_{\beta_2}\cos\omega T_0 + o_{\beta_2}\sin\omega T_0 + q_{\beta_2}e^{a_1(T_{00} - T_0)} + u_{s_2}e^{a_2(T_{00} - T_0)})$$

32

where

$$
\begin{aligned}
a_{s2} &= \tfrac{g_0}{a_2}, \quad b_{s2} = \tfrac{a_2 g_1 - 2\omega g_2}{a_2^2 + 4\omega^2}, \quad c_{s2} = \tfrac{2\omega g_1 + a_2 f_2}{a_1^2 + 4\omega^2}, \quad d_{s2} = -\tfrac{g_{10}}{a_1 - a_2} \\
e_{s2} &= -\tfrac{(a_1 - a_2) g_3 + \omega g_4}{(a_1 - a_2)^2 + \omega^2}, \quad f_{s2} = -\tfrac{(a_1 - a_2) g_4 - \omega g_3}{(a_1 - a_2)^2 + \omega^2}, \quad g_{s2} = -\tfrac{g_6}{\omega}, \quad h_{s2} = \tfrac{g_5}{\omega}, \\
i_{s2} &= -\tfrac{g_7}{a_1}, \quad j_{s2} = \tfrac{a_2 g_{11} - 2 g_{12}\omega}{a_2^2 + 4\omega^2}, \quad k_{s2} = \tfrac{a_2 g_{12} + 2 g_{12}\omega}{a_2^2 + 4\omega^2}, \quad l_{s2} = \tfrac{a_2 g_{13} - g_{14}\omega}{a_2^2 + \omega^2}, \\
m_{s2} &= \tfrac{a_2 g_{14} + g_{13}\omega}{a_2^2 + \omega^2}, \quad n_{s2} = \tfrac{a_2 g_{16} - g_{17}\omega}{a_2^2 + \omega^2}, \quad o_{s2} = \tfrac{a_2 g_{17} + g_{16}\omega}{a_2^2 + \omega^2}, \quad p_{s2} = -\tfrac{g_{15}}{a_1 - a_2}, \\
s_{s2} &= -a_{s2} - b_{s2} \cos 2\omega T_{00} - c_{s2} \sin 2\omega T_{00} - d_{s2} - e_{s2} \cos \omega T_{00} - f_{s2} \sin \omega T_{00} \\
&\quad -g_{s2} \cos \omega T_{00} - h_{s2} \sin \omega T_{00} - i_{s2} - r_{s2}, \quad q_{s2} = -\tfrac{g_{18}}{a_1 - a_2}, \quad r_{s2} = -\tfrac{g_8 + g_9}{a_2}, \\
t_{s2} &= -j_{s2} \cos 2\omega T_{00} - k_{s2} \sin 2\omega T_{00} - l_{s2} \cos \omega T_{00} - m_{s2} \sin \omega T_{00} - p_{s2}, \\
u_{s2} &= -n_{s2} \cos \omega T_{00} - o_{s2} \sin \omega T_{00} - q_{s2}.
\end{aligned}
\tag{2.59}
$$

The second order term in the expansion of the tumbling parameter $\lambda$ is

$$
\lambda_2 = \tfrac{2a}{3 s_{eq}^3} \left( s_{eq}(1 + s_{eq})\beta_2 - s_{eq} s_2 + s_1^2 - (2 + s_{eq}) s_1 \beta_1 + (1 + s_{eq})\beta_1^2 \right).
\tag{2.60}
$$

In order to find $\bar{\psi}_1(T_2)$, the still unknown portion of $\psi_1$, we now examine the third order balance of the angle equation

$$
\tfrac{\partial \psi_1}{\partial T_2} + \tfrac{\partial \psi_2}{\partial T_1} + \tfrac{\partial \psi_3}{\partial T_0} = \cos \omega T_0 \left( (2\lambda_0 \psi_1^2 - \lambda_2) \cos 2\psi_0 + 2(\lambda_1 \psi_1 + \lambda_0 \psi_2) \sin 2\psi_0 \right),
\tag{2.61}
$$

or

$$
\begin{aligned}
\tfrac{\partial \psi_3}{\partial T_0} = &-\tfrac{d\bar{\psi}_1}{dT_2} - \tfrac{B_1 \lambda_0}{2} \sin 2\psi_0 \sin 4\psi_0 \tfrac{\sin \omega T_0 - \sin \omega T_{00}}{\omega} - \tfrac{\partial \tilde{\psi}_2}{\partial T_1} \\
&+ \cos \omega T_0 \Big( H_1 + H_2 \cos 2\omega T_0 + H_3 \sin 2\omega T_0 + H_{13} e^{2a_1(T_{00} - T_0)} \\
&\quad + (H_4 + H_6 \bar{\psi}_1) \cos \omega T_0 + (H_5 + H_7 \bar{\psi}_1) \sin \omega T_0 + H_{14} e^{2a_2(T_{00} - T_0)} \\
&\quad + e^{a_1(T_{00} - T_0)}(H_8 \cos \omega T_0 + H_9 \sin \omega T_0 + H_{15} + H_{17}\bar{\psi}_1) \\
&\quad + e^{a_2(T_{00} - T_0)}(H_{10} \cos \omega T_0 + H_{11} \sin \omega T_0 + H_{16} + H_{17}\bar{\psi}_1) \\
&\quad + H_{12} e^{(a_1 + a_2)(T_{00} - T_0)} + H_{18} \bar{\psi}_0 e^{a_2(T_{00} - T_0)} + H_{19}\bar{\psi}_1^2 + H_{20}\bar{\psi}_1 + H_{21}\tilde{\psi}_2 \Big),
\end{aligned}
\tag{2.62}
$$

where the $H_i$ are known functions of $T_2$ through $\psi_0(T_2)$:

$$
\begin{aligned}
H_1 &= \lambda_0 \sin 2\psi_0 \left( (1 - \lambda_0 \cos 2\psi_0) \left( \frac{\lambda_0 \cos 2\omega T_{00} - 4B_2\omega}{4\omega^2} \sin 2\psi_0 + \frac{\lambda_0 \sin^2 2\omega T_{00}}{\omega} \right) \right. \\
&\quad + \frac{\sin 4\psi_0}{2} \left( \frac{B_3(a_1 \cos \omega T_{00} - \omega \sin \omega T_{00})}{a_1^2 + \omega^2} + \frac{B_4(a_2 \cos \omega T_{00} - \omega \sin \omega T_{00})}{a_2^2 + \omega^2} \right. \\
&\quad \left. \left. + \frac{B_2 \cos 2\omega T_{00} - B_1 \sin 2\omega T_{00}}{2\omega} \right) \right) + \cos 2\psi_0 \left( \frac{\lambda_0(1 + 2\sin^2 \omega T_{00})}{4\omega^2} (1 - \lambda_0 \cos 2\psi_0)^2 - h_1 \right), \\
H_2 &= \sin^2 2\psi_0 \left( \frac{2B_2}{\omega} \cos 2\psi_0 (1 - \lambda_0 \cos 2\psi_0) - \right. \\
&\qquad\qquad \left. \lambda_0 \left( \frac{B_2}{2\omega} \cos 2\psi_0 + \frac{\lambda_0}{4\omega^2} (1 - \lambda_0 \cos 2\psi_0) \right) \right) \\
&\quad + \cos 2\psi_0 \left( \frac{\lambda_0(1 + 2\sin^2 \omega T_{00})}{4\omega^2} (1 - \lambda_0 \cos 2\psi_0)^2 - h_1 \right), \\
H_3 &= \frac{B_1}{2\omega} \sin^2 2\psi_0 \left( \frac{\lambda_0}{4} - 1 + \lambda_0 \cos 2\psi_0 \right) - h_3 \cos 2\psi_0, \\
H_4 &= \frac{2B_1 \sin \omega T_{00}}{\omega} \sin^2 2\psi_0 (1 - \lambda_0 \cos 2\psi_0) - h_4 \cos 2\psi_0, \\
H_5 &= \frac{2B_2\omega - \lambda_0^2 \sin 2\omega T_{00}}{\omega^2} \sin^2 2\psi_0 (1 - \lambda \cos 2\psi_0) \\
&\quad - \cos 2\psi_0 \left( \frac{\sin \omega T_{00}}{2\omega^2} (1 - \lambda_0 \cos 2\psi_0)^2 + h_5 \right), \\
H_6 &= 4B_1 \sin^2 2\psi_0 - h_6 \cos 2\psi_0, \\
H_7 &= \frac{4B_2\omega - 2\lambda_0^2}{\omega} \sin^2 2\psi_0 - \left( \frac{\lambda_0}{\omega} (1 - \lambda_0 \cos 2\psi_0) + h_7 \right) \cos 2\psi_0, \\
H_8 &= -\cos 2\psi_0 \left( h_8 + \frac{B_3\lambda_0 a_1}{a_1^2 + \omega^2} \sin^2 2\psi_0 \right), \quad H_{10} = -\cos 2\psi_0 \left( h_{10} + \frac{B_4\lambda_0 a_2}{a_2^2 + \omega^2} \sin^2 2\psi_0 \right), \\
H_9 &= \frac{B_3 \sin^2 2\psi_0}{\omega} \left( 1 + \frac{\lambda_0(1 - \omega^2)}{a_1^2 + \omega^2} \cos 2\psi_0 \right) - h_9 \cos 2\psi_0, \\
H_{11} &= -h_{11} \cos 2\psi_0 - \frac{B_4 \sin^2 2\psi_0}{\omega} \left( 1 + \frac{\lambda_0(1 + \omega^2)}{a_2^2 + \omega^2} \cos 2\psi_0 \right) \\
H_{12} &= -h_{12} \cos 2\psi_0, \quad H_{15} = \frac{B_3\lambda_0 \sin 2\omega T_{00}}{\omega} (1 - \lambda_0 \cos 2\psi_0) \sin^2 2\psi_0 - h_{15} \cos 2\psi_0, \\
H_{13} &= -h_{13} \cos 2\psi_0, \\
H_{14} &= -h_{14} \cos 2\psi_0, \\
H_{16} &= -h_{16} \cos 2\psi_0 + \frac{B_4\lambda_0 \sin 2\omega T_{00}}{\omega} (1 - \lambda_0 \cos 2\psi_0) \sin^2 2\psi_0, \quad H_{21} = 2\lambda_0 \sin 2\psi_0 \\
H_{17} &= \frac{B_3\lambda_0}{\omega} \sin^2 2\psi_0 - h_{17} \cos 2\psi_0, \\
H_{18} &= \frac{B_4\lambda_0}{\omega} \sin^2 2\psi_0 - h_{18} \cos 2\psi_0, \\
H_{19} &= 2\lambda_0 \cos 2\psi_0, \quad H_{20} = \frac{2\lambda_0 \sin \omega T_{00}}{\omega} (1 - \lambda_0 \cos 2\psi_0) \cos 2\psi_0 + \frac{2\lambda_0^2 \sin \omega T_{00}}{\omega} \sin^2 \psi_0,
\end{aligned}
$$

$$(2.63)$$

where the $h_i$ are the appropriate coefficients from $\lambda_2$. We can integrate with respect to $T_0$ to

34

get

$$
\begin{aligned}
\psi_3 = \;& (T_0 - T_{00}) \left( -\frac{d\bar{\psi}_1}{dT_2} + \frac{B_1\lambda_0}{2\omega} \sin \omega T_{00} \sin 2\psi_0 \sin 4\psi_0 - \frac{\partial \tilde{\psi}_2}{\partial T_1} + \frac{H_4 + H_6\bar{\psi}_1}{2} \right) \\
&+ \left( \frac{B_1\lambda_0}{2\omega} \sin 2\psi_0 \sin 4\psi_0 - \frac{H_3}{2} \right) \frac{\cos \omega T_0 - \cos \omega T_{00}}{\omega} \\
&+ \frac{H_2}{6} \frac{\sin 3\omega T_0 - \sin 3\omega T_{00}}{\omega} - \frac{H_3}{6} \frac{\cos 3\omega T_0 - \cos 3\omega T_{00}}{\omega} + \frac{H_4 + H_6\bar{\psi}_1}{4} \frac{\sin 2\omega T_0 - \sin 2\omega T_{00}}{\omega} \\
&+ \left( H_1 + H_{19}\bar{\psi}_1^2 + H_{20}\bar{\psi}_1 + H_{21}\tilde{\psi}_2 + \frac{H_2}{2} \right) \frac{\sin \omega T_0 - \sin \omega T_{00}}{\omega} \\
&- \frac{H_5 + H_7\bar{\psi}_1}{4} \frac{\cos 2\omega T_0 - \cos 2\omega T_{00}}{\omega} \\
&- e^{a_1(T_{00} - T_0)} \left( \frac{H_8}{2a_1} + \frac{a_1 H_8 + 2\omega H_9}{2(a_1^2 + 4\omega^2)} \cos 2\omega T_0 + \frac{a_1 H_9 - \omega H_8}{2(a_1^2 + \omega^2)} \sin 2\omega T_0 \right) + \frac{H_8}{2a_1} \\
&- e^{a_2(T_{00} - T_0)} \left( \frac{H_{10}}{2a_2} + \frac{a_2 H_{10} + 2\omega H_{11}}{2(a_2^2 + 4\omega^2)} \cos 2\omega T_0 + \frac{a_2 H_{11} - \omega H_{10}}{2(a_2^2 + 4\omega^2)} \sin 2\omega T_0 \right) + \frac{H_{10}}{2a_2} \\
&+ \left( \frac{a_1 H_8 + 2\omega H_9}{2(a_1^2 + 4\omega^2)} + \frac{a_2 H_{10} + 2\omega H_{11}}{2(a_2^2 + 4\omega^2)} \right) \cos 2\omega T_{00} \\
&+ \left( \frac{a_1 H_9 - \omega H_8}{2(a_1^2 + 4\omega^2)} + \frac{a_2 H_{11} - \omega H_{10}}{2(a_2^2 + 4\omega^2)} \right) \sin 2\omega T_{00} \\
&- H_{12} \left( e^{(a_1 + a_2)(T_{00} - T_0)} \frac{(a_1 + a_2) \cos \omega T_0 - \omega \sin \omega T_{00}}{(a_1 + a_2)^2 + \omega^2} - \frac{(a_1 + a_2) \cos \omega T_{00} - \omega \sin \omega T_0}{(a_1 + a_2)^2 + \omega^2} \right) \\
&- H_{13} \left( e^{2a_1(T_{00} - T_0)} \frac{2a_1 \cos \omega T_0 - \omega \sin \omega T_{00}}{4a_1^2 + \omega^2} - \frac{2a_1 \cos \omega T_{00} - \omega \sin \omega T_0}{4a_1^2 + \omega^2} \right) \\
&- H_{14} \left( e^{2a_2(T_{00} - T_0)} \frac{2a_2 \cos \omega T_0 - \omega \sin \omega T_{00}}{4a_2^2 + \omega^2} - \frac{2a_2 \cos \omega T_{00} - \omega \sin \omega T_0}{4a_2^2 + \omega^2} \right) \\
&- (H_{15} + H_{17}\bar{\psi}_1) \left( e^{a_1(T_{00} - T_0)} \frac{a_1 \cos \omega T_0 - \omega \sin \omega T_{00}}{a_1^2 + \omega^2} - \frac{a_1 \cos \omega T_{00} - \omega \sin \omega T_0}{a_1^2 + \omega^2} \right) \\
&- (H_{16} + H_{18}\bar{\psi}_1) \left( e^{a_2(T_{00} - T_0)} \frac{a_2 \cos \omega T_0 - \omega \sin \omega T_{00}}{a_2^2 + \omega^2} - \frac{a_2 \cos \omega T_{00} - \omega \sin \omega T_0}{a_2^2 + \omega^2} \right).
\end{aligned}
\tag{2.64}
$$

In order for $\psi_3$ to be bounded as a function of $T_0$, we require as a solvability condition

$$
\frac{\partial \tilde{\psi}_2}{\partial T_1} = -\frac{d\bar{\psi}_1}{dT_2} + \frac{B_1\lambda_0 \sin \omega T_{00}}{2\omega} \sin 2\psi_0 \sin 4\psi_0 + \frac{H_4 + H_6\bar{\psi}_1}{2}
\tag{2.65}
$$

so that

$$
\tilde{\psi}_2 = T_1 \left( -\frac{d\bar{\psi}_1}{dT_2} + \frac{B_1\lambda_0 \sin \omega T_{00}}{2\omega} \sin 2\psi_0 \sin 4\psi_0 + \frac{H_4 + H_6\bar{\psi}_1}{2} \right) + \bar{\psi}_2(T_2).
\tag{2.66}
$$

Thus, in order for $\psi_1$ to remain bounded as a function of $T_1$, we impose the solvability condition

$$
\frac{d\bar{\psi}_1}{dT_2} = \frac{B_1\lambda_0 \sin \omega T_{00}}{2\omega} \sin 2\psi_0 \sin 4\psi_0 + \frac{H_4 + H_6\bar{\psi}_1}{2}
\tag{2.67}
$$

This can be expressed as

$$
\begin{aligned}
\frac{d\bar{\psi}_1}{dT_2} = \quad & \bar{\psi}_1 \left( 2B_1 \sin^2 2\psi_0(T_2) + \frac{2a^2}{3s_{eq}^2} \cos^2 2\psi_0(T_2)((1 + s_{eq})n_{\beta_2} - n_{s_2}) \right) \\
& + \sin \omega T_{00} \left[ \left( \frac{B_1}{\omega} \sin^2 2\psi_0(T_2) \right. \right. \\
& \quad + \frac{2a^2}{3s_{eq}^2} \cos^2 2\psi_0(T_2)(1 - \lambda_0 \cos 2\psi_0(T_2)) \times \\
& \quad \left. \left. \left( \frac{a_1 a_4 (1 + s_{eq})}{\omega(a_1^2 + \omega^2)} + \frac{1}{a_2^2 + \omega^2} \left( \frac{a_3 a_4 (\omega - a_2 a_3)}{a_1^2 + \omega^2} + \frac{a_2 a_3 a_5}{\omega} \right) \right) \right) \right].
\end{aligned}
\tag{2.68}
$$

The solution for $\bar{\psi}_1(T_2)$ can be expressed using hypergeometric functions; however, the important thing to notice from this equation is that $\bar{\psi}_1$ is proportional to $\sin \omega T_{00}$. Therefore, if we choose to start the clock at $T_{00} = 0$, then $\bar{\psi}_1 \equiv 0$. We will choose to do so for the remainder of this dissertation.

### 2.4.4 Summary

We now summarize the results of our multiple timescale perturbation analysis taking into account the choice of using $T_{00} = 0$ before comparing the asymptotics to a numerical solution in the next section. First for the director angle, at zeroth order, we see exponential decay – exponential, but driven by the slow time $T_2$ – of the tangent of twice the director angle:

$$
\psi_0(T_2) = \frac{1}{2} \tan^{-1}(e^{B_1 T_2} \tan 2\Psi_0) + \frac{\pi(sgn(\Psi_0) - sgn(\tan 2\Psi_0))}{4},
\tag{2.69}
$$

for $B_1 = \frac{a^2}{3s_{eq}^2}((1 + s_{eq})a_{\beta_1} - a_{s_1})$. Using the two order parameter decay rates,

$$
a_1 = N s_{eq}, \quad a_2 = \frac{N}{3}\left(s_{eq} + 2 - \frac{6}{N}\right),
\tag{2.70}
$$

which are both positive, is it easy to see that $B_1$ is negative by expressing it in the form

$$
B_1 = -\frac{a^2(a_1 a_2(3a_1 + a_2) + (a_1 + 3a_2)\omega^2)}{2N s_{eq}^2(a_1^2 + \omega^2)(a_2^2 + \omega^2)}.
\tag{2.71}
$$

From (2.69), we observe that

$$\sin 2\psi_0 = \begin{cases} -\dfrac{e^{B_1 T_2}\tan 2\Psi_0}{\sqrt{1+e^{2B_1 T_2}\tan^2 2\Psi_0}}, & \text{if } \frac{\pi}{4} < |\Psi_0| < \frac{\pi}{2}, \\[4mm] \dfrac{e^{B_1 T_2}\tan 2\Psi_0}{\sqrt{1+e^{2B_1 T_2}\tan^2 2\Psi_0}}, & \text{if } |\Psi_0| < \frac{\pi}{4}, \end{cases} \tag{2.72}$$

$$\cos 2\psi_0 = \begin{cases} -\dfrac{1}{\sqrt{1+e^{2B_1 T_2}\tan^2 2\Psi_0}}, & \text{if } \frac{\pi}{4} < |\Psi_0| < \frac{\pi}{2}, \\[4mm] \dfrac{1}{\sqrt{1+e^{2B_1 T_2}\tan^2 2\Psi_0}}, & \text{if } |\Psi_0| < \frac{\pi}{4}, \end{cases} \tag{2.73}$$

From this, we note that $\sin^2 2\psi_0(T_2)$ exhibits logistic decay with $T_2$.

The first order term is rapid oscillation with a small and slowly varying amplitude

$$\psi_1(T_0, T_2) = -\frac{1}{2\omega}\sin\omega T_0\left(1 - \lambda_0\cos 2\psi_0(T_2)\right). \tag{2.74}$$

Thus, to first order, we can write the angle as

$$\psi(T_0, T_2) = \begin{cases} -\frac{\pi}{2} + \frac{1}{2}\tan^{-1}(e^{B_1 T_2}\tan 2\Psi_0) \\ \quad -De\left(1 + \dfrac{\lambda_0}{\sqrt{1+e^{2B_1 T_2}\tan^2 2\Psi_0}}\right)\dfrac{\sin\omega T_0}{2\omega}, & \text{if } -\frac{\pi}{2} < \Psi_0 < -\frac{\pi}{4}, \\[6mm] \frac{1}{2}\tan^{-1}(e^{B_1 T_2}\tan 2\Psi_0) \\ \quad -De\left(1 - \dfrac{\lambda_0}{\sqrt{1+e^{2B_1 T_2}\tan^2 2\Psi_0}}\right)\dfrac{\sin\omega T_0}{2\omega}, & \text{if } -\frac{\pi}{4} < \Psi_0 < \frac{\pi}{4}, \\[6mm] \frac{\pi}{2} + \frac{1}{2}\tan^{-1}(e^{B_1 T_2}\tan 2\Psi_0) \\ \quad -De\left(1 + \dfrac{\lambda_0}{\sqrt{1+e^{2B_1 T_2}\tan^2 2\Psi_0}}\right)\dfrac{\sin\omega T_0}{2\omega}, & \text{if } \frac{\pi}{4} < \Psi_0 < \frac{\pi}{2}. \end{cases} \tag{2.75}$$

For the order parameters, we find that to first order, they are

$$\begin{aligned} \beta_1(T_0, T_2) &= a\sin 2\psi_0(T_2)\left(a_{\beta_1}\cos\omega T_0 + b_{\beta_1}\sin\omega T_0 - a_{\beta_1}e^{-a_1 T_0}\right) \\ s_1(T_0, T_2) &= a\sin 2\psi_0(T_2)\left(a_{s_1}\cos\omega T_0 + b_{s_1}\sin\omega T_0 - \frac{a_{\beta_1}}{2}e^{-a_1 T_0} + c_{s_1}e^{-a_2 T_0}\right), \end{aligned} \tag{2.76}$$

where

$$\begin{aligned} a_{\beta_1} &= \frac{a_1 a_4}{a_1^2+\omega^2}, \quad b_{\beta_1} = \frac{\omega a_4}{a_1^2+\omega^2}, \\ a_{s_1} &= \frac{a_3(a_2 a_{\beta_1} - \omega b_{\beta_1}) + a_5 a_2}{a_2^2+\omega^2}, \quad b_{s_1} = \frac{a_3(\omega a_{\beta_1} + a_2 b_{\beta_1}) + a_5\omega}{a_2^2+\omega^2}, \quad c_{s_1} = -a_{s_1} + \frac{a_{\beta_1}}{2}. \end{aligned} \tag{2.77}$$

The second order terms are

$$
\begin{aligned}
\beta_2 \;=\;& a^2 \sin^2 2\psi_0 \Big[ a_{\beta_2} + b_{\beta_2} \cos 2\omega T_0 + c_{\beta_2} \sin 2\omega T_0 \\
&+ e^{-a_1 T_0}(d_{\beta_2} + e_{\beta_2} \cos \omega T_0 + f_{\beta_2} \sin \omega T_0) \\
&+ e^{-a_2 T_0}(g_{\beta_2} \cos \omega T_0 + h_{\beta_2} \sin \omega T_0) + i_{\beta_2} e^{-(a_1+a_2)T_0} \Big] \\
&+ a \cos 2\psi_0 (1 - \lambda_0 \cos 2\psi_0) \left( j_{\beta_2} \cos 2\omega T_0 + k_{\beta_2} \sin 2\omega T_0 - j_{\beta_2} e^{-a_1 T_0} \right) \\
s_2 \;=\;& a^2 \sin^2 2\psi_0 \Big[ a_{s_2} + b_{s_2} \cos 2\omega T_0 + c_{s_2} \sin 2\omega T_0 \\
&+ e^{-a_1 T_0}(d_{s_2} + e_{s_2} \cos \omega T_0 + f_{s_2} \sin \omega T_0) \\
&+ e^{-a_2 T_0}(s_{s_2} + g_{s_2} \cos \omega T_0 + h_{s_2} \sin \omega T_0) + i_{s_2} e^{-(a_1+a_2)T_0} + r_{s_2} e^{-2a_2 T_0} \Big] \\
&+ a \cos 2\psi_0 (1 - \lambda_0 \cos 2\psi_0) \left( j_{s_2} \cos 2\omega T_0 + k_{s_2} \sin 2\omega T_0 + p_{s_2} e^{-a_1 T_0} + t_{s_2} e^{-a_2 T_0} \right)
\end{aligned}
\tag{2.78}
$$

where

$$
\begin{aligned}
a_{\beta_2} =\;& \tfrac{f_1+f_2}{2a_1}, \; b_{\beta_2} = \tfrac{a_1(f_1-f_2)-2\omega f_3}{2(a_1^2+4\omega^2)}, \quad c_{\beta_2} = \tfrac{2\omega(f_1-f_2)+a_1 f_3}{2(a_1^2+4\omega^2)}, \quad e_{\beta_2} = -\tfrac{f_5}{\omega}, \\
d_{\beta_2} =\;& -a_{\beta_2} - b_{\beta_2} - e_{\beta_2} - g_{\beta_2} - i_{\beta_2}, \quad f_{\beta_2} = \tfrac{f_4}{\omega}, \quad g_{\beta_2} = \tfrac{(a_1-a_2)f_6-\omega f_7}{(a_1-a_2)^2+\omega^2}, \\
h_{\beta_2} =\;& \tfrac{(a_1-a_2)f_7+\omega f_6}{(a_1-a_2)^2+\omega^2}, \quad i_{\beta_2} = -\tfrac{f_8}{a_2}, \quad j_{\beta_2} = -\tfrac{a_4}{a_1^2+4\omega^2}, \quad k_{\beta_2} = \tfrac{a_1 a_4}{2\omega(a_1^2+4\omega^2)} \\
a_{s_2} =\;& \tfrac{g_0}{a_2}, \quad b_{s_2} = \tfrac{a_2 g_1 - 2\omega g_2}{a_2^2+4\omega^2}, \quad c_{s_2} = \tfrac{2\omega g_1 + a_2 f_2}{a_1^2+4\omega^2}, \quad d_{s_2} = -\tfrac{g_{10}}{a_1-a_2} \\
e_{s_2} =\;& -\tfrac{(a_1-a_2)g_3+\omega g_4}{(a_1-a_2)^2+\omega^2}, \quad f_{s_2} = -\tfrac{(a_1-a_2)g_4-\omega g_3}{(a_1-a_2)^2+\omega^2}, \quad g_{s_2} = -\tfrac{g_6}{\omega}, \quad h_{s_2} = \tfrac{g_5}{\omega}, \\
i_{s_2} =\;& -\tfrac{g_7}{a_1}, \quad j_{s_2} = \tfrac{a_2 g_{11} - 2g_{12}\omega}{a_2^2+4\omega^2}, \quad k_{s_2} = \tfrac{a_2 g_{12} + 2g_{12}\omega}{a_2^2+4\omega^2}, \quad p_{s_2} = -\tfrac{g_{15}}{a_1-a_2}, \\
r_{s_2} =\;& -\tfrac{g_8+g_9}{a_2}, \quad s_{s_2} = -a_{s_2} - b_{s_2} - d_{s_2} - e_{s_2} - g_{s_2} - i_{s_2} - r_{s_2}, \\
t_{s_2} =\;& -j_{s_2} - p_{s_2}.
\end{aligned}
\tag{2.79}
$$

where the $f_i$ and the $g_i$ are given by (2.53) and (2.57), respectively.

Also, we can fully describe the orientation tensor to first order as

$$
\mathbf{Q} = \mathbf{Q}_0(T_2) + De\mathbf{Q}_1(T_0, T_2) + O(De^2),
\tag{2.80}
$$

which we can write as a linear combination of these three matrices

$$\mathbf{A}_0 \;=\; \frac{1}{6}\begin{bmatrix} 1 & 0 & 0 \\ 0 & 1 & 0 \\ 0 & 0 & -2 \end{bmatrix}, \tag{2.81}$$

$$\mathbf{A}_1(T_2) \;=\; \frac{1}{2\sqrt{1+e^{2B_1 T_2}\tan^2 2\Psi_0}}\begin{bmatrix} 1 & e^{B_1 T_2}\tan^2 \Psi_0 & 0 \\ e^{B_1 T_2}\tan^2 2\Psi_0 & -1 & 0 \\ 0 & 0 & 0 \end{bmatrix}, \tag{2.82}$$

$$\mathbf{A}_2(T_2) \;=\; \frac{1}{2\sqrt{1+e^{2B_1 T_2}\tan^2 2\Psi_0}}\begin{bmatrix} -e^{B_1 T_2}\tan^2 \Psi_0 & 1 & 0 \\ 1 & e^{B_1 T_2}\tan^2 2\Psi_0 & 0 \\ 0 & 0 & 0 \end{bmatrix}. \tag{2.83}$$

In terms of this basis,

$$\mathbf{Q}_0(T_2) = \begin{cases} s_{eq}(\mathbf{A}_0 - \mathbf{A}_1(T_2)), & \text{if } \frac{\pi}{4} < |\Psi_0| < \frac{\pi}{2}, \\ s_{eq}(\mathbf{A}_0 + \mathbf{A}_1(T_2)), & \text{if } |\Psi_0| < \frac{\pi}{4}, \end{cases} \tag{2.84}$$

and

$$\mathbf{Q}_1(T_0,T_2) = \begin{cases} s_1(T_0,T_2)(\mathbf{A}_0 - \mathbf{A}_1(T_2)) + \beta_1(T_0,T_2)(\mathbf{A}_0 + \mathbf{A}_1(T_2)) \\ \quad + s_{eq}\psi_1(T_0,T_2)\mathbf{A}_2(T_2), & \text{if } \frac{\pi}{4} < |\Psi_0| < \frac{\pi}{2}, \\ s_1(T_0,T_2)(\mathbf{A}_0 + \mathbf{A}_1(T_2)) + \beta_1(T_0,T_2)(\mathbf{A}_0 - \mathbf{A}_1(T_2)) \\ \quad - s_{eq}\psi_1(T_0,T_2)\mathbf{A}_2(T_2), & \text{if } |\Psi_0| < \frac{\pi}{4}, \end{cases} \tag{2.85}$$

## 2.5 Analysis and comparison to numerical solution

### 2.5.1 Slow drift of the director angle

Our asymptotic model for the director angle (2.75) predicts rapid oscillation around a slowly varying mean. This mean is simply $\psi_0(T_2)$, and its drift towards either $0$ or $\pm\frac{\pi}{2}$ drives the phenomena that we detail in the following sections.

The amplitude of the oscillation about $\psi_0$ is small, and its envelope is also a function of $T_2$.

We can characterize the amplitude by defining the envelop of the oscillation with

$$\psi_\pm(T_2) = \psi\left(\pm\frac{\pi}{2\omega}, T_2\right). \tag{2.86}$$

We note that $\psi_+$ is often the bottom edge of the envelope. The asymptotic values of $\psi_\pm$ are

$$\psi_\pm^\infty = \begin{cases} -\frac{\pi}{4} \mp \frac{De}{2\omega}(1 + \lambda_0) & \text{if } -\frac{\pi}{2} < \Psi_0 < -\frac{\pi}{4}, \\ \mp\frac{De}{2\omega}(1 - \lambda_0) & \text{if } |\Psi_0| < \frac{\pi}{4}, \\ \frac{\pi}{4} \mp \frac{De}{2\omega}(1 + \lambda_0) & \text{if } \frac{\pi}{4} < \Psi_0 < \frac{\pi}{2}. \end{cases} \tag{2.87}$$

Figures 2.4 and 2.5 show $\psi_0(T_2)$ and $\psi_\pm(T_2)$ plotted on top numerical solutions for $\psi$ for rod-shaped nematics, and Figures 2.6 and 2.7 show the similar plots for disks. Figures 2.4 and 2.6 depict the response of rods ($a = 0.8$) and disks ($a = -0.8$) that tumble under steady shear ($|\lambda_0| < 1$) while Figures 2.5 and 2.7 show thinner rods ($a = 0.9$) and disks ($a = -0.9$) that tumble under steady shear ($|\lambda_0| < 1$).

It is interesting to compare this to the response to steady shear. In steady shear, the dominant parameter in determining the nature of the response is the tumbling parameter $\lambda_0$, a material parameter that depends on the concentration $N$ and molecular shape parameter $a$. However, in oscillatory shear, the initial value of the director angle $\Psi_0$ determines the longtime asymptotic response. Compare Figures 2.4 and 2.5 with Figure 2.1. For the mean director angle $\psi_0$, there is no difference between rods and the disks with the reciprocal aspect ratio, or in other words, $\psi_0$ depends not on $a$ but on $|a|$. When $|\Psi_0| < \frac{\pi}{4}$, the mean drifts towards zero, but when $\frac{\pi}{4} < |\Psi_0| < \frac{\pi}{2}$, the mean drifts towards $\pm\frac{\pi}{2}$. However, as illustrated in the comparison of Figures 2.4 and 2.5 with Figures 2.6 and 2.7, there is a difference in the amplitude of the oscillations between rods and disks. When $|\Psi_0| < \frac{\pi}{4}$, for rods, the amplitude slowly decreases whereas for disks, the amplitude slowly increases. This behavior is reversed when $\frac{\pi}{4} < |\Psi_0| < \frac{\pi}{2}$. In this case, it is the disks that exhibit the slowly decreasing amplitude while the amplitude slowly increases for rods.

For both rods and disks, there is a qualitative dependence on $\lambda_0$ in oscillatory shear, but it is much subtler than the steady shear. First consider $|\lambda_0| > 1$ so that the steady shear alignment
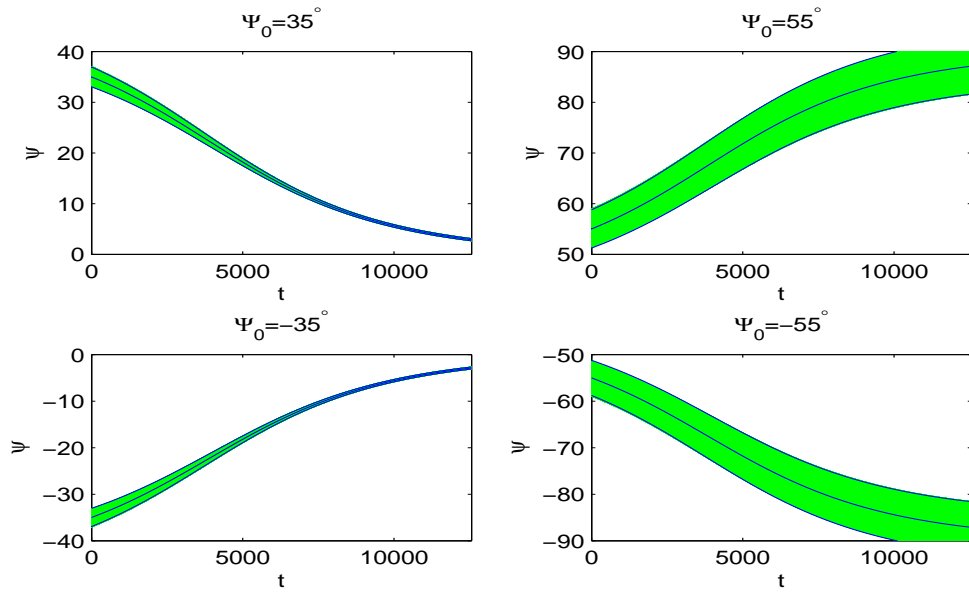
Figure 2.4: For rods, the oscillating numerical solution compared with our predicted predicted mean $\psi_0$ and envelope $\psi_\pm$ for the same parameters as Figure 2.3. These parameter values for steady shear are in the tumbling regime.



Figure 2.5: The oscillating numerical solution compared with our predicted predicted mean $\psi_0$ and envelope $\psi_\pm$ for the same concentration and flow parameters as Figure 2.4, but for thinner rods with $a = 0.9$ (or $\lambda_0 = 1.04$). These parameter values are in the steady shear flow-aligning regime.

Figure 2.6: For disks, the oscillating numerical solution compared with our predicted predicted mean $\psi_0$ and envelope $\psi_\pm$ for $a = -0.8$. These parameter values for steady shear are in the tumbling regime.
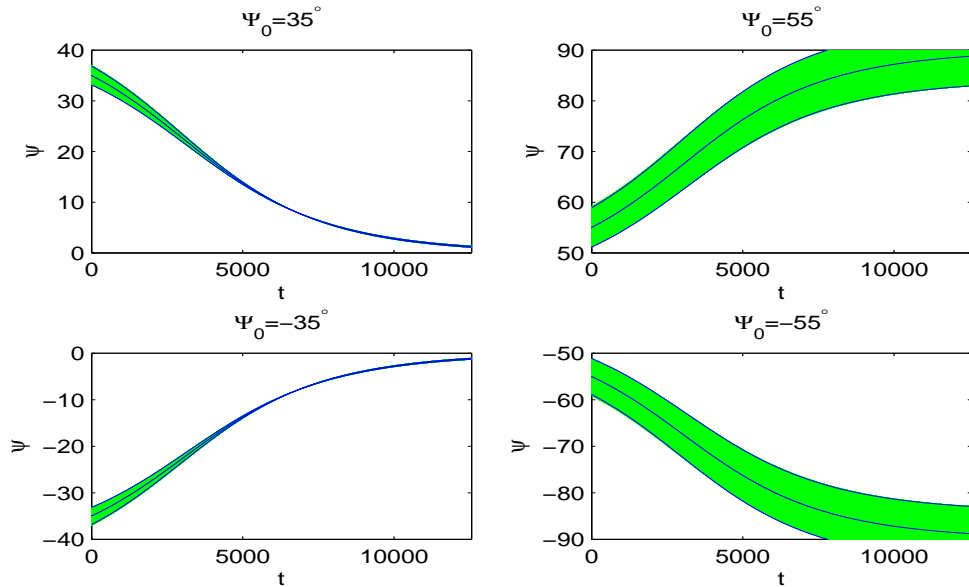


Figure 2.7: The oscillating numerical solution compared with our predicted predicted mean $\psi_0$ and envelope $\psi_\pm$ for the same concentration and flow parameters as Figure 2.6, but for flatter disks with $a = 0.9$ (or $\lambda_0 = 1.04$). These parameter values are in the steady shear flow-aligning regime.
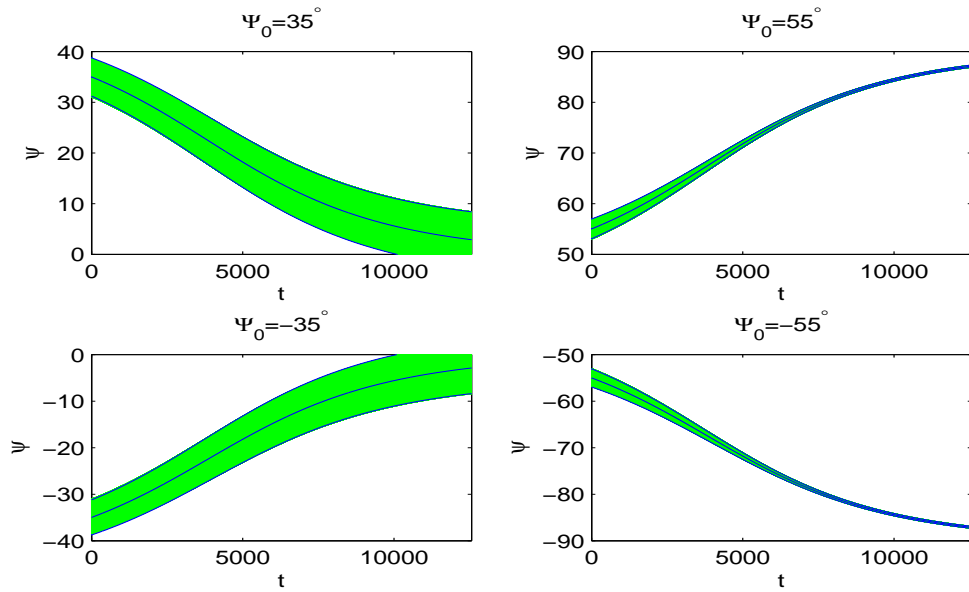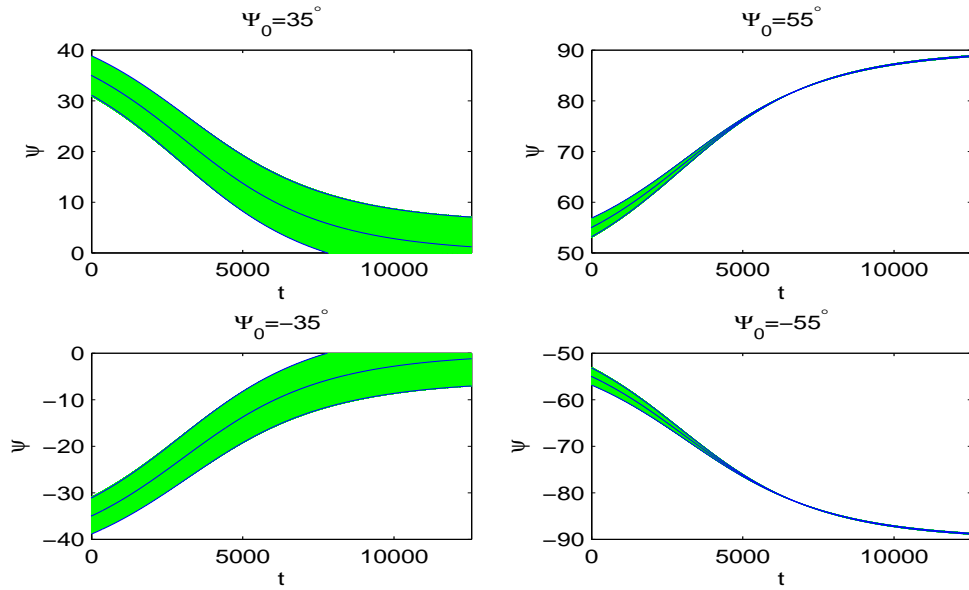
angle $\psi_L$ is defined. For rods, suppose

$$\psi_L < |\Psi_0| < \frac{\pi}{4}, \tag{2.88}$$

(or for disks with $\lambda_0 < -1$, when $\frac{\pi}{4} < |\Psi_0| < -\psi_L$). Thus $\psi_0(T_2)$ starts at $\Psi_0$ and begins to slowly drift towards zero, and therefore, there is a moment when $\psi_0$ passes through $\pm\psi_L$. At this moment, the envelope pinches with $\psi_+ = \psi_- = \pm\psi_L$, as illustrated in Figure 2.8. The close-up shows that our predicted envelope may slightly overestimate the value of the angle, but the amplitude of the numerical solution is at its minimum near $\psi_L$, which is represented by the horizontal dashed line. At this point, given the definition of $\psi_L$, $1 - \lambda_0 \cos 2\psi_L = 0$, and thus for a brief window of time, the first order term $De\,\psi_1$ is actually smaller than the second order term $De^2\psi_2$. If we simplify $\psi_2$ from (2.47) by ignoring the term proportional to $(1 - \lambda_0 \cos 2\psi_L)$, the exponential terms, and unknown term $\bar{\psi}_2$, to

$$\psi_2 = \frac{\sin 4\psi_0}{4} \left( \frac{B_1}{2\omega} \sin 2\omega T_0 - \frac{B_2}{2\omega} \cos 2\omega T_0 - \frac{B_3 a_1}{a_1^2 + \omega^2} - \frac{B_4 a_2}{a_2^2 + \omega^2} \right), \tag{2.89}$$

and so near $\psi_0 = \psi_L$, the first harmonics become suppressed in favor of the second harmonics. The vertical dotted lines in Figure 2.8 have been add at the beginning of each period to highlight this effect. Figure 2.9 shows the result of the addition of the second order term from (2.89) compared to the numerical solution.

Additionally, it is interesting to note that initially, the angle oscillations are $180°$ out of phase with the plates, that is, $\psi$ decreases when the top plate is moving in the forward. However, when the first harmonic terms return to dominance after $\psi$ passes through $\pm\psi_L$, $\psi$ is now in phase with the plates. This brief emergence of the second harmonics and the phase shift do not occur for values of $\Psi_0$ that do not satisfy (2.88) when $|\lambda_0| > 1$, or for any value of $\Psi_0$ when $|\lambda_0| < 1$.
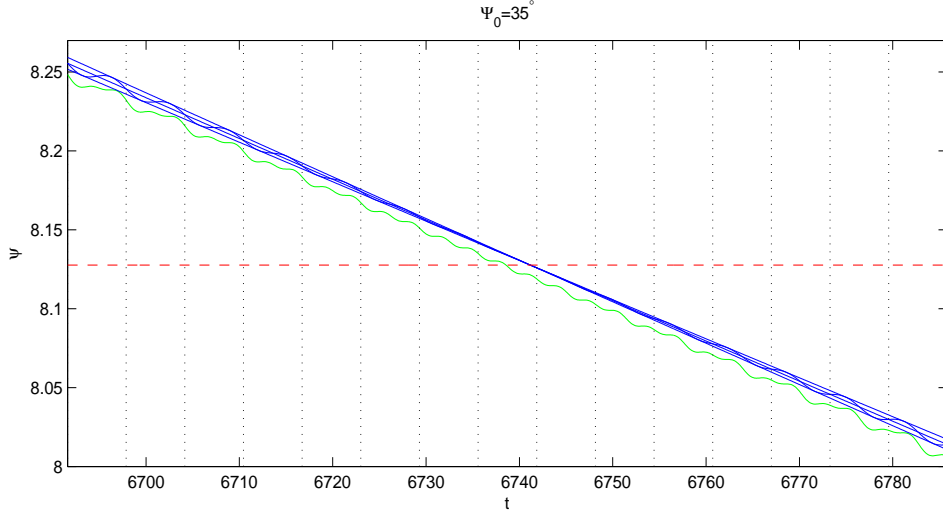
Figure 2.8: When $|\lambda_0| > 1$, the predicted envelope edges cross if $\psi$ passes through $|\psi_L|$. The dashed line is $\psi_L = 8.128°$ for $\lambda_0 = 1.04$. $[N = 6,\ a = 0.9,\ De = 0.1,\ \omega = 1,\ \Psi_0 = 35°.]$
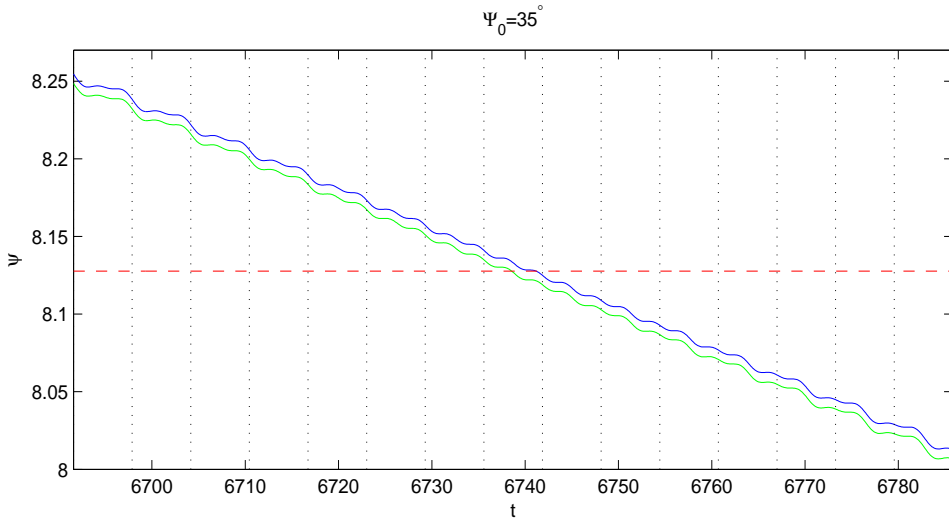


Figure 2.9: The addition of the second order term $\psi_2$ given by (2.89) (the dark line) and the numerical solution (the light line) for $\lambda_0 = 1.04$. $[N = 6,\ a = 0.9,\ De = 0.1,\ \omega = 1,\ \Psi_0 = 35°.]$

### 2.5.2  Frequency dependency of the slow decay rate

Although from (2.69), we see that $\tan 2\psi_0$ decays exponentially with the slow time $T_2$ for all frequencies, we observe that the decay rate

$$B_1 = -\frac{a^2(a_1 a_2(3a_1 + a_2) + (a_1 + 3a_2)\omega^2)}{2N s_{eq}^2(a_1^2 + \omega^2)(a_2^2 + \omega^2)}, \tag{2.90}$$

44

Figure 2.10: The decay rate $B_1$ shows a strong dependence upon the frequency, being $O(\omega^{-2})$ as $\omega \to \infty$.

has a dependence on $\omega$. Figure 2.10 shows a logarithmic plot of $B_1$ as a function of $\omega$. We observe that $B_1 = O(\omega^{-2})$ as $\omega \to \infty$. Thus, for higher frequencies, the slow drift in the director angle is less observable, and so the effects outlined below 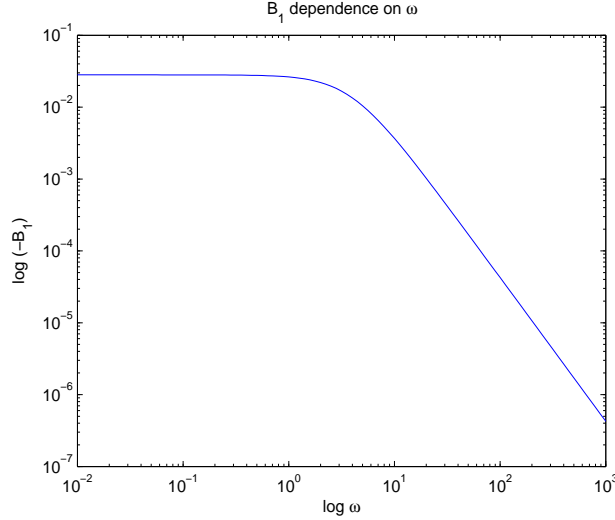are also less observable for higher frequencies. This effect is often compounded by our choice to measure quantities in terms of number of periods of oscillation, which for higher frequencies also gives a shorter time for the director to drift compared to lower frequencies.

In the above analysis, we assumed that $\omega >> De$, but since the middle time $T_1 = De\,t$ did not appear in the analysis and since we see that $B_1$ is relatively constant with respect to small frequencies, we will now ease this restriction to $\omega >> De^2$. Additionally we observe good agreement between our asymptotics and numerical solutions in this regime, and some of the effects below are easier to observe for these smaller frequencies.

### 2.5.3 Order parameters

In general, the order parameters have roughly elliptical orbits in $s$-$\beta$ phase space, but the fluctuations of $\beta$ from zero are very small indicating that the shear-induced biaxiality is a weak effect. Figure 2.11 demonstrates the effect of the initial angle on the order parameters, tracking numerical solutions in $s$-$\beta$ space for twenty plate oscillations. The amplitude of the order parameters starts large for $|\Psi_0|$ near $\frac{\pi}{4}$ and small for $|\Psi_0|$ near 0 or $\pm\frac{\pi}{2}$ and then decays,
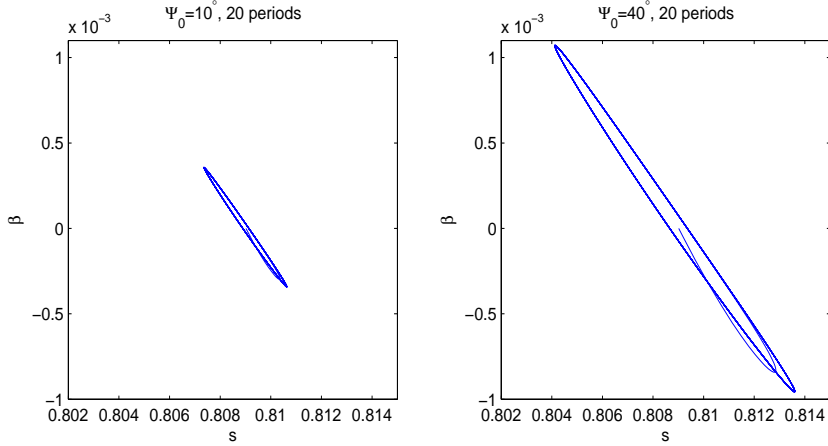
Figure 2.11: The numerical solutions tracked in $s$-$\beta$. Notice that the amplitude is much smaller for $|\Psi_0|$ near 0 than for $|\Psi_0|$ near $\pm\frac{\pi}{4}$. [$N = 6$, $a = 0.8$, $De = 0.1$, $\omega = 1$]
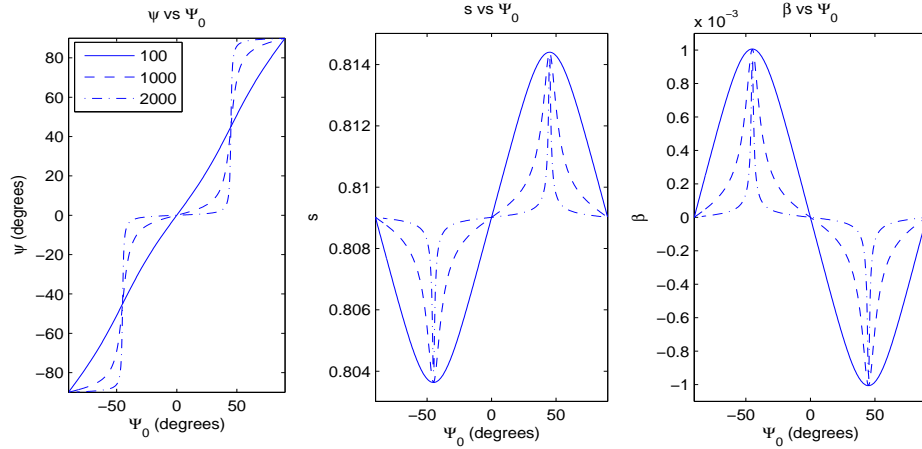


Figure 2.12: The dependence of the director angle and the order parameters on $\Psi_0$. [$N = 6$, $a = 0.8$, $De = 0.1$, $\omega = 1$]

as illustrated in Figure 2.12. Our first order asymptotic predictions of $s$ and $\beta$ from (2.76) match these very well, and given that they are proportional to $\sin 2\psi_0(T_2)$, they predict the dependence on $\Psi_0$ shown in the numerical solutions, and also predict the slow decay in the amplitude with $T_2$, with the square of the amplitude decaying logistically from (2.72). These decay effects are much less dramatic for rapid oscillations due to the effect in Section 2.5.2.

### 2.5.4 Order parameter period halving

We observe an interesting phenomenon that is easier to see when $\omega \approx De$ and $\Psi_0$ is small. Figure 2.13 shows snapshots of the order parameters for two periods of plate oscillation for the first two periods, and periods 101 and 102, 501 and 502, and 1001 and 1002 with $\omega = De = 0.1$ and $\Psi_0 = 5°$. Notice that the order parameter oscillations start out with the same period as the plates and the director angle, but these oscillations are not exactly sinusoidal in nature. However, after a hundred plate oscillations, as the amplitudes of the order parameter decreases, the shape of the waveform changes. Then after five hundred plate oscillations, the decrease in the amplitude of the oscillations stops with the order parameters finally decaying to a constant amplitude oscillation at twice the frequency of the plates and the director angle. Since both the numerical and our asymptotics are plotted in Figure 2.13, we find that this phenomenon can be readily explained from the asymptotic forms.

From (2.76) and (2.78), if the terms that decay exponentially with the fast time $T_0$ are ignored, the order parameters to second order take the forms

$$
\begin{aligned}
s = \ & s_{eq} + De\,a\sin 2\psi_0\,(a_{s_1}\cos\omega T_0 + b_{s_1}\sin\omega T_0) \\
& + De^2 a^2 \sin^2 2\psi_0\Big[a_{s_2} + b_{s_2}\cos 2\omega T_0 + c_{s_2}\sin 2\omega T_0\Big] \\
& + De^2 a\cos 2\psi_0(1 - \lambda_0\cos 2\psi_0)\Big[j_{s_2}\cos 2\omega T_0 + k_{s_2}\sin 2\omega T_0\Big] \\
\beta = \ & De\,a\sin 2\psi_0\Big[a_{\beta_1}\cos\omega T_0 + b_{\beta_1}\sin\omega T_0\Big] \\
& + De^2 a^2 \sin^2 2\psi_0\Big[a_{\beta_2} + b_{\beta_2}\cos 2\omega T_0 + c_{\beta_2}\sin 2\omega T_0\Big] \\
& + De^2 a\cos 2\psi_0(1 - \lambda_0\cos 2\psi_0)\Big[j_{\beta_2}\cos 2\omega T_0 + k_{\beta_2}\sin 2\omega T_0\Big].
\end{aligned}
\tag{2.91}
$$

Since the terms that oscillate at the frequency of the plates are $O(De)$ they are initially the dominant terms, but they are also proportional to $\sin 2\psi_0$, which decays with $T_2$. In this situation, they decay far enough so that the $O(De^2)$ proportional to $\cos 2\psi_0(1 - \lambda_0\cos 2\psi_0)$, which oscillate at twice the plate frequency, become the dominant terms. Thus, in the $T_2 \to \infty$ limit, we have

$$
\begin{aligned}
s^\infty(T_0) = \ & s_{eq} + De^2 a(1 - \lambda_0)\Big[j_{s_2}\cos 2\omega T_0 + k_{s_2}\sin 2\omega T_0\Big] \\
\beta^\infty(T_0) = \ & De^2 a(1 - \lambda_0)\Big[j_{\beta_2}\cos 2\omega T_0 + k_{\beta_2}\sin 2\omega T_0\Big].
\end{aligned}
\tag{2.92}
$$
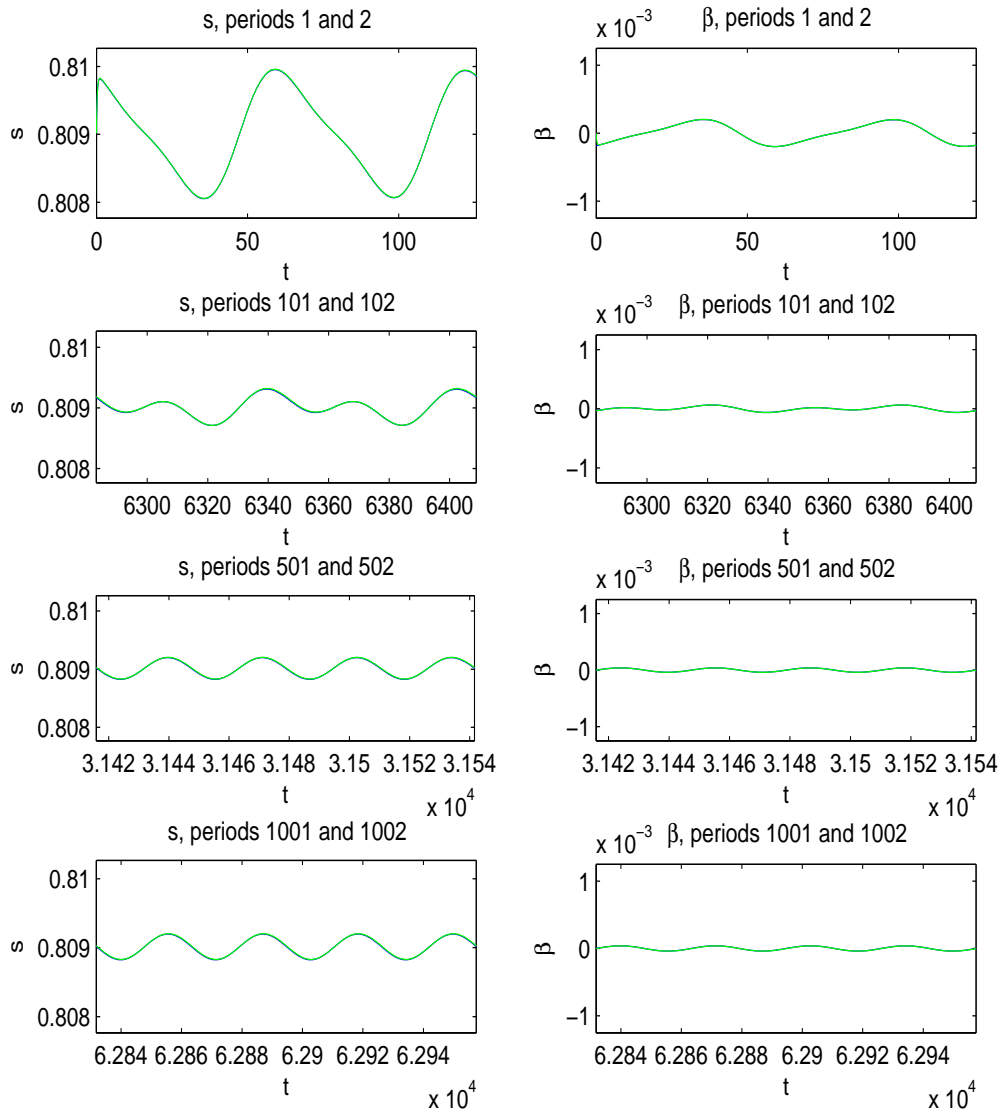
Figure 2.13: Snapshots of the order parameters strobed for two periods of plate oscillation after 100, 500, and 1000 periods. Initially, the order parameters have the same period as the plates and the director angle. However, over the course of the first 200 plate oscillations, the order parameter oscillations slowly double in frequency, unlike $\psi$ remains at the plate frequency. [$N = 6$, $a = 0.8$, $De = 0.1$, $\omega = 0.1$, $\Psi_0 = 5°$]

When $\psi_0 \to \pm\frac{\pi}{2}$, the $1 - \lambda_0$ is replaced by $-1 - \lambda_0$.

## 2.6 Rheological properties

Now that we have $s$, $\beta$, and $\psi$ (and equivalently $\mathbf{Q}$) to first order, we can construct the stress tensor to first order. Given the monodomain restrictions, only the viscous stress $\boldsymbol{\tau}^{Vis}$ (1.26) and the nematic elastic stresses $\boldsymbol{\tau}^{NE}$ (1.28) are present. We will nondimensionalize the stress here with $\tau = 3\nu k_B T \approx 10^5$ Pa so that the stress tensor is now

$$\boldsymbol{\tau} = a\big(\mathbf{Q} - N(\mathbf{M} \cdot \mathbf{M} - \mathbf{M} : \mathbf{M}\mathbf{M})\big) + \mu_1(\mathbf{D} \cdot \mathbf{M} + \mathbf{M} \cdot \mathbf{D}) + \mu_2 \mathbf{D} : \mathbf{M}\mathbf{M} + \mu_3 \mathbf{D}, \qquad (2.93)$$

where $\mu_1 = 6D_r \zeta_1$, $\mu_2 = 6D_r \zeta_2$, and $\mu_3 = \frac{8D_r \eta_s}{\nu k_B T} + 6D_r \zeta_3$. To order first order, $\tau^{Vis}$ can be computed using just $s_{eq}$ and $\psi_0(T_2)$, but nematic elastic stress, $s_1$ and $\beta_1$ arise:

$$\boldsymbol{\tau}^{NE} = De\, a\Big((a_2 s_1 - a_3 \beta_1)\bar{\mathbf{n}}_1 \bar{\mathbf{n}}_1 + a_1 \beta_1 \bar{\mathbf{n}}_2 \bar{\mathbf{n}}_2\Big), \qquad (2.94)$$

where $\bar{\mathbf{n}}_1 = (\cos\psi_0, \sin\psi_0, 0)$ and $\bar{\mathbf{n}}_2 = (-\sin\psi_0, \cos\psi_0, 0)$. Since from (2.76), $s_1$ and $\beta_1$ are both proportional to $\sin 2\psi_0(T_2)$, when $\psi_0$ is near $0$ or $\pm\frac{\pi}{2}$, there are no elastic stresses in the monodomain prediction at leading order. This was observed in Larson and Mead (1989a), but now with our slow-time dependence of $\psi_0$, we are able to say that in the system slowly migrates to oscillation about one of these to elastic-stress free states.

We can also express the extra stress to order $De$ using an integral as

$$\boldsymbol{\tau} = \int_0^{T_0} \mathbf{G}(T_0 - T_0')\mathbf{D}(T_0')\, dT_0' \qquad (2.95)$$

where the relaxation modulus is

$$
\begin{aligned}
\mathbf{G}(u)(\cdot) = \quad & a^2 \left((a_1 a_4 e^{-a_1 u} + a_2(2a_5 - a_4)e^{-a_2 u}) ((\cdot) : \mathbf{n}_1 \mathbf{n}_1)\left(\mathbf{n}_1 \mathbf{n}_1 - \tfrac{\mathbf{I}}{3}\right)\right. \\
& \left. -2a_1 a_4 e^{-a_1 u}((\cdot) : \mathbf{n}_2 \mathbf{n}_2)\left(\mathbf{n}_2 \mathbf{n}_2 - \tfrac{\mathbf{I}}{3}\right)\right) \\
& +\delta(u)\left(\left(\tfrac{2}{3}\mu_1 + \mu_3\right)(\cdot) + \mu_1 s_+ ((\cdot) \cdot \mathbf{n}_1 \mathbf{n}_1 + \mathbf{n}_1 \mathbf{n}_1 \cdot (\cdot))\right. \\
& \left. +\mu_2 s_+^2 ((\cdot) : \mathbf{n}_1 \mathbf{n}_1)\mathbf{n}_1 \mathbf{n}_1\right).
\end{aligned}
\qquad (2.96)
$$

In the limit $a = 1$, if the viscous terms are dropped, then the $e^{-a_2 u}$ term is the same as the one in (Larson and Mead, 1989a) restricted to the in-plane case, but our $e^{-a_1 u}$ terms are different

due to the presence of the biaxial $\mathbf{n}_2\mathbf{n}_2$ term.

### 2.6.1 Shear stress and storage and loss moduli

In order to make a prediction of the storage modulus $G'(\omega)$ and the loss modulus $G''(\omega)$, we need to write the shear stress in the form of (1.45). To do this, we will first wait until the transient terms that decay exponentially with the fast time $T_0$ have become small enough to ignore. The only $T_0$-dependence that remains in the shear stress is a dependence upon either $\cos\omega T_0$ or $\sin\omega T_0$. Therefore we will proceed by allowing the storage and loss moduli to not only be a function of the plate frequency $\omega$ but also to retain a dependence on the slow time $T_2$.

To define the moduli from (1.45), we must first define a macroscopic shear strain in the form of (1.43). Given our nondimensional monodomain velocity $v_x = De\,y\cos\omega t$, the appropriate macroscopic shear strain is

$$\gamma = \frac{De}{\omega}\sin\omega t = \gamma_0\sin\omega t. \tag{2.97}$$

The viscous part of the shear stress is

$$\tau_{xy}^{Vis}(T_0,T_2) \;=\; De\cos\omega T_0\left(\frac{\mu_1}{6}(2+s_{eq}) + \frac{\mu_3}{2} + \frac{\mu_2}{4}s_{eq}^2\sin^2 2\psi_0(T_2)\right). \tag{2.98}$$

Notice that this is entirely out-of-phase with the strain (2.97) and hence can contribute only to the loss modulus. The nematic elastic part however takes the form

$$\begin{aligned}
\tau_{xy}^{NE}(T_0,T_2) &= De\,a\sin 2\psi_0(T_2)\left[\tfrac{a_2}{2}s_1(T_0,T_2) - \tfrac{a_2+a_1}{4}\beta_1(T_0,T_2)\right] \\
&= De\,a^2\sin^2 2\psi_0(T_2)\left[\cos\omega T_0\left(\tfrac{a_2}{2}a_{s_1} - \tfrac{a_2+a_1}{4}a_{\beta_1}\right)\right. \\
&\quad \left. + \sin\omega T_0\left(\tfrac{a_2}{2}b_{s_1} - \tfrac{a_2+a_1}{4}b_{\beta_1}\right)\right].
\end{aligned} \tag{2.99}$$

Since this has both $\sin\omega T_0$ and $\cos\omega T_0$ terms, it also contributes to the loss modulus, and it provides the only terms in the storage modulus, which we can now write as

$$G'(\omega,T_2) = C_1(\omega)\sin^2 2\psi_0(T_2) \tag{2.100}$$

where

$$C_1(\omega) = \omega\left(\frac{a_2}{2}b_{s_1}(\omega) - \frac{a_2 + a_1}{4}b_{\beta_1(\omega)}\right)$$

$$= \frac{a^2(1 - s_{eq})}{12}\frac{a_2(a_1^2 + a_2^2(3 + 6s_{eq}))\omega^2 + (a_1 + a_2(3 + 6s_{eq}))\omega^4}{(a_1^2 + \omega^2)(a_2^2 + \omega^2)}. \qquad (2.101)$$

The loss modulus is

$$G''(\omega, T_2) = \hat{\eta}\omega + C_2(\omega)\sin^2 2\psi_0(T_2), \qquad (2.102)$$

where

$$\hat{\eta} = \frac{\mu_1(2 + s_{eq})}{6} + \frac{\mu_3}{2} \qquad (2.103)$$

$$C_2(\omega) = \frac{\mu_2 s_{eq}^2}{4}\omega + \omega\left(\frac{a_2}{2}a_{s_1}(\omega) - \frac{a_2 + a_1}{4}a_{\beta_1(\omega)}\right)$$

$$= \frac{\mu_2 s_{eq}^2}{4}\omega + \frac{a^2(1 - s_{eq})}{12}\frac{a_1^2 a_2^2(4 + 6s_{eq})\omega + (a_1^2 + (3 + 6s_{eq})a_2^2)\omega^3}{(a_1^2 + \omega^2)(a_2^2 + \omega^2)}. \qquad (2.104)$$

If the viscous terms are dropped (that is, the $\mu_i$ are set to zero), then in the limit $a = 1$ these are the same as those given in (Larson and Mead, 1989a) with the exception of the dependence on $T_2$. The $\omega$-dependence of the storage and loss moduli are depicted in Figure 2.14 after 10, 100, and 1000 plate oscillations. As $T_2$ increases, the moduli slowly decay, an effect much more apparent for low frequencies due the $\omega$-dependence of $B_1$ detailed in Section 2.5.2. Figure 2.15 shows the same information as Figure 2.14, but it highlights the effect of the differing values of the initial angle $\Psi_0$. When the initial angle $\Psi_0$ is near $\pm\frac{\pi}{2}$, the storage modulus shows an increase of approximately an order or magnitude over those with $\Psi_0$ near 0 or $\frac{\pi}{2}$. The loss modulus also shows an increase near $|\Psi_0| = \frac{\pi}{4}$, but the effect is smaller, only on the order of a factor of 2. Before the slow decay takes effect, we observe that asymptotically, the storage modulus behaves as

$$G'(\omega) \approx \frac{a^2(1-s_{eq})(a_1^2 + a_2^2(3 + 6s_{eq}))}{12a_1^2 a_2}\frac{e^{2B_1^{(0)}De^2 t}\tan^2 2\Psi_0}{1 + e^{2B_1^{(0)}De^2 t}\tan^2 2\Psi_0}\omega^2, \quad \text{as } \omega \to 0,$$

$$G'(\omega) \approx \frac{a^2(1-s_{eq})(a_1 + a_2(3 + 6s_{eq}))}{12}\sin^2 2\Psi_0, \qquad \text{as } \omega \to \infty, \qquad (2.105)$$
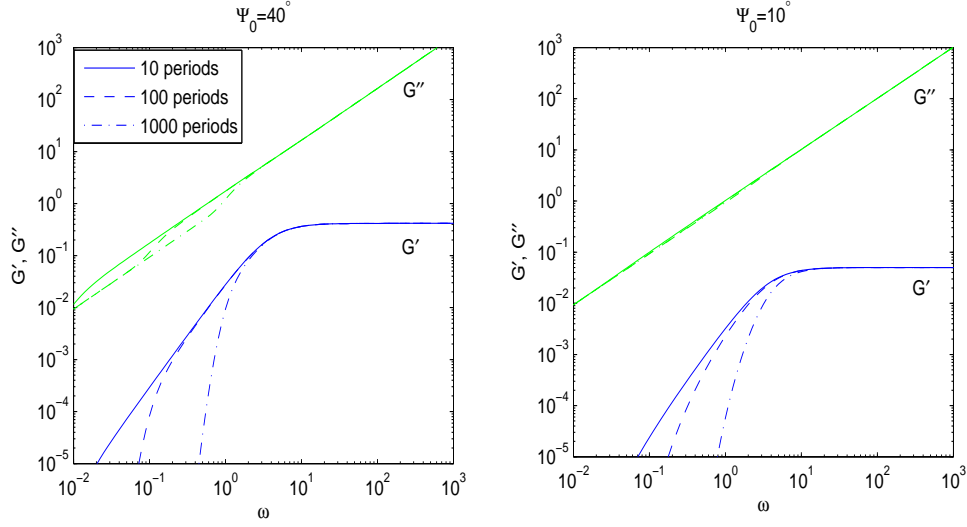
Figure 2.14: The storage modulus $G'$ (dark lines) and loss modulus $G''$ (light lines) for $\Psi_0 = 40°$ and $\Psi_0 = 10°$ highlighting the slow-time decay that is more evident for lower frequencies. $[a = 0.9, N = 6, \zeta^{(0)} = 0.01]$
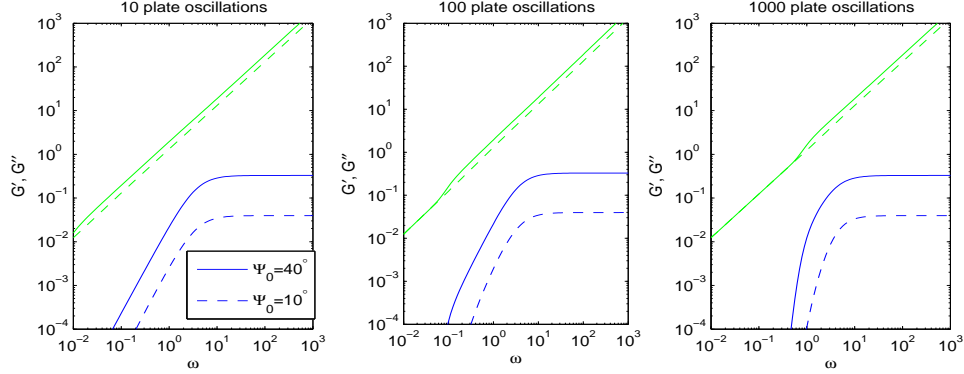


Figure 2.15: The storage modulus $G'$ (dark lines) and loss modulus $G''$ (light lines) for $\Psi_0 = 40°$ and $\Psi_0 = 10°$ highlighting the effect of the initial angle $\Psi_0$. $[a = 0.9, N = 6, \zeta^{(0)} = 0.01]$

where $B_1^{(0)} = -\frac{a^2(3a_1+a_2)}{2N^2 s_{eq}^2 a_1^2 a_2^2}$. The loss modulus is

$$
\begin{aligned}
G''(\omega) &\approx \left[\hat{\eta} + \left(\frac{\mu_2 s_{eq}^2}{4} + \frac{a^2(1-s_{eq})(2+3s_{eq})}{6}\right) \frac{e^{2B_1^{(0)}De^2 t}\tan^2 2\Psi_0}{1+e^{2B_1^{(0)}De^2 t}\tan^2 2\Psi_0}\right]\omega, &\quad \text{as } \omega \to 0, \\
G''(\omega) &\approx \left[\hat{\eta} + \frac{\mu_2 s_{eq}^2}{4}\sin^2 2\Psi_0\right]\omega, &\quad \text{as } \omega \to \infty.
\end{aligned}
\tag{2.106}
$$

52

### 2.6.2 Comparison to experiments

From (2.72), the key factor in the long-time behavior of $G'$ and $G''$ becomes explicit:

$$\sin^2 2\psi_0(T_2) = \frac{e^{2B_1 T_2} \tan^2 2\Psi_0}{1 + e^{2B_1 T_2} \tan^2 2\Psi_0} \ . \tag{2.107}$$

We immediately deduce that the dynamic moduli $G'$ and $G''$ obey a logistic long-time decay law. Figure 2.16 illustrates this property for three different values of $\Psi_0$.

The solid lines in Figure 2.16 represent starting the oscillatory shear with the initial angle $\Psi_0$ aligned with the steady shear flow-aligning angle $\psi_L$. In (Larson and Mead, 1989b; Moldenaers and Mewis, 1986), flow-aligning solutions of PBLG were subjected to a lengthy period of steady shear to pre-align the molecules with $\psi_L$ before the application of oscillatory shear for a long period of time. While the initial conditions of our "theoretical experiment" differs from the laboratory experiments slightly[2], the predictions in Figure 2.16 are consistent with the experimental data for $G''$ and the scaled $G'' = \frac{G''(t=\infty)-G''(t)}{G''(t=\infty)-G''(t=0)}$ in spite of the claim in (Larson and Mead, 1989b) that the monodomain theory cannot predict this decay. The decay of $G'$ is consistent with their experiments in that they do observe decay; however they observe two effects that we do not. First, we predict that $G'$ decays to zero, whereas they observe it decaying to a finite plateau greater than zero. Additionally, in some but not all of the experiments of Larson and Mead (1989b), it was observed that $G'$ after a lengthy period of decay slowly began to increase slightly, which is an effect that we do not predict.

In addition, it was experimentally observed that $t_c$, the characteristic time required for the dynamic moduli to complete one-third of their decay, was inversely proportional to the shear rate of the pre-aligning shear. Since our set-up has no pre-aligning shear rate, we cannot speak directly to this; however, we can compute the characteristic decay time for quiescent initial data and find that $t_c = \frac{1}{2B_1 De^2} \ln \frac{2}{3 + \tan^2 2\Psi_0}$.

---

[2] The initial conditions of our order parameters are at their zero-shear equilibrium values whereas if a steady shear had been applied immediately prior to the oscillatory shear, the order parameters would be given by (2.35).
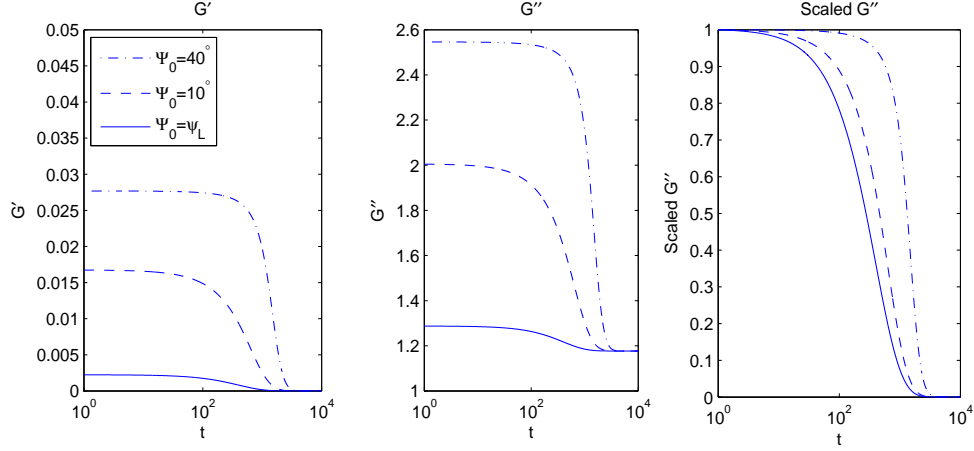
Figure 2.16: $G'$, $G''$, and the scaled $G'' = \frac{G''(t=\infty)-G''(t)}{G''(t=\infty)-G''(t=0)}$ for $N = 6$, $a = 0.9(\psi_L = 8.128°)$, for $\Psi_0 = \psi_L$, $\Psi_0 = 25°$ and $\Psi_0 = 40°$. [$De = 0.2$, $\omega = 1$]

### 2.6.3 First and second normal stress differences

The first normal stress difference is

$$N_1 = \tau_{xx} - \tau_{yy} = De \cos 2\psi_0 \left( \frac{\mu_2 s_{eq}^2}{2} \sin 2\psi_0 \cos \omega T_0 + a \left( a_2 s_1 - \frac{a_1+a_2}{2}\beta_1 \right) \right), \qquad (2.108)$$

and it can be expressed using the shear stress notation from (2.101) and (2.104):

$$N_1 = De \sin 4\psi_0 \left( \frac{C_2(\omega)}{\omega} \cos \omega T_0 + \frac{C_1(\omega)}{\omega} \sin \omega T_0 \right), \qquad (2.109)$$

where the terms that decay exponentially with $T_0$ have been ignored. The second normal stress difference is

$$
\begin{aligned}
N_2 &= \tau_{yy} - \tau_{zz} \\
&= De \Big[ \left( \frac{\mu_1 s_{eq}}{2} + \frac{\mu_2 s_{eq}^2}{2} \sin^2 \psi_0 \right) \sin 2\psi_0 \cos \omega T_0 \\
&\quad + a \left( \frac{a_2}{2} s_1 + \frac{3a_1-a_2}{4}\beta_1 - \left( \frac{a_2}{2} s_1 - \frac{a_1+a_2}{4}\beta_1 \right) \cos 2\psi_0 \right) \Big] \\
&= De \sin 2\psi_0 \left( (D_1 + D_2 \cos 2\psi_0) \cos \omega T_0 + (D_3 + D_4 \cos 2\psi_0) \sin \omega T_0 \right).
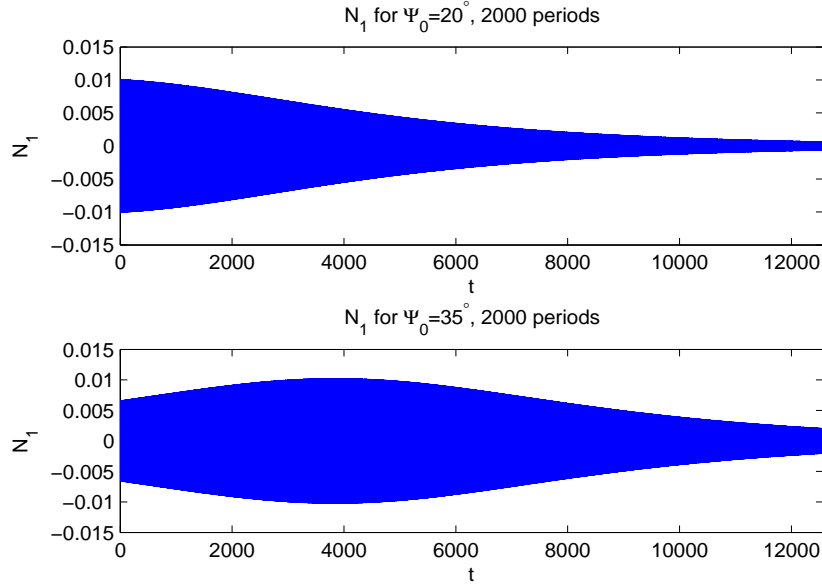\end{aligned}
\qquad (2.110)
$$

54

Figure 2.17: The first normal stress differences for oscillatory shear with $\Psi_0 = 15°$, $\Psi_0 = 35°$ and $\Psi_0 = 55°$. [$N = 6$, $a = 0.8$, $De = 0.1$, $\omega = 1$]

where the terms that decay exponentially with $T_0$ have been ignored and

$$
\begin{aligned}
D_1 &= \tfrac{\mu_1 s_{eq}}{2} + \tfrac{\mu_2 s_{eq}^2}{4} + a^2\big(\tfrac{a_2}{2} a_{s_1} + \tfrac{3a_1 - a_2}{4} a_{\beta_1}\big), \\
D_2 &= -\tfrac{C_2(\omega)}{\omega}, \\
D_3 &= a^2\big(\tfrac{a_2}{2} b_{s_1} + \tfrac{3a_1 - a_2}{4} b_{\beta_1}\big), \\
D_4 &= -\tfrac{C_1(\omega)}{\omega}.
\end{aligned}
\tag{2.111}
$$

The normal stress differences also show a slow time effect. As shown in Figure 2.17, the first normal stress difference oscillates around zero, but the amplitude varies slowly. If $\Psi_0$ is in $\left(-\tfrac{\pi}{2}, -\tfrac{3\pi}{8}\right)$, $\left(-\tfrac{\pi}{8}, \tfrac{\pi}{8}\right)$, or $\left(\tfrac{3\pi}{8}, \tfrac{\pi}{2}\right)$, then the amplitude slowly decreases, decaying to zero. However, if $\Psi_0$ is in either $\left(-\tfrac{3\pi}{8}, -\tfrac{\pi}{8}\right)$ or $\left(\tfrac{\pi}{8}, \tfrac{3\pi}{8}\right)$, then as $\psi_0(T_2)$ drifts, the amplitude of $N_1$ will slowly increase until $T_2 = -\tfrac{1}{2B_1} \ln \tan^2 2\Psi_0$, when $N_1$ reaches its maximum amplitude, and then it will slowly decrease, eventually decaying to zero. The zeroes of the amplitude of $N_1$ are when $\psi_0$ is $0, \pm\tfrac{\pi}{4}$, or $\pm\tfrac{\pi}{2}$, and the maxima occur when (and if) $\psi_0$ passes through $\pm\tfrac{\pi}{8}$ or $\pm\tfrac{3\pi}{8}$.

The slow time effects are more apparent for the second normal stress difference, as depicted in Figure 2.18. The amplitude of $N_2$ can exhibit behavior qualitatively similar to $N_1$ for some values of $\Psi_0$, However, the amplitude of $N_2$ can have local extrema or other zeroes in between
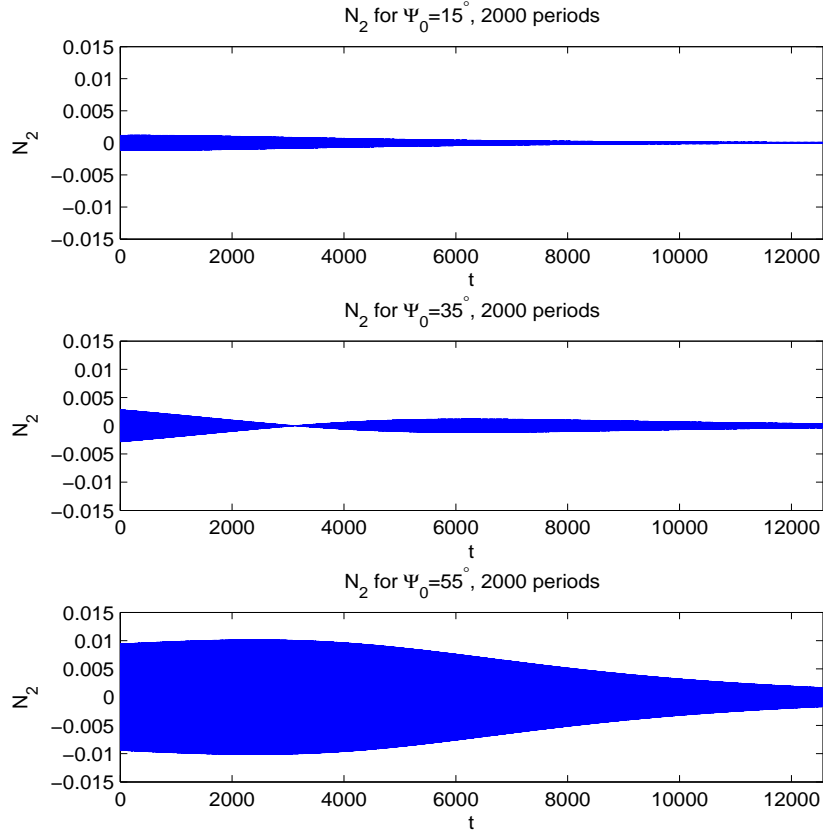
Figure 2.18: The second normal stress differences for oscillatory shear with $\Psi_0 = 15°$ $\Psi_0 = 35°$ and $\Psi_0 = 55°$. [$N = 6$, $a = 0.8$, $De = 0.1$, $\omega = 1$]

the zeroes at $0$ and $\pm\frac{\pi}{2}$, the location of which depend upon $N$, $a$, and $\omega$. As $T_2$ increases, $\psi_0$ can drive the amplitudes of $N_1$ and $N_2$ through these extrema or zeros. An additional difference between $N_1$ and $N_2$ lies in their phase shifts relative to the plates. For $N_1$, the phase shift is $\tan^{-1} \frac{C_1(\omega)}{C_2(\omega)}$ and is independent of the initial angle. However for $N_2$, the phase shift is $\tan^{-1} \frac{D_3 + D_4 \cos 2\psi_0(T_2)}{D_1 + D_2 \cos 2\psi_0(T_2)}$, and thus, $N_2$ can experience a change in the phase shift during the course of the experiment.

## 2.7 Concluding remarks

### 2.7.1 An alternative derivation

The derivation in Section (2.4) can be seen from a different point of view as taking the prediction

$$\psi_{LE} = \Psi \left( De \frac{\sin \omega T_0}{\omega} + \phi_0 \right), \tag{2.112}$$

but instead of using the constant $\phi_0$ of (2.69), we now allow it to be an unknown function of $T_2$. Once $\phi_0(T_2)$ is determined, the approximation

$$\psi(T_0, T_2) = \Psi(\phi_0(T_2)) + De\Psi'(\phi_0(T_2)) \frac{\sin \omega T_0}{\omega} + O(De^2) \tag{2.113}$$

is the same as (2.75).

### 2.7.2 Other closure approximations

We now briefly address the robustness of these drift phenomena to closure approximation used to approximate the fourth moment $\mathbf{M}_4$ as a function of $\mathbf{M}$. The two other algebraic closures addressed in (Forest and Wang, 2003) (those of Tsuji-Rey (Tsuji and Rey, 1997) and Hinch-Leal 1 (Hinch and Leal, 1976)) produce the same qualitative behavior as the Doi closure presented here: the same two stress-free asymptotic states with the same basins of attraction, independent of closure, and the long-time decrease of the dynamic moduli. The non-algebraic Hinch-Leal 2 closure yields similar behavior for sufficiently low nematic concentrations. However, at higher concentrations it predicts different bi-stable asymptotic states where $\psi_0(T_2)$ drifts toward $\pm\frac{\pi}{4}$, which are not elastic stress free, and it predicts a long-time increase in the dynamic moduli. These modified properties appear to be a nonphysical closure artifact.

### 2.7.3 Conclusion

We have examined the mesoscopic monodomain in-plane Doi-Hess tensor model for a nematic liquid crystal polymer subjected to an imposed small amplitude oscillatory shear flow. A multiple timescale perturbation analysis predicts sensitivity in the director angle and storage and loss moduli to initial value of the director angle $\Psi_0$ that is experimentally relevant on long

timescales. This analysis was motivated by a return to the classical papers of Moldenaers and Mewis (Moldenaers and Mewis, 1986) and Larson and Mead (Larson and Mead, 1989a) on linear viscoelasticity of nematic polymers, armed with current analytical understanding of the role of orientational degeneracy of nematic equilibria in simple shear.

Specifically, we predict a slow drift dynamics of the major director of the orientational distribution. The drift phenomenon is due to the coupling of the director to order parameter fluctuations, and thus would not be observed in small molecule liquid crystals and the Leslie-Ericksen model. The envelope and mean of the drift dynamics is explicitly characterized, which predicts bistable longtime asymptotic orientational states, one with the major director along the flow axis and the other along the flow-gradient axis. These states are distinguished in that they are the minima of the purely elastic shear stress component, as noted in (Larson and Mead, 1989a). Remarkably, the basins of attraction of the bistable longtime states do not depend on material parameters (e.g., the Leslie tumbling parameter which determines tumbling versus flow-alignment in simple steady shear); rather, the initial director orientation angle alone determines the two drift dynamic routes and final states. These results are then converted into predictions of the storage and loss moduli, which are predicted to obey a logistic long-time decay law consistent with experimental observations of (Moldenaers and Mewis, 1986). The bistable drift dynamics yield the same order of magnitude loss modulus, yet an order of magnitude difference in storage modulus which is due solely to the initial director orientation angle. Experiments which bias the initial director of the nematic sample, as with steady pre-shear, would thereby not observe this sensitivity in storage modulus.

The monodomain predictions of linear viscoelastic properties in oscillatory shear are a precursor to structure-dependent properties of nematic polymers and rigid rod suspensions. The present monodomain results predict the loss modulus dominates the storage modulus at essentially all frequencies. On the other hand, defect-ridden nematic polymer suspensions have been observed to obey the opposite extreme, with nearly solid-like linear viscoelastic response (Colby et al., 2001).

# Chapter 3

# One-dimensional heterogeneity in small amplitude oscillatory flow

We now relax the monodomain restriction of the previous chapter and allow the orientation tensor and the velocity to vary in the $y$ direction. Oscillatory shear flows of small molecule nematic liquid crystals have been studied by Burghardt (Burghardt, 1991) and de Andrade Lima and Rey (de Andrade Lima and Rey, 2006) using Leslie-Ericksen theory under the single Frank constant approximation. This includes spatial distortions in the director angle generated by isotropic elasticity and flow feedback; here we extend their analysis to allow for excluded volume effects, or variations in the degree of orientation, and unequal Frank elasticity constants with the Marrucci-Greco potential (1.19). The present analysis also extends our results of Cui *et al.* (Cui *et al.*, 2006) on the importance of anisotropic elasticity in steady shear flows, from the zero frequency limit to the full spectrum.

We formulate the flow-nematic equations and boundary conditions in such a way that the same moduli predictions arise for oscillatory flow, stress, and pressure driving conditions, what one might call "rheological equivalence between shear and Poiseuille flows." The analysis is tractable for both tangential and homeotropic anchoring, allowing for their explicit comparison, which reveals strong variability of linear viscoelastic response to wall anchoring conditions. Further studies on the anchoring dependence of storage and loss moduli will require numerical simulations.

## 3.1 Dimensional analysis and boundary conditions

In this chapter, we consider oscillatory flow between parallel plates driven either by drag from moving plates or by pressure gradients. To establish equivalence between shear flow and

Poiseuille flow for measuring and modeling of the storage and loss moduli, we find it useful to consider slightly different geometrical setups for the two flows. The separation of the plates is $h$ for shear flow, but $2h$ for Poiseuille flow, as depicted in Figure 1.2. In each case, we nondimensionalize the gap dimension $y$ by $h$ and choose $y = 0$ to correspond to the midpoint of the gap. This choice, in essence, identifies the bottom half of a Poiseuille response with the full gap of a shear response.

To make contact with scaling analysis of Burghardt, de Andrade Lima and Rey, and using connections from the tensor model to the Leslie-Ericksen model from (Wang, 2002), we choose as a characteristic stress the Frank stress

$$\tau_F = \frac{K}{h^2} = \frac{\nu k T N \mathcal{L}^2 s_{eq}^2}{8h^2}, \tag{3.1}$$

where $K$ is the Frank constant. This is a measure of the stress caused by spatial gradients in molecular orientation. We define a characteristic Leslie viscosity

$$\eta_0 = \frac{\nu k T s_{eq}^2}{D_r}, \tag{3.2}$$

and then we define the characteristic timescale as

$$t_0 = \frac{\eta_0}{\tau_F} = \frac{8h^2}{N \mathcal{L}^2 D_r}. \tag{3.3}$$

The velocity scale is taken to be $\frac{h}{t_0}$.

We now identify two nondimensional parameters that arise in the flow-nematic equations and boundary conditions. The Ericksen number $Er$ is the ratio of the viscous stress to the Frank stress, and the Deborah number $De$ is the ratio of the characteristic shear rate to the rotational diffusion rate. These numbers take different forms depending upon the type of flow imposed, which we amplify next.

For shear flow, if we impose the boundary condition

$$\tau_{xy}\left(y = \pm\tfrac{1}{2}\right) = \tau_0 \cos \omega t \tag{3.4}$$

on the stress, then we can use the characteristic viscosity to convert this into the effective shear rate $\dot\gamma_{eff} = \frac{\tau_0}{\eta_0}$ so that

$$Er = \frac{\tau_0}{\tau_F}, \quad De = \frac{\dot\gamma_{eff}}{D_r}. \tag{3.5}$$

This definition of $Er$ is consistent with the Leslie-Ericksen theory (Burghardt, 1991; de Andrade Lima and Rey, 2006); however, since there is no molecular relaxation rate in LE theory, there is no analogue of $De$.

For the velocity boundary condition

$$v_x\big(y = \pm\tfrac{1}{2}\big) = \pm v_0 \cos\omega t, \tag{3.6}$$

different definitions must be used. We can use the gap width $h$ to define a shear rate $\dot\gamma_0 = \frac{v_0}{h}$, and then we can use the characteristic viscosity to convert this to an effective viscous stress $\tau_{eff} = \dot\gamma_0 \eta_0$ in order to define

$$Er = \frac{\tau_{eff}}{\tau_F}, \quad De = \frac{\dot\gamma_0}{D_r}. \tag{3.7}$$

Thus for shear flow, the nondimensional boundary conditions are

$$\begin{cases} \tau_{xy}\big(y = \pm\tfrac{1}{2}\big) = Er \cos\omega t, & \text{for imposed stress,} \\[2ex] v_x\big(y = \pm\tfrac{1}{2}\big) = \pm Er \cos\omega t, & \text{for imposed velocity.} \end{cases} \tag{3.8}$$

For Poiseuille flow, we use the pressure gradient

$$\nabla p = \left(\left(\tfrac{\partial p}{\partial x}\right)_0 \cos\omega t, 0, 0\right), \tag{3.9}$$

where $\left(\frac{\partial p}{\partial x}\right)_0$ is constant and negative, and then nondimensionalize so that

$$Er = -\tfrac{h}{2\tau_F}\left(\tfrac{\partial p}{\partial x}\right)_0, \quad De = -\tfrac{h}{2\eta_0 D_r}\left(\tfrac{\partial p}{\partial x}\right)_0, \tag{3.10}$$

and the nondimensional pressure gradient is

$$\nabla p = (2Er\cos\omega t, 0, 0). \tag{3.11}$$

For all flows, the above definitions satisfy

$$\frac{Er}{De} = \frac{8h^2}{N\mathcal{L}^2}. \tag{3.12}$$

While the following equations reduce to Leslie-Ericksen-type behavior in the limit $De \to 0$, we observe that one drawback to this nondimensionalization is that the limit $Er \to \infty$ does not recover the monodomain equations.

Under this nondimensionalization, (1.22) becomes

$$
\begin{aligned}
\tfrac{\partial}{\partial t}\mathbf{M} =\ & \mathbf{\Omega}\cdot\mathbf{M} - \mathbf{M}\cdot\mathbf{\Omega} + a(\mathbf{D}\cdot\mathbf{M} + \mathbf{M}\cdot\mathbf{D} - 2\mathbf{D}:\mathbf{M}_4) \\
& -6\tfrac{Er}{De}[\mathbf{Q} - N(\mathbf{M}\cdot\mathbf{M} - \mathbf{M}:\mathbf{M}_4)] + \Delta\mathbf{M}\cdot\mathbf{M} + \mathbf{M}\cdot\Delta\mathbf{M} - 2\Delta\mathbf{M}:\mathbf{M}_4 \\
& +\tfrac{\theta}{2}[(\nabla\nabla\mathbf{M}) \vdots \mathbf{M}_4 + ((\nabla\nabla\mathbf{M}) \vdots \mathbf{M}_4)^T + \mathbf{M}_4 \vdots \nabla\nabla\mathbf{M} + (\mathbf{M}_4 \vdots \nabla\nabla\mathbf{M})^T \\
& \quad +\mathbf{M}\cdot(\nabla\nabla:\mathbf{M}_4) + (\nabla\nabla:\mathbf{M}_4)\cdot\mathbf{M} - 4\mathbf{M}_6 :: \nabla\nabla\mathbf{M} - 2\mathbf{M}_4 : (\nabla\nabla:\mathbf{M}_4)].
\end{aligned}
\tag{3.13}
$$

On the boundary, $\mathbf{M}$ is assumed to take the fixed uniaxial nematic equilibrium form

$$\mathbf{M}\big(y = \pm\tfrac{1}{2}\big) = s_{eq}\Big(\mathbf{n}_0\mathbf{n}_0 - \tfrac{\mathbf{I}}{3}\Big) + \tfrac{\mathbf{I}}{3} \tag{3.14}$$

where $\mathbf{n}_0$ is an arbitrary unit vector in the $x$-$y$ plane. (These are the boundary conditions for shear flow. The only difference for Poiseuille flow is that they are applied at $y = \pm 1$.) In terms of the spectral variables, the boundary conditions are

$$s(y = \pm\tfrac{1}{2}) = s_{eq}, \quad \beta(y = \pm\tfrac{1}{2}) = 0, \quad \psi(y = \pm\tfrac{1}{2}) = \psi_0 \tag{3.15}$$

where $\psi_0$ is an arbitrary constant director angle.

The dimensionless parts of the stress tensor are

$$\boldsymbol{\tau}^{Vis} = \mu_1(\mathbf{D} \cdot \mathbf{M} + \mathbf{M} \cdot \mathbf{D}) + \mu_2 \mathbf{D} : \mathbf{M}_4 + \mu_3 \mathbf{D}, \tag{3.16}$$

$$\boldsymbol{\tau}^{NE} = \frac{3a}{s_0^2}\frac{Er}{De}[\mathbf{Q} - N(\mathbf{M} \cdot \mathbf{M} - \mathbf{M} : \mathbf{M}_4)], \tag{3.17}$$

$$\boldsymbol{\tau}^{IE} = \frac{1-a}{2s_0^2}\mathbf{M} \cdot \Delta\mathbf{M} - \frac{1+a}{2s_0^2}\Delta\mathbf{M} \cdot \mathbf{M} + \frac{a}{s_0^2}\Delta\mathbf{M} : \mathbf{M}_4$$
$$- \frac{1}{4s_0^2}(M_{kl,i}M_{kl,j} - \mathbf{M} : \nabla\nabla\mathbf{M}), \tag{3.18}$$

$$\boldsymbol{\tau}^{AE} = \theta[\frac{a}{2s_0^2}(2\mathbf{M}_6 :: \nabla\nabla\mathbf{M} + \mathbf{M}_4 : (\nabla\nabla : \mathbf{M}_4))$$
$$- \frac{1+a}{4s_0^2}(\nabla\nabla\mathbf{M}\vdots\mathbf{M}_4 + (\mathbf{M}_4\vdots\nabla\nabla\mathbf{M})^T + (\nabla\nabla : \mathbf{M}_4) \cdot \mathbf{M}) \tag{3.19}$$
$$+ \frac{1-a}{4s_0^2}((\nabla\nabla\mathbf{M}\vdots\mathbf{M}_4)^T + \mathbf{M}_4\vdots\nabla\nabla\mathbf{M} + \mathbf{M} \cdot (\nabla\nabla : \mathbf{M}_4))],$$

where $\mu_1 = \frac{3\zeta_1 D_r}{s_0^2}$, $\mu_2 = \frac{3\zeta_2 D_r}{s_0^2}$, and $\mu_3 = 2\frac{\eta_s}{\eta_0} + \frac{3\zeta_3 D_r}{s_0^2}$.

The dimensionless linear momentum balance is

$$Re\,\frac{\partial\mathbf{v}}{\partial t} = \nabla \cdot (-p\mathbf{I} + \boldsymbol{\tau}), \tag{3.20}$$

where $Re = \frac{\rho h^2}{\tau_F t_0^2}$ defines a Reynolds number. For large molecule LCPs, $t_0$ can be $10^3$s or larger, and so with $\rho \approx 10^3$kg/m$^3$, $h \approx 10^{-4}$m, and $\tau_F \approx 0.1$Pa, we estimate $Re \approx 10^{-10}$ so that we can safely ignore the fluid inertia term. In our analysis below, the equations are still tractable when inertia is included, but our solutions confirm the effect is negligible, and so we omit the details.

Given the chosen boundary conditions (3.8) for shear and our pressure condition (3.11) for Poiseuille flow, the appropriate asymptotic limit to examine the linear response is the small Ericksen number limit. Therefore we propose the solution ansatz for the orientation tensor and flow:

$$\begin{aligned} s &= s_0 + \sum_{k=1}^{\infty} Er^k s^{(k)}(y,t), & \beta &= 0 + \sum_{k=1}^{\infty} Er^k \beta^{(k)}(y,t), \\ \psi &= \psi_0 + \sum_{k=1}^{\infty} Er^k \psi^{(k)}(y,t), & v_x &= 0 + \sum_{k=1}^{\infty} Er^k v_x^{(k)}(y,t). \end{aligned} \tag{3.21}$$

Equivalently, we can expand $\mathbf{Q}$ in powers of $Er$ as $\mathbf{Q} = \mathbf{Q}_0 + \sum_{k=1}^{\infty} Er^k \mathbf{Q}^{(k)}(y,t)$ for which

$$\mathbf{Q}^{(1)} = s_0 \psi^{(1)} \begin{bmatrix} -\sin 2\psi_0 & \cos 2\psi_0 & 0 \\ \cos 2\psi_0 & \sin 2\psi_0 & 0 \\ 0 & 0 & 0 \end{bmatrix} + \frac{s^{(1)} - \beta^{(1)}}{2} \begin{bmatrix} \cos 2\psi_0 & \sin 2\psi_0 & 0 \\ \sin 2\psi_0 & -\cos 2\psi_0 & 0 \\ 0 & 0 & 0 \end{bmatrix}$$

$$+ \frac{s^{(1)} + \beta^{(1)}}{6} \mathbf{I}. \tag{3.22}$$

Additionally, we represent the stress by $\boldsymbol{\tau} = \sum_{k=1}^{\infty} Er^k \boldsymbol{\tau}^{(k)}$.

At $O(Er)$, the nondimensionalized system (1.34)-(1.37) transforms to

$$\frac{\partial s^{(1)}}{\partial t} = \left(\frac{2}{N} + \theta\left(\frac{2(1+s_{eq})}{3N} - \frac{5+18s_{eq}}{9N}\cos 2\psi_0\right)\right)\frac{\partial^2 s^{(1)}}{\partial y^2}$$
$$- \frac{2(1-s_{eq})}{3}\left(2 + \theta\left(\frac{s_{eq}(s_{eq}+5)}{6} - \frac{8+25s_{eq}+45s_{eq}^2}{18}\cos 2\psi_0\right)\right)\frac{\partial^2 \beta^{(1)}}{\partial y^2} \tag{3.23}$$
$$+ \sin 2\psi_0 \left(a\frac{1+2s_{eq}-3s_{eq}^2}{3}\frac{\partial v_x^{(1)}}{\partial y} + \theta\frac{s_{eq}(1+s_{eq})}{N}\frac{\partial^2 \psi^{(1)}}{\partial y^2}\right),$$

$$\frac{\partial \beta^{(1)}}{\partial t} = -\sin 2\psi_0\left(a\frac{1-s_{eq}}{3}\frac{\partial v_x}{\partial y} + \frac{\theta s_{eq}}{N}\frac{\partial^2 \psi^{(1)}}{\partial y^2}\right) + \frac{4\theta}{9N}\cos 2\psi_0 \frac{\partial^2 s^{(1)}}{\partial y^2}$$
$$+ \frac{1-s_{eq}}{27}\left(18 + \frac{\theta}{2}(4 + s_{eq} + (10-7s_{eq})\cos 2\psi_0)\right)\frac{\partial^2 \beta^{(1)}}{\partial y^2}, \tag{3.24}$$

$$\frac{\partial \psi^{(1)}}{\partial t} = -\frac{1}{2}\left(1 - \lambda_L \cos 2\psi_0\right)\frac{\partial v_x^{(1)}}{\partial y} + \frac{2+s_{eq}}{3}\left[1 + \frac{\theta s_{eq}}{2}(\frac{\lambda_L}{a} - \cos 2\psi_0)\right]\frac{\partial^2 \psi^{(1)}}{\partial y^2}$$
$$+ \frac{\theta \lambda_L}{36a}\sin 2\psi_0\left((1+5s_{eq})\frac{\partial^2 s^{(1)}}{\partial y^2} + (1-4s_{eq})\frac{\partial^2 \beta^{(1)}}{\partial y^2}\right), \tag{3.25}$$

$$0 = \begin{cases} \frac{\partial \tau_{xy}^{(1)}}{\partial y}, & \text{for shear flow}, \\ 2\cos\omega t + \frac{\partial \tau_{xy}^{(1)}}{\partial y}, & \text{for Poiseuille flow}, \end{cases} \tag{3.26}$$

$$\tau_{xy}^{(1)} = \left(\frac{\mu_1(s_{eq}+2)}{6} + \frac{\mu_2 s_{eq}^2}{4}\sin^2 2\psi_0 + \frac{\mu_3}{2}\right)\frac{\partial v_x^{(1)}}{\partial y} + \frac{1}{2}\Big[1 - \lambda_L \cos 2\psi_0$$
$$+ \theta\left(\frac{(2+s_{eq})(1+a)}{6} - \frac{3s_{eq}+(2+s_{eq})\lambda_L}{6}\cos 2\psi_0 - \frac{a(2N-3)}{6N}\sin^2 2\psi_0\right)\Big]\frac{\partial^2 \psi^{(1)}}{\partial y^2}$$
$$- \sin 2\psi_0\Big[\left(\frac{a}{2Ns_{eq}^2} - \theta\left(\frac{1+5s_{eq}}{72s_{eq}} - a\left(\frac{1+s_{eq}}{6Ns_{eq}^2} + \frac{Ns_{eq}^2-18}{48Ns_{eq}^2}\cos 2\psi_0\right)\right)\right)\frac{\partial^2 s^{(1)}}{\partial y^2} \tag{3.27}$$
$$- \left(\frac{a(1-s_{eq}^2)}{6s_{eq}^2} - \theta\left(\frac{1-4s_{eq}}{72s_{eq}^2} + a\left(\frac{s_{eq}^3-3s_{eq}^2+4}{72s_{eq}^2} - \frac{3-5s_{eq}^2+s_{eq}}{24s_{eq}}\cos 2\psi_0\right)\right)\right)\frac{\partial^2 \beta^{(1)}}{\partial y^2}\Big],$$

where $\lambda_L = \frac{a(2+s_{eq})}{3s_{eq}}$ is the Leslie tumbling parameter (Forest and Wang, 2003).

## 3.2 Normal and tangential anchoring

At this point, we restrict to two special anchoring conditions, which identify both a dramatic simplification of the new model equations (3.23)-(3.27) and a protocol that highlights the most

transparent relationship between experimental data and linear viscoelastic moduli. If the anchoring is either parallel to the flow direction (tangential anchoring, $\psi_0 = 0$), or perpendicular to the plates (normal or homeotropic anchoring, $\psi_0 = \frac{\pi}{2}$), then as observed in (Larson and Mead, 1989a), the nematic elastic stress of a monodomain, which comes only from being out of equilibrium, is zero at leading order. Additionally, as observed in Chapter 2, a monodomain under small amplitude oscillatory shear flow will asymptotically drift to oscillations around one of these two orientations.

### 3.2.1 Decoupling of order parameters from director angle and velocity

These special anchoring conditions provide the significant modeling advantage that the system of four equations (3.23)-(3.27) decouples into two systems of two equations, one for the order parameters and another for the angle and velocity. The order parameter system is

$$
\begin{aligned}
\frac{\partial s^{(1)}}{\partial t} &= \left(\frac{2}{N} + \theta\left(\frac{2(1+s_{eq})}{3N} \mp \frac{5+18s_{eq}}{9N}\right)\right)\frac{\partial^2 s^{(1)}}{\partial y^2} \\
&\quad - \frac{2(1-s_0)}{3}\left(2 + \theta\left(\frac{s_{eq}(s_{eq}+5)}{6} \mp \frac{8+25s_{eq}+45s_{eq}^2}{18}\right)\right)\frac{\partial^2 \beta^{(1)}}{\partial y^2}, \\
\frac{\partial \beta^{(1)}}{\partial t} &= \pm\frac{4\theta}{9N}\frac{\partial^2 s^{(1)}}{\partial y^2} + \frac{1-s_{eq}}{27}\left(18 + \frac{\theta}{2}(4 + s_{eq} \pm (10 - 7s_{eq}))\right)\frac{\partial^2 \beta^{(1)}}{\partial y^2}.
\end{aligned}
\tag{3.28}
$$

Since $s^{(1)}$ and $\beta^{(1)}$ are zero at the boundary of this linear system, we find that $s^{(1)}(y,t) \equiv \beta^{(1)}(y,t) \equiv 0$.

Therefore, near these two orientations, at leading order, the only elastic stresses are distortional, and the leading order dynamics dominated by the director angle and velocity. Thus, the leading order asymptotic description of the director angle and fluid velocity reduces to the same basic form as those derived for normal anchoring with LE theory (Burghardt, 1991; de Andrade Lima and Rey, 2006):

$$
\frac{\partial \psi^{(1)}}{\partial t} = A\Theta(\theta)\frac{\partial^2 \psi^{(1)}}{\partial y^2} + B\frac{\partial v_x^{(1)}}{\partial y},
\tag{3.29}
$$

$$
0 = \begin{cases} \frac{\partial \tau_{xy}^{(1)}}{\partial y}, & \text{for shear flow,} \\ 2\cos\omega t + \frac{\partial \tau_{xy}^{(1)}}{\partial y}, & \text{for Poiseuille flow,} \end{cases}
\tag{3.30}
$$

$$
\tau_{xy}^{(1)} = -B\Theta(\theta)\frac{\partial^2 \psi^{(1)}}{\partial y^2} + C\frac{\partial v_x^{(1)}}{\partial y},
\tag{3.31}
$$

where $A = \frac{s_{eq}+2}{3}$, $C = \frac{\mu_1(s_{eq}+2)}{6} + \frac{\mu_3}{2}$,

$$
B = \begin{cases} -\frac{1-\lambda_L}{2}, & \text{if } \psi_0 = 0, \\ -\frac{1+\lambda_L}{2}, & \text{if } \psi_0 = \frac{\pi}{2}, \end{cases} \tag{3.32}
$$

and where the anisotropy of the molecular elasticity is encoded by

$$
\Theta(\theta) = \begin{cases} 1 + \theta\frac{1-s_{eq}}{3}, & \text{if } \psi_0 = 0, \\ 1 + \theta\frac{1+2s_{eq}}{3}, & \text{if } \psi_0 = \frac{\pi}{2}. \end{cases} \tag{3.33}
$$

Since $\theta \geq -1$, $(AC + B^2)\Theta(\theta) > 0$, and as shown in (Cui *et al.*, 2006), all steady solutions of the system (3.29)-(3.31) are stable for both steady shear and steady Poiseuille flows.

### 3.2.2 Effect of anisotropic elasticity

We now observe one additional advantage of the normal and tangential anchoring conditions: the anisotropic distortional elasticity may now be scaled out of the problem by rescaling the characteristic stress as $\tau_F \to \Theta\tau_F$ and the time as $t_0 \to \frac{t_0}{\Theta}$. From (3.1) and (3.3), this renormalization is equivalent to rescaling $\mathcal{L}^2$ by $\Theta$ and rescales the Ericksen number as $Er \to \frac{Er}{\Theta}$. Notice that from (3.2), $\eta_0$ is unaffected by this rescaling. *Therefore, at these special anchoring conditions, the effects due to anisotropic distortional elasticity can be absorbed into the isotropic distortional elasticity by a simple scaling law.* This simplification does not hold for tilted anchoring. Since $\theta > 0$ for rods and $\theta < 0$ for disks, the anisotropic distortional elasticity effectively increases the isotropic distortional elasticity for rods but decreases it for disks. In both cases, the effect of normal anchoring is stronger than tangential. For the remainder of the paper, we analyze the system (3.29)-(3.31) in the isotropic elastic limit $\theta = 0$ so that $\Theta(\theta) = 1$.

We comment that the above analysis establishes the most efficient and transparent protocols for the prediction of linear viscoelastic moduli of nematic polymers. The model parameters can be fit for using these anchoring conditions, and then the full model can be studied numerically to ascertain the linear response for tilted anchoring conditions.

## 3.3 Linear viscoelasticity moduli for shear flow

We now establish the stress-strain relationship needed to define the storage and loss moduli for shear flow. Along the way, we find that this relationship is independent of the choice to impose stress or plate velocity boundary conditions, and indeed, the solutions for these two boundary conditions are equivalent up to a rescaling and phase shift. Since the system (3.29)-(3.31) is linear, and the driving conditions are sinusoidal in time, the standard analysis for determination of the linear viscoelastic moduli is to suppress transients and seek a frequency-locked solution of the form

$$
\psi^{(1)}(y,t) \;=\; \psi_1(y)\cos\omega t + \psi_2(y)\sin\omega t,
$$

$$
v_x^{(1)}(y,t) \;=\; v_1(y)\cos\omega t + v_2(y)\sin\omega t. \tag{3.34}
$$

After substituting (3.34) into (3.29)-(3.31), we obtain the following general solution for the resulting system of ordinary differential equations

$$
\psi_1(y) = \; C_1\cosh ry\cos ry + C_2\sinh ry\sin ry - \tfrac{B}{C\omega}\tau_2,
$$

$$
\psi_2(y) = \; C_2\cosh ry\cos ry - C_1\sinh ry\sin ry + \tfrac{B}{C\omega}\tau_1, \tag{3.35}
$$

$$
v_1(y) = \; -\tfrac{Br}{C}[(C_1 - C_2)\cosh ry\sin ry - (C_1 + C_2)\sinh ry\cos ry] + \tfrac{\tau_1}{C}y,
$$

$$
v_2(y) = \; -\tfrac{Br}{C}[(C_1 + C_2)\cosh ry\sin ry + (C_1 - C_2)\sinh ry\cos ry] + \tfrac{\tau_2}{C}y, \tag{3.36}
$$

where $r = \sqrt{\frac{C\omega}{2(AC+B^2)}}$.

Although we have not yet applied boundary conditions to determine the constant coefficients $C_1, C_2, \tau_1$, and $\tau_2$ in (3.35) and (3.36), we recognize that from (3.30) and (3.31), the frequency-locked shear stress is independent of $y$ and takes the form

$$
\tau_{xy}^{(1)} = \tau_1\cos\omega t + \tau_2\sin\omega t. \tag{3.37}
$$

For both imposed shear and imposed velocity, the director boundary conditions are

$$\psi_1(\pm\tfrac{1}{2}) = 0, \quad \psi_2(\pm\tfrac{1}{2}) = 0. \tag{3.38}$$

Applying these to (3.35) allows us to express $C_1$ and $C_2$ as functions of $\tau_1$ and $\tau_2$:

$$C_1 = \tau_1 \frac{2B}{C\omega} \frac{\sin\frac{r}{2}\sinh\frac{r}{2}}{\cosh r + \cos r} + \tau_2 \frac{2B}{C\omega} \frac{\cos\frac{r}{2}\cosh\frac{r}{2}}{\cosh r + \cos r},$$

$$\tag{3.39}$$

$$C_2 = -\tau_1 \frac{2B}{C\omega} \frac{\cos\frac{r}{2}\cosh\frac{r}{2}}{\cosh r + \cos r} + \tau_2 \frac{2B}{C\omega} \frac{\sin\frac{r}{2}\sinh\frac{r}{2}}{\cosh r + \cos r}.$$

Thus, if we define the motion of the upper plate as

$$V = V_1 \cos\omega t + V_2 \sin\omega t, \tag{3.40}$$

with $V_i = v_i(\frac{1}{2})$ using (3.39) in (3.36), we establish a direct relationship between the components of the shear stress and the components of velocity at the upper plate:

$$V_1 = E_2\tau_1 + E_1\tau_2, \qquad V_2 = -E_1\tau_1 + E_2\tau_2,$$

$$\tag{3.41}$$

$$E_1 = \frac{B^2 r}{C^2\omega} \frac{\sinh r - \sin r}{\cosh r + \cos r}, \quad E_2 = \frac{1}{2C} - \frac{B^2 r}{C^2\omega} \frac{\sinh r + \sin r}{\cosh r + \cos r}.$$

Therefore, (3.37) and the macroscopic strain

$$\gamma = \tfrac{2}{\omega}(V_1 \sin\omega t - V_2 \cos\omega t) \tag{3.42}$$

provide the stress-strain relationship that we need in order to identify the storage and loss

moduli as, respectively,

$$G'(\omega) \quad = \frac{\omega}{2}\frac{\tau_2 V_1 - \tau_1 V_2}{V_1^2 + V_2^2} = \frac{\omega}{2}\frac{E_1}{E_1^2 + E_2^2}$$

(3.43)

$$= \frac{2B^2 C^2 \omega^2 r(\sinh r - \sin r)}{(8B^4 r^2 + C^2 \omega^2)(\cosh r + \cos r) - 16B^4 r^2 \cos r - 4B^2 Cr\omega(\sin r + \sinh r)},$$

$$G''(\omega) \quad = \frac{\omega}{2}\frac{\tau_1 V_1 + \tau_2 V_2}{V_1^2 + V_2^2} = \frac{\omega}{2}\frac{E_2}{E_1^2 + E_2^2}$$

(3.44)

$$= \frac{C^2 \omega^2 (C\omega(\cosh r + \cos r) - 2B^2 r(\sinh r + \sin r))}{(8B^4 r^2 + C^2 \omega^2)(\cosh r + \cos r) - 16B^4 r^2 \cos r - 4B^2 Cr\omega(\sin r + \sinh r)}.$$

Thus we have predicted the storage and loss moduli independent of the choice to impose oscillatory stress or velocity on the plates. Figure 3.1 shows the effect of normal versus tangential anchoring on the storage and loss moduli. There is no qualitative difference in the dynamic moduli between the steady shear distinction of flow-aligning ($\lambda_L > 1$) and tumbling nematics ($\lambda_L < 1$) regimes, a prediction that is consistent with the monodomain predictions of Chapter 2. We plot only the flow-aligning case with $a = 0.9$ ($\lambda_L = 1.04$). Given the scaling laws for anisotropic elasticity in Section 3.2.2, the effect of $\theta$ on the moduli is also a simple scaling:

$$G(\omega;\theta) = \Theta(\theta)G(\frac{\omega}{\Theta(\theta)};0). \tag{3.45}$$

For normal anchoring, (3.43)) and (3.44) predict similar behavior of $G'$ and $G''$ with respect to $\omega$ for nematic polymers as those found in (Burghardt, 1991; de Andrade Lima and Rey, 2006) for heterogeneous liquid crystals with normal anchoring. We discuss this behavior now in order to highlight the significant differences normal anchoring and tangential anchoring conditions, which were not specified in (Burghardt, 1991; de Andrade Lima and Rey, 2006).

Except for a region of moderate frequencies, the loss modulus $G''(\omega)$ exhibits nearly linear behavior at high and low frequencies with a low frequency offset:

$$\begin{aligned} G''(\omega) &= \left(C + \frac{B^2}{A}\right)\omega, \quad \text{as } \omega \to 0, \\ G''(\omega) &= C\,\omega, \quad\quad\quad \text{as } \omega \to \infty. \end{aligned} \tag{3.46}$$
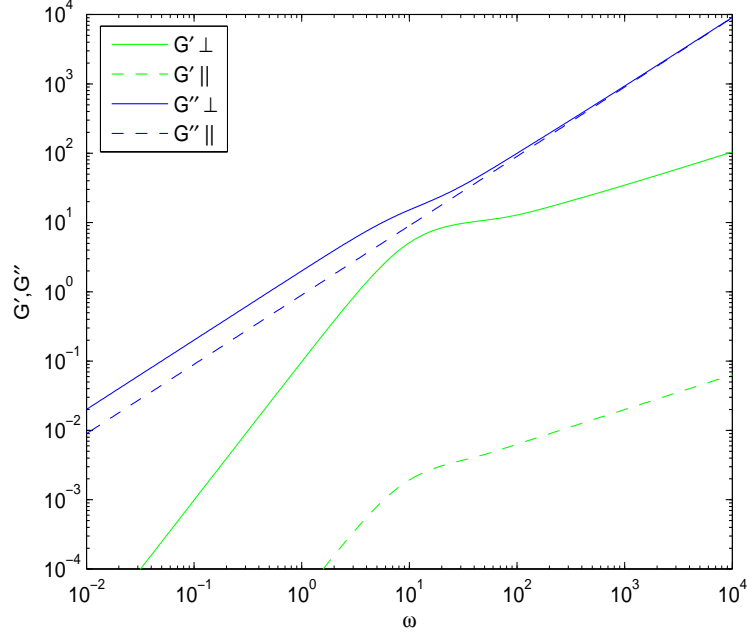
Figure 3.1: The effect of normal (solid lines) and tangential (dashed lines) anchoring on the dynamic moduli in the isotropic elasticity limit, $\theta = 0$.

The constant shift between the high and low frequency limit, $\frac{B^2}{A} = \frac{3(1 \mp \lambda_L)^2}{4(s_0+2)}$, is always positive. However, we get an immediate insight into the difference between tangential and normal anchoring and rods versus platelets: for rods (when $\lambda_L \approx 1$) with normal anchoring, $B^2 = \frac{(1+\lambda_L)^2}{4} \approx 1$, whereas for tangential anchoring, $B^2 = \frac{(1-\lambda_L)^2}{4} \approx 0$. Thus, normal anchoring exhibits an increased loss modulus for low frequencies over tangential anchoring, but for high frequencies, the two anchoring conditions yield approximately the same values. However, for platelets, $\lambda_L \approx -1$ so that the effect of anchoring is reversed with tangential anchoring showing a low frequency increase over normal anchoring.

For the storage modulus, we also find different asymptotic regimes for high and low frequencies, but they have distinct scaling behaviors:

$$G'(\omega) = \quad \frac{B^2}{12A^2}\omega^2, \qquad \text{as } \omega \to 0,$$

$$(3.47)$$

$$G'(\omega) = \quad B^2\sqrt{\frac{2C}{AC+B^2}}\sqrt{\omega}, \quad \text{as } \omega \to \infty.$$

For reasons similar to the loss modulus behavior at low frequencies, the overall factor of $B^2$

is the dominant feature in both regimes, accounting for the two to three orders of magnitude difference in $G'(\omega)$ between normal and tangential anchoring shown in Figure 3.1.

## 3.4   Comparison to monodomains

Now we turn our attention to how these moduli predictions of heterogeneous polymers differ from those of a monodomain in shear flow. Since the nondimensionalization employed in this chapter was not designed to recover the monodomain equations analyzed in Chapter 2 in any particular asymptotic limit, some caution should be made in a direct comparison of the present results with those of Chapters 2. Nevertheless, each model provides a prediction of the storage and loss moduli, and so some degree of comparison is possible.

For the nondimensionalization and asymptotic analysis used in this chapter, the monodomain solution ansatz for (3.23)-(3.27), *i.e.*, $s^{(1)}$, $\beta^{(1)}$, and $\psi^{(1)}$ are functions of $t$ only and $\frac{\partial v_x^{(1)}}{\partial y} = \cos \omega t$, yields different predictions than that used in Chapter 2. Specifically, in this case the shear stress has no elastic component and is given by

$$\tau_{xy,monodomain}^{(1)} = \left( \frac{\mu_1(s_0+2)}{6} + \frac{\mu_2 s_0^2}{4} \sin^2 2\psi_0 + \frac{\mu_3}{2} \right) \cos \omega t. \tag{3.48}$$

Thus, under this nondimensionalization, $G'(\omega) = 0$ and $G''(\omega) = (C + \frac{\mu_2 s_0^2}{4} \sin^2 2\psi_0)\omega$. Both this monodomain prediction and that from Chapter 2, the two special anchoring conditions in our present discussion restrict to the same prediction. When $\psi_0 = 0$ or $\frac{\pi}{2}$,

$$G'(\omega) = 0, \quad G''(\omega) = C\omega. \tag{3.49}$$

Note that $\hat{\eta}$ from (2.103) is equal to $C$ in terms of the dependence on the nondimensional parameters $\mu_1$ and $\mu_3$, but the definitions of these nondimensional parameters are different in each chapter. The main advantage of the different approaches of the two chapters is the comparison of the effect of the nematic elastic stresses generated by a monodomain with a tilted angle in Chapter 2 with the effect of heterogeneity, which the present chapter has elucidated when the effects of tilted anchoring are suppressed.

The major qualitative difference between the nematic elastic stress from a tilted mon-

odomain and the isotropic elastic stress from a heterogeneous sample with normal or tangential anchoring lies in the scaling law for $G'(\omega)$ for high frequencies. From (2.106), $G'(\omega) = O(1)$ as $\omega \to \infty$ in contrast to the scaling $G'(\omega) = O(\sqrt{\omega})$ found in (3.47).

## 3.5 Equivalence of flows

Now we examine the equivalence between imposed velocity and imposed stress boundary conditions in further detail. In this section, the subscript $\tau$ represents the coefficients for imposed stress boundary conditions, and the subscript $v$ indicates imposed velocity boundary conditions.

If the stress is imposed, then we have

$$\tau_{1,\tau} = 1, \quad \tau_{2,\tau} = 0, \tag{3.50}$$

and so from (3.41),

$$V_{1,\tau} = E_2, \qquad\qquad V_{2,\tau} = -E_1,$$

$$\tag{3.51}$$

$$C_{1,\tau} = \frac{2B}{C\omega} \frac{\sin \frac{r}{2} \sinh \frac{r}{2}}{\cosh r + \cos r}, \quad C_{2,\tau} = -\frac{2B}{C\omega} \frac{\cos \frac{r}{2} \cosh \frac{r}{2}}{\cosh r + \cos r}.$$

However for imposed velocity, the boundary conditions are

$$V_{1,v} = 1, \quad V_{2,v} = 0, \tag{3.52}$$

and so

$$\tau_{1,v} = \frac{2G''}{\omega} = \frac{E_2}{E_1^2 + E_2^2}, \qquad \tau_{2,v} = \frac{2G'}{\omega} = \frac{E_1}{E_1^2 + E_2^2},$$

$$\tag{3.53}$$

$$C_{1,v} = C_{1,\tau}\tau_{1,v} - C_{2,\tau}\tau_{2,v}, \quad C_{2,v} = C_{2,\tau}\tau_{1,v} + C_{1,\tau}\tau_{2,v}.$$

It can be shown that within the gap, the solutions from these two boundary conditions differ only by a rescaling and a phase shift of $\chi = -\tan^{-1}\frac{E_1}{E_2}$:

$$\psi_\tau^{(1)}(y,t) = \sqrt{E_1^2 + E_2^2}\, \psi_v^{(1)}\left(y, t - \frac{\chi}{\omega}\right), \quad v_{x,\tau}^{(1)}(y,t) = \sqrt{E_1^2 + E_2^2}\, v_{x,v}^{(1)}\left(y, t - \frac{\chi}{\omega}\right). \tag{3.54}$$
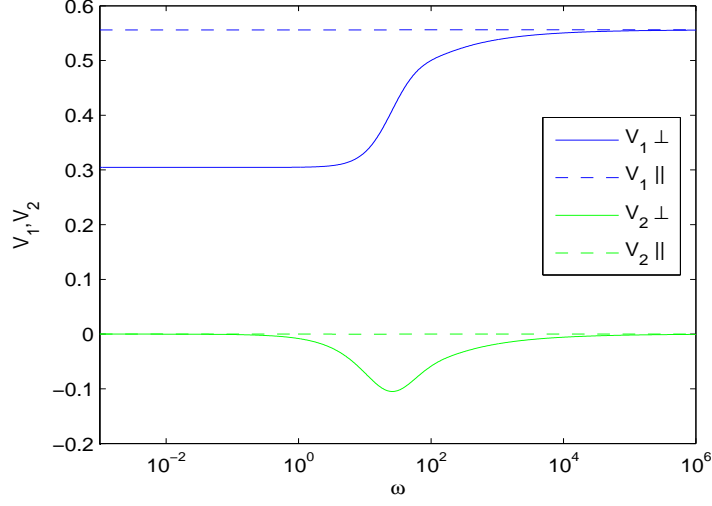
Figure 3.2: The in-phase $V_1$ and out-of-phase $V_2$ response of the upper plate velocity to imposed stress for tangential (dashed lines) and normal (solid lines) anchoring.

For imposed stress, the velocity components of the upper plate are shown in Figure 3.2. For tangential anchoring, there is no observable frequency dependence. For normal anchoring under high frequencies, the plate motion is the same as for tangential anchoring. However, for moderate frequencies, there is a significant out-of-phase response, and for lower frequencies, there is a significant decrease in the velocity compared to tangential anchoring, as indicated by the presence of the $B^2$ term the low-frequency limit compared to the high-frequency limit:

$$\lim_{\omega \to 0} V_1 = \frac{A}{2(AC+B^2)} \ , \quad \lim_{\omega \to \infty} V_1 = \frac{1}{2C}. \tag{3.55}$$

To help us compare the macroscopic response of the velocity and the director angle with the imposed stress $\tau_{xy}^{(1)} = \cos \omega t$, we write the plate velocity as

$$V = V_0 \cos(\omega t - \delta), \tag{3.56}$$

where $\tan \delta = \frac{G''}{G'}$ is the loss tangent, and we define

$$\Psi = \psi^{(1)}(0,t) = \Psi_0 \cos(\omega t - \phi) \tag{3.57}$$

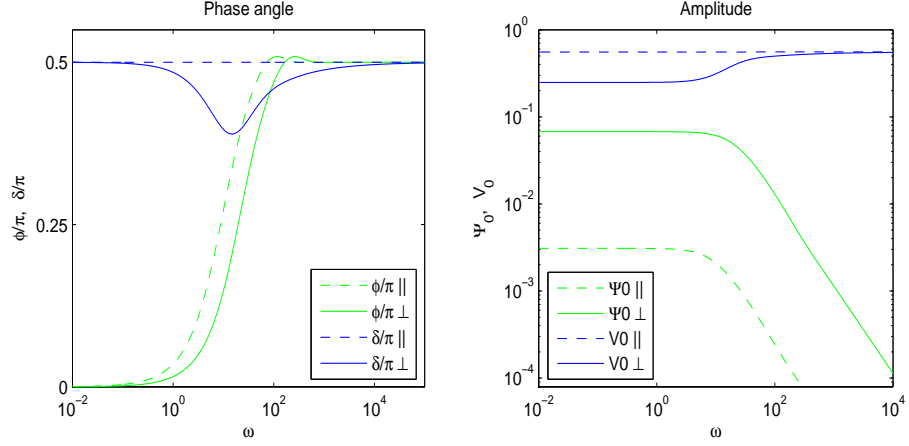to be the director angle at the midpoint between the plates. Figure 3.3 shows plots of phase

Figure 3.3: The phase angles with respect to the imposed stress $\delta$ (plate velocity) and $\phi$ (director angle at $y = 0$), and the amplitudes $V_0$ (plates) and $\Psi_0$ (director angle at $y = 0$).

angles $\delta$ and $\phi$, and the amplitudes $V_0$ and $\Psi_0$ as functions of $\omega$. For normal anchoring at high and low frequencies and at tangential anchoring for all frequencies, the velocity is always out of phase with the stress by $\frac{\pi}{2}$. However, for normal anchoring with moderate frequencies, the plates are closer to in-phase with the stress. The angle is in-phase with the stress for low frequencies, but for larger frequencies it is in-phase with the plates. This transition occurs at a lower frequency for tangential anchoring than normal. The amplitude of the angle is constant for low frequencies, but is $O(\omega^{-1})$ for high frequencies and much larger for normal than tangential anchoring.

### 3.5.1 Poiseuille Flows

Now we turn our attention to the linear viscoelasticity generated by an imposed small amplitude oscillatory Poiseuille flow. Again, we seek solutions to (3.29)-(3.31) of the form (3.34) and find

that

$$\psi_1(y) = D_1 \cosh ry \sin ry + D_2 \sinh ry \cos ry,$$

$$\psi_2(y) = -D_2 \cosh ry \sin ry + D_1 \sinh ry \cos ry - \frac{2B}{C\omega}y,$$

(3.58)

$$v_1(y) = \frac{Br}{C}[(D_1 + D_2) \cosh ry \cos ry + (D_1 - D_2) \sinh ry \sin ry] + D_3 - \frac{y^2}{C},$$

$$v_2(y) = \frac{Br}{C}[(D_1 - D_2) \cosh ry \cos ry - (D_1 + D_2) \sinh ry \sin ry] + D_4$$

where $r$ is the same as for oscillatory shear. Applying the boundary conditions

$$\psi_1(\pm 1) = \psi_2(\pm 1) = v_1(\pm 1) = v_2(\pm 1) = 0 \tag{3.59}$$

determines that

$$D_1 = \frac{4B \cos r \sinh r}{C\omega(\cosh 2r - \cos 2r)}, \qquad D_2 = -\frac{4B \sin r \cosh r}{C\omega(\cosh 2r - \cos 2r)},$$

(3.60)

$$D_3 = \frac{1}{C} - \frac{2B^2 r(\sinh 2r - \sin 2r)}{C^2\omega(\cosh 2r - \cos 2r)}, \quad D_4 = -\frac{2B^2 r(\sinh 2r + \sin 2r)}{C^2\omega(\cosh 2r - \cos 2r)}.$$

At the middle of the gap where the fluid undergoes its maximum displacement, we define the components of the macroscopic fluid velocity as

$$V_1 = v_1(0) = \frac{Br}{C}(D_1 + D_2) + D_3 = 2E_2,$$

(3.61)

$$V_2 = v_2(0) = \frac{Br}{C}(D_1 - D_2) + D_4 = -2E_1,$$

where $E_1$ and $E_2$ are the same quantities defined in (3.41) for shear flow. Thus, the motion of the midline of the fluid relative to the bottom plate in Poiseuille flow is the same as the motion of the top plate in shear flow with imposed stress of relative to the bottom plate.

The stress components are simply $\tau_1 = -2y$ and $\tau_2 = 0$, and if we use the average stress

$$\bar{\tau}_{xy}^{(1)} = \int_{-1}^{0} \tau_1 \cos \omega t + \tau_2 \sin \omega t \, dy = \cos \omega t \tag{3.62}$$

75

to compute the storage and loss moduli relative to the macroscopic strain rate

$$\gamma = \frac{1}{\omega}(V_1 \sin \omega t - V_2 \cos \omega t), \tag{3.63}$$

we find that $G'(\omega)$ and $G''(\omega)$ give exactly the same formulas as those for oscillatory shear given by (2.102) and (2.100). Thus in a macroscopic sense, the bottom half of the channel in Poiseuille flow can be seen as oscillatory "plate" of fluid moving against a fixed bottom plate, "rheologically equivalent" to a shear flow.

### 3.5.2 Heterogeneity of shear and Poiseuille flows

We have carefully scaled the Poiseuille flow experiment so that from a macroscopic perspective, it can be seen as a fluid trapped between two plates separated by the same distance, moving at the same relative velocity, and having the same average stress across the gap as the shear flow experiment with imposed stress boundary conditions. Furthermore, since $\psi^{(1)}$ is an odd function of $y$ in Poiseuille flow, we effectively have the same anchoring conditions at the virtual plate top plate as the physical plate in shear flow. We now look closer and examine the interior of the responses where we find both similarities and differences.

First, the plate frequency induces a new length scale $\frac{1}{r}$ which defines a "boundary layer" near the plates with thickness proportional to $\frac{1}{\sqrt{\omega}}$. However, since the thickness of the boundary layer increases as the frequency decreases, if $\omega < 8(A + \frac{B^2}{C})$, then in shear flow the boundary layers are thick enough that they collide, filling the entire gap. It is different for Poiseuille flow since the boundary layer is present at the physical plate but not at the virtual plate.

In Figure 3.4, we plot the velocity profiles of the two flows for normal anchoring. To plot them on the same coordinate axes, we have shifted the shear flow so that the lower plate coincides with that of Poiseuille flow. While the Poiseuille flow is faster in both the in-phase and out-of-phase components, the out-of-phase components of both flows are only significant for moderate frequencies. For tangential anchoring, the velocity profiles have no significant dependence on $\omega$.

In Figure 3.5, we plot $\psi_i^*(y) = \frac{\psi_i(y)}{\Psi_0}$, which are the director angle profiles for both shear and Poiseuille flows scaled by $\Psi_0$ from Figure 3.3, the magnitude of $\psi^{(1)}$ halfway between the
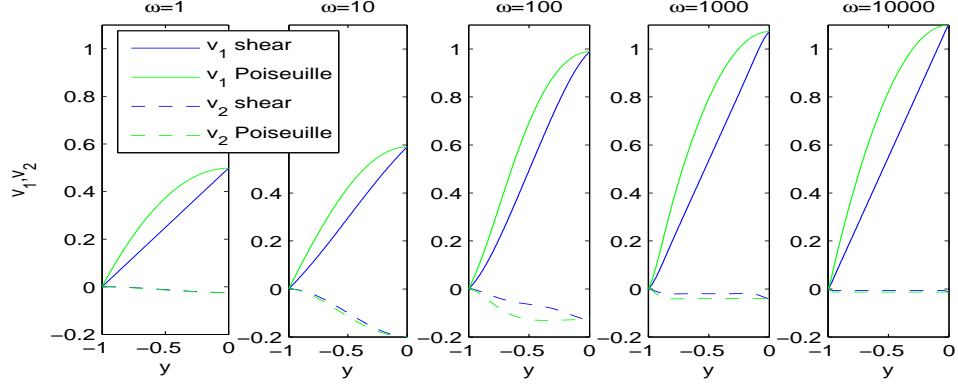
Figure 3.4: The profiles of $v_1$ (solid lines) and $v_2$ (dashed lines) across the gap for shear flow with imposed stress and Poiseuille flow for normal anchoring.
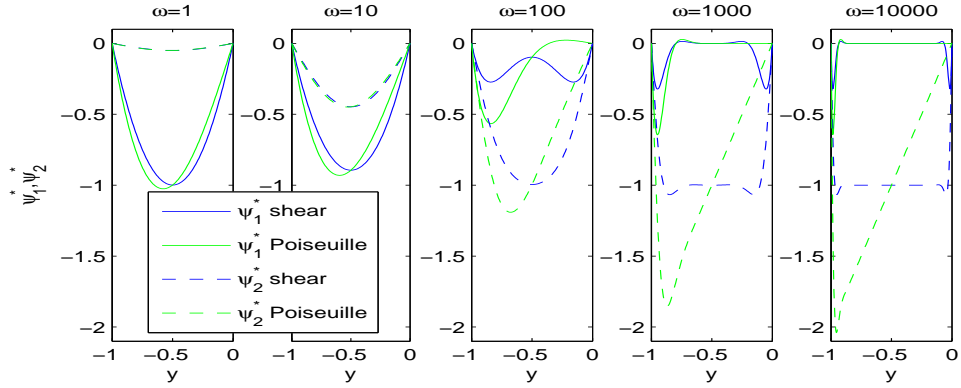


Figure 3.5: The scaled in-phase $\psi_1^*$ (solid line) and out-of-phase $\psi_2^*$ (dashed line) director angles for normal anchoring.

plates for shear flow. Both flows have a similar dependence on the frequency in that for low frequencies, $\psi_1$ is dominant, with $\psi_2$ being insignificant, but as $\omega$ increases, $\psi_2$ increases and eventually surpasses $\psi_1$ in dominance, although $\psi_2$ is $O(\omega^{-1})$ as $\omega \to \infty$. For low frequencies, the profiles of the two flows are quite similar in shape, but as the frequency increases, the profiles become less similar.

## 3.6 Conclusion

We have examined small amplitude oscillatory shear and Poiseuille flows of nematic polymers, using a Doi-Hess-Marrucci-Greco mesoscopic tensor model, incorporating heterogeneity and highlighting the effects of normal versus tangential anchoring at the plates. At these two special anchoring conditions, the nematic polymer response simplifies dramatically, and we recover

Leslie-Ericksen-type dynamics for the velocity and the major axis of the orientation tensor (the primary director). The order parameters are then driven by the flow-director response functions. Furthermore, at these two anchoring conditions, the effects of anisotropic molecular elasticity to be absorbed into the one-constant Frank elastic potential by a simple rescaling.

Through a judicious nondimensionalization, we show rheological equivalence between shear flow with both imposed stress or velocity boundary conditions and Poiseuille flow; both experiments yield the same storage and loss moduli when anchoring conditions at the plates are identical (either tangential or homoetropic). An important physical prediction is the strong dependence of the storage and loss moduli on plate anchoring conditions of the nematic director, with two-to-three orders of magnitude in the storage modulus between normal and tangential anchoring. A deeper investigation into the effect of plate anchoring conditions is warranted, which will require numerical simulations.

# Bibliography

Burghardt, W.R. (1991). "Oscillatory shear flow of nematic liquid crystals." *J. Rheol.*, **35**(1), 49-62.

Choate, E.P., and Forest, M.G. (2006). "A classical problem revisited: Rheology of nematic polymer monodomains in small amplitude oscillatory shear." *Rheol. Acta*, **46**, 83-94.

Colby, R.H., Nentwich, L.M., Clingman, S.R., and Ober, C.K. (2002). "Defect-mediated creep of structured materials." *Europhys. Lett.*, **54**, 269-274.

Cui, Z., Forest, M.G., Wang, Q., and Zhou, H. (2006). "On weak plane shear and Poiseuille flows of rigid rod and platelet ensembles." *SIAM J. Appl. Math.*, **66**(4), 1227-1260.

de Andrade Lima, L.R.P., and Rey, A.D. (2004). "Superposition and universality in the linear viscoelasticity of Leslie-Ericken liquid crystals." *J. Rheol.*, **48**(5), 1067-1084.

de Andrade Lima, L.R.P. and Rey, A.D. (2006). "Superposition principles for small amplitude oscillatory shearing of nematic mesophases." *Rheol. Acta*, **45**, 591-600.

Doi, M., and Edwards, S.F. (1986). *The Theory of Polymer Dynamics.* Oxford U. Press (Clarendon), London New York.

Forest, M.G., and Wang, Q. (2003). "Monodomain response of finite-aspect-ratio macromolecules in shear and related linear flows." *Rheol. Acta*, **42**, 26-42.

Forest, M.G., Zhou, R., and Wang, Q. (2003). "Full-tensor alignment criteria for sheared nematic polymers." *J. Rheol.*, **47**, 105-127.

Forest, M.G., Zhou, R., and Wang, Q. (2005). "Kinetic structure simulations of nematic polymers in plane Couette cells II: In-plane structure transitions." *Multiscale Model. Simul.*, **4**, 1280-1304.

Hess S. (1976). "Fokker-Planck-Equation Approach to Flow Alignment in Liquid Crystals." *Z. Naturforsch.*, **31a**, 1034-1037.

Hess S., and Kröger, M. (2004). "Regular and chaotic orientational and rheological behaviour of liquid crystals." *J. Phys.: Condens. Matter*, **16**, S3835-S3859

Hinch, E.J., and Leal, L.G. (1976). "Constituative equations in suspension mechanics. Part 2. Approximate forms for a suspension of rigid particles affected by Brownian rotations." *J. Fluid Mech.*, **76**, 187-208.

Larson R.G. (1999). *The Structure and Rheology of Complex Fluids.* Oxford University Press, New York Oxford.

Larson, R.G., and Mead, D.W. (1989a). "Linear Viscoelasticity of Nematic Liquid Crystilline Polymers." *J. Rheol.*, **33**, 185-206.

Larson, R.G., and Mead, D.W. (1989b). "Time and Shear-Rate Scaling Laws for Liquid Crystal Polymers." *J. Rheol.*, **33**, 1251-1281.

Lee, J., Forest, M.G., and Zhou, R. (2006). "Alignment and rheo-oscillator criteria for sheared nematic polymer films in the monodomain limit." *Disc. Cont. Dyn. Syst. B*, **6**, 339-356.

Marrucci, G., and Greco, F. (1993). "Flow behavior of liquid crystalline polymers." *Adv. Chem. Phys.*, **86**, 331-404.

Moldenaers, P., and Mewis, J. (1986). "Transient Behavior of Liquid Crystalline Solutions of Poly(benzylglutamate)." *J. Rheol.*, **30**, 567-584.

Rienäcker, G., and Hess, S. (1999). "Orientational dynamics of nematic liquid crystals under steady shear flow." *Physica A*, **267**, 294-321.

Rienäcker, G., Kröger M., and Hess, S. (2002a). "Chaotic orientational behavior of a nematic liquid crystal subjected to a steady shear flow." *Phys. Rev. E*, **60**, 040702 DOI:10.1103/PhysRevE.66.040702

Rienäcker, G., Kröger, M., and Hess, S. (2002b). "Chaotic and regular shear-induced orientational dynamics of nematic liquid crystals." *Physica A*, **315**, 537-568.

Tsuji, T., and Rey, A.D. (1997). "Effect of long range order on sheared liquid crystalline materials Part 1: compatibility between tumbling behavior and fixed anchoring." *J Non-Newtonian Fluid Mech.*, **73**, 127-152.

Vicente Alonso, E., Wheeler, A.A., and Sluckin, T.J. (2003). "Nonlinear Dynamics of a Nematic Liquid Crystal in the Presence of a Shear Flow." *Proc. R. Soc. London Ser. A*, **459**, 195-220.

Wang, Q. (2002). "A hydrodynamic theory of nematic liquid crystalline polymers of different configurations," *J. Chem. Phys.*, **116**(20), 9120-9136.